National Library of Canada
Acquisitions and Bibliographic Services Branch
395 Wellington Street
Ottawa, Ontario
K1A 0N4

Bibliothèque nationale du Canada
Direction des acquisitions et des services bibliographiques
395, rue Wellington
Ottawa (Ontario)
K1A 0N4

Your file Votre référence

Our file Notre référence

NOTICE

The quality of this microform is heavily dependent upon the quality of the original thesis submitted for microfilming. Every effort has been made to ensure the highest quality of reproduction possible.

If pages are missing, contact the university which granted the degree.

Some pages may have indistinct print especially if the original pages were typed with a poor typewriter ribbon or if the university sent us an inferior photocopy.

AVIS

La qualité de cette microforme dépend grandement de la qualité de la thèse soumise au microfilmage. Nous avons tout fait pour assurer une qualité supérieure de reproduction.

S'il manque des pages, veuillez communiquer avec l'université qui a conféré le grade.

La qualité d'impression de certaines pages peut laisser à désirer, surtout si les pages originales ont été dactylographiées à l'aide d'un ruban usé ou si l'université nous a fait parvenir une photocopie de qualité inférieure.

Canada

The phase space volume of ion clouds in Paul traps

by

Matthew David Norwood Lunney
B.Eng. McGill University, 1984
M.Eng. McGill University, 1986

A thesis submitted to the Faculty of Graduate Studies and Research
in partial fulfillment of the requirements for the degree of
Doctor of Philosophy

Computational Analysis and Design Laboratory
Department of Electrical Engineering and
Foster Radiation Laboratory
Department of Physics
McGill University
Montreal, Canada

submitted: June, 1992
defended: September, 1992

ISBN 0-315-80474-2

ABSTRACT

A new technique is presented for measuring the spatial and momentum distributions of a buffer-gas cooled ion cloud in a Paul trap by extracting it from the trap and fitting the time profile of the extracted ion signal. A thermodynamic model based on the Gibbs distribution has been developed which describes the initial ion cloud phase space volume and fits the measured time distributions of the extracted cloud using only one parameter: temperature. A time-of-flight system has been built to systematically vary the ion extraction conditions and compare predictions of the model to various measurements of the ion cloud time profile. A new numerical method using a multipole expansion was developed to compute the extraction fields. Agreement between the ion simulations and the time-of-flight data is better than 2% of the total flight time.

Ion cloud temperatures were measured for seven different trap loadings of potassium ions and four loadings of sodium ions, in both cases down to clouds of about 1000 ions. This is the first time that temperature measurments have been made for such small numbers of buffer-gas cooled ions. The results show that the temperature of the ions above the buffer gas temperature appears to be proportional to the two-thirds power of the number of ions in the cloud.

Dynamic manipulation of the extracted ion cloud phase space volume was also accomplished using a time-varying acceleration voltage to change the ion cloud energy spread in flight.

A concept is also outlined to measure the detailed phase space area of the extracted cloud using the projection-slice theorem of tomographic imaging.

These measurements have applications for the use of ion traps as beam collectors for nuclear physics experiments at isotope separator facilities and possibly for nano-circuit fabrication.

RESUME

Une nouvelle technique est présentée pour la mesure détaillée de la distribution spatiale et en moment du nuage d'ions refroidi par gaz tampon dans une trappe Paul. La mesure est réalisée par déconvolution du spectre en temps de vol des ions extraits de la trappe. Un modèle thermodynamique basé sur les distributions de Gibbs a été développé pour décrire l'évolution en temps de l'espace de phase à partir des conditions initiales du nuage d'ions. Le modèle reproduit les distributions en temps des ions après extraction avec un seul parametre: la température. Un système de mesure de temps de vol a été construit qui permet le contrôle détaillé des conditions d'extraction. Les prédictions du modèle ont pu ainsi être comparées aux mesures pour différentes conditions d'extraction. Une nouvelle méthode numérique basée sur une expension multipolaire a été développée pour le calcul des champs d'extraction. Un accord meilleur que 2% à été obtenu entre les simulations et les mesures de temps de vol.

La température du nuage d'ions a été mesurée pour sept différentes conditions de concentration en ions de potasium et quatre concentrations en ions de sodium avec dans les deux cas un nuage minimum de 1000 ions. La présente mesure de température est une première pour de si petits nombres d'ions refroidis par gaz tampon. Les résultats montrent que la température des ions au dessus de la température du gaz tampon est proportionelle à la puissance deux tiers du nombre d'ions dans le nuage.

Des manipulations dynamiques de l'espace de phase du nuage d'ions ont aussi été accompli à l'aide d'un voltage d'accélération dépendant du temps.

Un concept est aussi ébauchée pour la mesure détaillée du projections du l'espace de phase du faiseau extrait qui utilise le théorème du projection du tranches en imagerie tomographique.

Les mesures décrites ont des applications pour l'utilisation de trappes d'ions comme collecteurs de faiseaux pour la réalisation d'expériences de physique nucléaire auprès d'installations de séparateurs d'ions en ligne et possiblement, aussi, pour la fabrication de nano-circuit.

When at the first I took my pen in hand
Thus for to write, I did not understand...
Some said...print it; others said, Not so;
Some said, It might do good; others said, No.
Now I was in a strait, and did not see
Which was the best thing to be done by me:
At last I thought, Since ye are thus divided,
I print it will, and so the case decided.
To prove, then, who advised for the best,
Thus I thought fit to put it to the test.
...O man of God,
Art thou offended? Dost thou wish I had
Put forth my matter in another dress?
Or that I had in things been more express?
...let me propound; then I submit
To those that are my betters, as it fit.
And now before I do put up my pen,
I'll show the profit of my book, and then
Commit both thee and it unto that Hand
That pulls the strong down, and makes weak ones stand.
This book it chalketh out before thine eyes
The man that seeks the everlasting prize...

From The Author's Apology to *The Pilgrim's Progress* by John Bunyan

TABLE OF CONTENTS

LIST OF FIGURES

LIST OF TABLES

FOREWORD

I know you: solitary griefs, desolate passions, aching hours.
The Precept of Silence by Lionel Pigot Johnson

The research work described in this dissertation began, unofficially, in June 1987. I say unofficially because: (1) I was not registered at the university (until September); (2) I was not paid; and (3) I was working, 20 hours a week, at Paramax Electronics in Montreal. For the next year, I spent about two days a week at the Foster Radiation Laboratory building a collinear laser spectroscopy system under the supervision of Fritz Buchinger. Fritz wanted to explore the ion trap collection ideas of Bob Moore in order to enhance the sensitivity of his laser spectroscopy measurements at CERN.

In June of 1988, I left Paramax and became, one again, a full-time student. I was registered in the department of Electrical Engineering but worked almost exclusively in the Physics department and was completely assimilated into the research program of the experimental nuclear physics group in the Foster Radiation Laboratory. Why? Having obtained a Bachelors degree in Electrical Engineering (in 1984), transfering to the Physics department would have involved another two or so years of extra coursework. On the other hand, my engineering background in some ways suited the instrumentation-oriented work that was needed at the Foster lab.

Moore recruited me first as a summer student in 1982 and 1983, and later into his research program at the Masters level in 1984. It was then that I built and tested McGill's first ion trap. After three years of exploring trap beam collector potential, with fellow graduate student Sid Gulick making the ultimate breakthrough, we were seemingly in position to apply these ideas to real experiments. It was here that the laser story started.

After three agonizing years of development, it became clear that laser spectroscopy on beams extracted from ion traps was not to be. It boiled down to the limited capacity of the trap coupled with its tremendous broadening of the velocity spread of the extracted beam. A paucity of funding also hindered the work to some degree. At this point the focus of the project shifted towards probing the extracted beam by non-optical methods, namely, time-of-flight. As the glow of the laser faded from sight, I diffused unto the direct supervision of "the Master" himself and ultimately, a successful characterization of trapped ion clouds emerged from the mire.

This project falls very much under the category of Engineering Physics, a program that used to exist at McGill. A side-effect of such potentially interesting inter-disciplinary study is the creation of odd-balls who don't fit in to the categories of today's *mission*-oriented existance. I found myself falling through the cracks as an unknown number in the department in which I was working but not registered and an unknown face in a department in which I was registered but not seen.

Overall, the experience has been quite positive, however. An "undergraduatehood" dream was realized when I participated in research performed in Geneva at CERN, the *mecca* of experimental physics. Research in experimental physics also provides more opportunities to play with various pieces of expensive equipment and inflict real damage unlike the increasingly computer-oriented nature of electrical engineering.

I would like now to acknowledge everyone who contributed to this humbling experience and made it possible. Bob Moore is the visionary from whom the whole reason for pursuing this

work comes. He is brimming with ideas and also works very hard towards their implementation. The ever-optimistic Fritz Buchinger was the original prime-mover in this project and is always available to help and encourage. Prof. Jean Barrette, our director at the Foster Lab (the boss), is an infinite fund of advice, idea sounding volume, encouragement and downright ass-kicking. His tireless dedication to the success of the lab and its inhabitants has revitalized the place. Prof. Jon Webb, who provides my lifeline into the electrical engineering world, likewise provides great encouragement, rigor and patience. His careful proof-reading of this thesis was invaluable. Prof. Steve McFee also provided me with some desperately sought-after guidance in the area of finite-element error analysis for which I am grateful. I also wish to thank Dave Lowther and Behzad Forghani of *Infolytica Corporation* for the use of their high-order solver and computing facilities. Marc Nantel contributed greatly to the project during his M.Sc. tenure at the lab and Philippe Archambeault provided valuable assistance and encouragement during the summer of 1990.

A special mention must be made for the *sine qua non* assistance of Leo Nikkinen, broadband electrotechnophile extraordinaire, and Steve Kecani, omni-material machinist superlatif. Their contributions towards the implementation of apparatus are truly crucial and appreciated.

I wish also to acknowledge the help of fellow graduate student Ali Alousi. In addition to the *Encyclopedia Alousica*, our lab is priviledged to possess the "Alousian Gauntlet," through which no unsound hypothesis (scientific or otherwise) can successfully pass. To Claude Pruneau, fellow patron of *McGill Pizza* and *Basha*, I render thanks for translation services rendered. I would like to thank all the lab members for making the place, at most times, a fun place to work.

I am indebted to Judith Marshall Cicon of *Vernon Rentals and Leasing* in Vancouver as well as Vaughn Denis and Barbara Morrison of *Greyvest Financial Services* for integrating me into their office and pool of computing assets during the summer of 1991.

I thank Stan Judek for the loan of the six degree-of-freedom acoustic resonator used for re-calibration after the experiments and data analysis and the following cast of characters for making life livable: Jehan Alain, Ralph Vaughan Williams, the McGill Faculty of Music, the "La Bamba" Redshift Blues Band, "So Sweet" Honeypot and "One Chance" Pearlfishers; Ross "OK, just *one* more beer" Thomson;† Geoff "OK, but *only* one beer" Soga;† Ian "walkin' through my window" Graham;† Steve "Brother!...Food!" Brauer;† Lou "educating Rita" Davey; Barbmeister "get me to the train on time" Roy; Stella "1.0" Laleff; Ute "eat that or you take it home" Moore; Philipp "string theory" Moore; Voytek "IF wammy THEN GOTO" Bandrowski; Darin "Dave, loook" Marshall; Mary-Ellen "could be done" Edwards; Steve "fancy a pint?" Rochefort; Michèle "what have I done, now?" McLaughlin; and Mrs. "off the balcony" Wag.

Finally, I've got to thank my Mom and Dad. During the latter stages of this work, I had to take something of a leave of absence to get myself serviced and recalibrated. The good old parental units provided just the right nurturing atmosphere of worry-free living and drinking which helped pull me through. Living with your parents when you turn 30 years old *can* be a great experience.

† Charter members of the Pathetic Losers Club, of which I am also one.

CHAPTER 1: INTRODUCTION

> As we jog on, either laugh with me, or at me, or in short do anything,- only keep your temper!
>
> *Tristram Shandy* by Laurence Stern

A: ION TRAPS AND THEIR USES

Late in 1989, a small community of scientists were elated to hear that the recipients of the Nobel prize for physics included Wolfgang Paul and Hans Dehmelt, respectively, the creator and preserver of the quadrupole ion trap. This same community, of which the author and his supervisor have become members, has been employing these interesting devices in a wide variety of fascinating applications since the seminal work of Paul and Dehmelt.

By containing a cloud of ions in free space, the ion trap provides an excellent, if not the ultimate, environment for perturbation-free observation. Ion traps can store isolated particles, even a solitary particle, for long durations and thus, in accordance with Heisenberg's uncertainty principle, enable the measurement of their properties with high accuracy.

The ion trap evolved from Paul's work in molecular-beam physics, mass spectrometry and particle accelerator physics in 1950-1955 at Bonn University where he used electric and magnetic fields to focus charged particles in two dimensions. From this work came the quadrupole mass filter in 1953 [PST], a two-dimensional, *path stability* mass analyzer that allows axial transmission of only a chosen charge to mass ratio. By extending this idea to three dimensions the ion trap was born. The trap is first discussed in the thesis of Berkling [BER] in 1956 and later by Fischer [FIS] in 1959 who demonstrated its use as a mass spectrometer. Paul gives an excellent account of the invention of the *Paul* trap, as it is now called, in his Nobel prize acceptance speech [PAU].

The trapping principle hinges on a quadrupole electric field which focuses in one dimension while defocusing in the other. The trap itself consists of a ring electrode with endcap electrodes on either side. The electrodes set up a net restoring force on charged particles towards the trap center. The Paul trap works at radiofrequency, changing the polarity of the field to restore an ion alternately along the radial and axial directions. There is a static brother of the Paul trap, the *Penning* trap, which employs the same geometry but with an axial magnetic field and a DC radial electric field used to contain the ions. This trap is an embodiment of the electric discharge containment principle developed by Penning [PEN] which is used extensively in vacuum gauge technology. Ion traps are generally constructed with volumes of a few cubic centimeters and can hold up to about a million ions for a few seconds depending on the vacuum. Single-ion traps are typically cubic millimeters in volume and can hold ions essentially in perpetuity. A detailed description of traps is given in chapter 2.

The pioneering physics experiment using a Paul trap was performed by Schuessler *et al.* [SFD] in 1969 by measuring the ground-state hyperfine splitting of $^3He^+$ twenty times more accurately than before. Dehmelt [DEHb] gives an excellent review of this, and other such experiments, as well as a comprehensive description of ion traps. Since then, the applications involving ion traps have taken two broad paths: mass spectrometry and precision measurements.

Mass spectrometry using ion traps and mass filters has seen enormous development by chemists for such applications as ion/molecule kinetics, reaction rates and photodissociation of ions. Traps have been operated with very high mass resolution and mass range which makes the study of extremely heavy and complicated molecules possible. March and Hughes [MHU] give an excellent review of these applications, and traps in general, in their recent book. An earlier book edited by Dawson [DAW] also chronicles the extensive contributions of the chemistry community to ion trap development and mass spectrometry.

Dehmelt, working at the University of Washington, continues to be a giant in the field of precision measurements with ion traps. In his Nobel prize acceptance speech [DEHa] he describes the "metastable pseudo-atom geonium" which is an individual electron permanently confined in a Penning trap so that it is bound to the earth by the trap potential. Using the geonium atom, the electron gyromagnetic ratio (g-factor) was measured with an accuracy almost 900 times greater than previous experiments [VSDa]. This measurement has far reaching theoretical consequences in determining if the electron is indeed a Dirac point particle or whether it has constituents. More recent measurements made on both the electron and the antielectron [VSDb] have made these g-factors the best known fundamental constants and have provided the most stringent test of charge-parity-time (CPT) invariance for a charged particle pair. Further Penning trap geonium experiments include the observation of relativistic cyclotron motion hysteresis during which the electron was trapped for 10 months [GDK]. A geonium review has been published by Brown and Gabrielse [BGA].

Using a Penning trap, Gabrielse *et al.* [GFO] have now measured the inertial mass of the antiproton a thousand times more accurately than before. This measurement, with its comparison to that of the proton, has provided the most stringent CPT test using baryons.

Another precision mass measurement program has been undertaken by Juergen Kluge's group at Mainz who are collecting long sequences of radioisotopes from the ISOLDE mass separator at CERN into a Penning trap system where the masses are measured by ion cyclotron resonance. Recent results of this work [SBB] were obtained with a resolving power of 10^6 and an accuracy of about 10^{-7}. Details of the experiment are given by Becker *et al.* [BBK].

Spectroscopy in ion traps has been developed to a phenomenal extent using both Paul and Penning traps. Paul traps offer ease of construction over Penning traps as no magnetic field is required. However, due to the large variation in velocity caused by the RF field, ions in Paul

traps exhibit large Doppler shifts that must be eliminated for spectroscopic work. The easiest remedy is buffer-gas cooling [MDE] in which the ions lose energy in collisions with light, neutral, background gas atoms. Günther Werth, working with Paul traps at Mainz University, has made a number of optical and microwave hyperfine structure measurements to accuracies of 10^{-9} for ion temperatures of about 1000° K [WERa, WERb]. This is close to the best accuracy possible with buffer-gas cooling due to the relativistic second-order Doppler shift.

Large ion clouds in Paul traps are subject to a process called RF heating which places a limit on the ion temperature. Furthermore, small buffer-gas cooled clouds cannot reach temperatures lower than the room temperature of the gas. A further reduction in ion temperature can be achieved using the dramatic method of laser cooling first proposed by Wineland and Dehmelt [WDE] and Hänsch and Schawlow [HSH]. By absorbing resonant laser light along one axis, ions generally lose kinetic energy on re-emission because the recoil direction is isotropic. Temperatures of mK are usual for laser cooling in a trap and the lowest temperature yet achieved is 47 μK [DFI]. While laser cooling offers the ultimate in ion refrigeration, the technique is severely limited to ions having a suitable, laser-accessible transition.

The advent of laser cooling brought about several intriguing observations using ion traps. The first of these was the trapping of a single ion by Dehmelt and colleagues [NHTc] in 1980 and Wineland and Itano [WITa] in 1981. This single-ion work has produced intense activity towards the development of new frequency standards due to the superior accuracy afforded by spectroscopic single-ion measurements. David Wineland, at the National Institute of Standards and Technology (NIST), has contributed extensively to this field and has provided a review [WIN]. Recent work by his group has produced a time standard of 10^{-13} accuracy [BHI]. Similar accuracy has been achieved by another group at Jet Propulsion Laboratories [PDM].

A beautiful consequence of storing a single ion is the observation of quantum jumps: the fluorescense produced when an atomic electron jumps from an excited state to a lower energy state. These fundamental entities of quantum mechanics have never before been witnessed in isolation. Recent contributors to this field include Dehmelt's group [NSD], Wineland's group [BHU] Toschek's group in Hamburg [SBN] and Walter's group in Munich [DWA]. A review of quantum jump observations is provided by Blatt and Zoller [BZO].

Laser cooling has also enabled the observation of stored ionic crystals the patterns of which are determined by the balance of the Coulomb force between the ions and the trap potential. In 1959, Wuerker *et al.* [WSL] published photographs of aluminum microparticles tracing out Lissajou trajectories in a Paul trap. When they added more particles, the cloud condensed into an ordered array. Only recently has this work again been explored. Due to RF heating, only a few ions (2-50) can form crystals in a Paul trap [DPC]. However, in a Penning trap thousands of

ions can be observed and cooled into a microplasma [GBW]. Microplasma work has interesting ramifications in the field of phase transitions and chaos [HDR].

Long term storage of single ions has also provided excellent measurements of metastable state lifetimes that cannot be studied in any other environment due to their long duration (up to seconds). Knight has reviewed these measurements in [VSK].

A number of popular articles have appeared concerning various aspects of ion trapping. An article in *Scientific American* by Ekstom and Wineland [EWI] discusses the g-factor of the electron. Another *Scientific American* article by Bollinger and Wineland [BWI] contains some nice pictures of microplasmas in traps. Richard Thompson has written a trapping article in *New Scientist* [THOa] as well as an excellent technical review [THOb]. Two more technical but general articles have appeared in *Physics Today* by Wineland and Itano [WITb] on laser cooling and by Walls and Dunn [WDU] on ion storage. The excellent *Search and Discovery* section of *Physics Today* also reports on some trapping milestones [SAD]. NIST has produced an awesome image-intensified video of a single ion, blinking with quantum jumps†, as well as some ionic crystals in both Paul and Penning traps. Dehmelt, ever the philosopher, has just given a banquet speech at the recent Interdisciplinary Laser Science Conference [ILS] entitled: *"That I may know the inmost force that binds the world and guides its course!"* His concluding section, an elegant summary of what ion traps offer, was subtitled: *"The simplest thing that ever was."*

B: PURPOSE OF THESIS

At McGill, work involving ion traps has progressed along a different avenue. Far from the world of single-ion traps, the McGill ion trap is being developed to store as many ions as possible. This inclination stems from research on properties of radioactive nuclei. In particular, two types of experiments which require short-lived radioisotopes stand limited by their lack of sensitivity to low yields of such isotopes: the Penning trap nuclear mass measurements mentioned above [SBB, BBK] and the study of nuclear ground state properties using collinear laser spectroscopy [NEU]. What is lacking is a universal, clean and efficient device for collecting weak radioactive beams and then delivering the ions to the apparatus all at once. When a radioisotope yield (number of ions per second) drops below a certain threshold, not enough signal can be observed due to the background. If all, or some critical fraction of this signal can be concentrated into a smaller observation time, then the background is reduced relative to the signal. If an ion trap could collect some weak radioactive beam and then deliver it all in one short pulse, the sensitivity of experiments measuring the properties of this radionuclide could then be improved. A simple analogy of this idea is illustrated in figure 1-1. The potential for such beam

† The blinking is actually produced when the ion is excited into a non-radiative, metastable state.

collection is encouraging: Moore *et al.* [MLR] have presented arguments which indicate possible compression factors approaching a million. Many techniques have been developed which offer enhancement by only a factor of two in sensitivity. These techniques are usually element specific also. Therefore, the collection potential of the ion trap invites serious investigation.

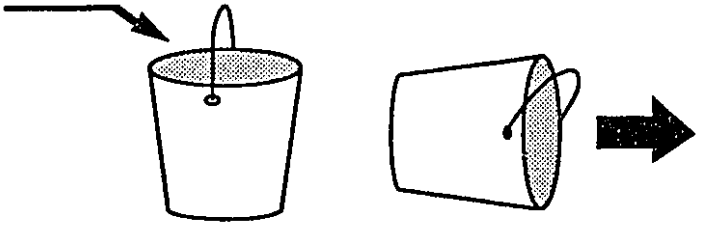

Figure 1-1: Simple analogy of the beam bunching process.

The continuous ion beam must be transformed into a pulsed beam, ideally without losing anything. This is called beam *bunching* as opposed to beam *pulsing* or *chopping* in which the yield is reduced according to the duty factor of the chopper. Efficient beam bunching requires meticulous engineering as dynamic manipulation of the beam is required. This requirement moves the ion trap from the table-tops of small labs to the beam-halls of large radioactive beam facilities and into the realm of the accelerator engineer where beamlines would be designed to include ion trap beam-collection stages and pulsed beam transport regions.†

Professor Robert Moore first envisioned a beam bunching trap several years ago. Since then, in spite of numerous technical problems, some major progress has been made. The problem has been approached from two directions: ion injection and ion extraction. The injection work started in 1985 with the Masters projects of the author [LUN] and Sid Gulick [GUL]. Gulick went on to produce a prototype bunching system [MGU]. Gary Rouleau continued the injection work for his doctoral thesis [ROU] and recently succeeded in capturing 60 kV ISOLDE beams of positive and negative ions with relatively good efficiency [MRO]. High efficiency is critical as we cannot afford to throw away any of these exceedingly rare radionuclides in the accumulation process.

The most crucial function of a successful beam collector is the ability to cool the beam once inside the trap. Just as the contents of a vessel must be settled to incorporate larger amounts, ions in a trap must also be settled, or cooled so that more ions can fit into the available storage

† Though the term beam *pulse* continues to be used, it is done so, synonymously with the term *bunch*, to indicate a collection of cooled ions extracted from a trap.

volume of the trap. Due to the large numbers of ions involved, the only practical cooling mechanism for such a beam buncher is buffer gas cooling.

Finally, the extracted beam must be extensively studied to ensure that it is suitable for delivery to other apparatus. Because the transport of the ion bunch is affected by its energy and spatial distributions, it is important to study these quantities in detail. For example, as an ion bunch drifts, its length, or time duration, changes in proportion to its velocity spread, or energy spread. If this bunch is to be transported to another trap, as in the mass measurement experiment, the bunch duration must be known in order to know how long to open the other trap. Since the study of the extracted beam requires knowledge of the ion cloud before extraction, it is the dynamics of trapped ion clouds that forms the subject of this thesis.

Previous studies of extracted ion beams have been quite inconclusive and rather incomplete. Extracted ions were first observed in 1974 by Dawson and Whetton [DWE] who concluded that the extraction process was "complex" and depended on the extraction amplitude and RF phase at extraction. More systematic measurements were made in 1979 by Waldren and Todd [WTO] varying extraction amplitude, width and RF phase. Again, these results are largely empirical with no information derived about the energy or time distributions. More recently (1987), time-of-flight studies by Mosburg *et al.* [MVZ], were reported that attempted to model the measured time distribution. However, their techniques were not refined enough to extract any information about the initial ion distributions. Champeau *et al.* [CCL] reported time-of-flight measurements in 1990 but were unable to determine the initial ion conditions. Brincourt *et al.* [BCZ] also reported time-of-flight measurements in 1990 but were only able to measure the collective ion oscillation frequency. Measurements of extracted ion kinetic energies were reported by Reiser *et al.* [RKS] in 1991 but yielded no insight into the trapped ion dynamics.

Further analysis of ion dynamics has been made using a method of ion extraction known as "ion tickling". A small driving frequency is applied to one, or both, endcaps that resonantly excites the collective motion of a particular ion mass eventually ejecting those ions from the trap. This method is used in analytical chemistry where several masses can be present in the trap. Tickling is also used for studying molecular collisional fragmentation by increasing the kinetic energy of the trapped ions. These techniques are reviewed by March and Hughes [MHU]. Ion tickling is not suitable for our purposes as the ions are extracted over a very long time period. This not only defeats the purpose of a beam buncher but can cause undesirable coupling between ion motions in each dimension.

In situ spectroscopic measurements on trapped ion clouds have been performed by several researchers with various results which are discussed in detail in chapter 4. The main premise in all of this work is that the concept of an ion temperature can be introduced which defines the spatial and velocity distributions of the ion cloud. However, much of this work does not actually

concern the temperature but the average kinetic energy and the relation between these quantities has not been well resolved in the literature. Overall, the published results are quite wide-ranging and consequently, there is a great deal of uncertainty regarding the temperature of ion clouds in Paul traps, particularly for small numbers of ions. This uncertainty carries over to the dynamics of an extracted beam which is important for the engineering of beam transport systems in which Paul traps are to be used as beam collectors.

The dynamics of the extracted beam are embodied in a description known as *phase space* which is comprised of two entities related to the beam velocity and displacement. The main problem in studying the spatial and momentum distributions of extracted ion clouds is that these distributions are folded together and it is extremely difficult to separate them.

The phase space volume of the beam contains all the information required to perform the engineering exercise of manipulating it for use by other apparatus. This quantity is determined by the original phase space volume of the ions inside the trap before extraction. The extraction process does not increase or decrease the phase space volume of the ion cloud but only modifies its different projections in energy and time. Two things must be therefore be known: the extraction mechanism and the initial phase space volume.

The extraction process is fairly easy to study as computing the ion dynamics through a well-defined transport system is relatively straightforward. It is the determination of the initial spatial and momentum distributions of the ion cloud that becomes the focal point of these investigations.

To completely map out the phase space of the extracted ion beam, a series of energy retardation measurements would have to be performed for each time slice of the beam pulse. Sampling these distributions is nearly impossible due to the extremely short time intervals with which ions are extracted. Furthermore, ion bunches are extracted from the trap with large momentum spreads that cause rapid diffusion of the bunch. This makes energy-analyzing measurements very difficult. In general, the time distribution can be measured with far greater accuracy that the energy distribution. The approach taken in this work, therefore, is to vary the extraction parameters and measure the time distribution under many different conditions. In this way, some information regarding the overall phase space projections may be gleaned.

Another way of probing the extracted beam is to use laser spectroscopy. By directing the laser beam collinearly with the extracted ion beam and scanning the laser frequency, a measurement of the velocity profile of the ion beam can, in principle, be obtained. This was actually the original intent of this project and considerable effort was expended to achieve this end. However, since the velocity spread of the extracted beam is so great, the resonance was broadened beyond detection sensitivity. A short synopsis of this work is given in Appendix 1. While not successful, these laser spectroscopy results are included to illustrate the nature of the problem and as a guide for further work in this area.

C: CONTRIBUTIONS OF THESIS

This thesis describes work in which a model was developed that computes the dynamics of stored, extracted and transported ion distributions. The model is based on phase space arguments and statistical mechanics so that an extracted-ion time distribution is computed based on spatial and momentum distributions that are governed by a chosen ion temperature. The temperature of the cloud is deduced from the best fit to the measured time distributions of the ion cloud after extraction from the trap under various systematic conditions.

The results which follow represent the first such measurement of the temperature of a trapped ion cloud. Ion temperature was measured as a function of trap loading down to the lowest number that could be detected (corresponding to about 1000 trapped ions) for two different ion masses and was found to be quite low, especially for small numbers of ions. The low temperatures considerably ease the engineering requirements for transporting the extracted beams to other apparatus. The ion temperatures were found to vary in proportion to the two-thirds power of the number of ions. Most other researchers have tended to measure ion temperature as a function of trap parameters keeping the ion number constant. The low ion number temperature measurements are the first for ions cooled by buffer gas.

A new mathematical model was developed for this work which incorporates a Gibbs distribution applied to the phase space density of a trapped ion cloud. This model is combined with a general numerical integration algorithm, also developed for this work, offering a powerful engineering tool for dynamic, ion-optics systems. This is important as existing beam optics codes generally do not handle time-varying fields. A new numerical method was developed to calculate the non-analytical ion trap extraction field based on a multipole expansion. This method was the subject of a publication which is included in the thesis as Appendix 2.

The first experimental evidence of the dynamic manipulation of the extracted ion beam phase space is also presented in this work. This result has far-reaching consequences for the use of Paul traps as beam bunchers.

Another way of interpreting the measured time distribution of the extracted ion beam is to view it as a one-dimensional projection of the initial phase space volume. A favorable consequence of performing detailed (brute force) calculation of the ion dynamics is that this single projection can be mapped back to the initial phase space volume. Many such projections can be obtained for different extraction and transport conditions and the orientation of the projection in the original phase space can be determined. This situation is analogous to the problem of reconstructing a two-dimensional image from a set of one-dimensional projectional

views. The best known example of this problem is non-invasive imaging of the brain by CAT† scan. Though conceived during the progression of this work, the idea was not pursued for the purpose of this thesis. However, it does offer extremely interesting possibilities for determination of phase space volumes of beams. Therefore, the idea for reconstruction of the phase space density from multiple time projections is presented in Appendix 3.

The major original contributions of this thesis are summarized here in point form:

- A new method for determining the spatial and momentum distributions of a trapped ion cloud has been developed that is based on extracting the ions and measuring the time-of-flight for various extraction conditions.
- A theoretical model has been formulated based on phase space arguments that describes the spatial and momentum distributions of trapped ion clouds by a temperature.
- New results for the temperature of ion clouds are presented for small numbers of ions. A systematic trend of the temperature versus trap loading has been identified and explanations presented over a greater range of trap loadings than previously published.

In addition, the following minor original contributions originating from this work are:

- A new combination of numerical applications has been developed for computing electric fields based on a multipole expansion for use in integration of charged particle motion .
- The dynamic manipulation of the phase space projection of an extracted ion cloud has been performed using a time-varying voltage in order to reduce its energy spread.
- A new idea for the determination of detailed phase space projections has been presented based on the tomographic reconstruction of images from multiple angular projections.

†Computerized Axial Tomography. A tomograph is an image of a two-dimensional slice (*tomos*) which is reconstructed from multiple projections around the central axis normal to the slice.

CHAPTER 2: THEORY

> You may have, sir, a good reason for saying that two and two make five,
> But they still make four.
>
> Samuel Johnson

A: QUADRUPOLE ION TRAPS

A heuristic introduction to ion traps comes directly from the equation for the quadrupole potential Φ:

$$\Phi = \Phi_o (ax^2 + by^2 + cz^2) \tag{2-1}$$

where a,b and c are constants. This equation tells us that the potential is uncoupled in each dimension, is zero at the origin and increases with distance from the origin. When this potential is subjected to the Laplace equation ($\nabla^2\Phi = 0$):

$$a + b + c = 0 \tag{2-2}$$

For the ion trap potential, we use cylindrical coordinates and set $a = b = \alpha$ and $c = -2\alpha$ to obtain:

$$\Phi = \frac{\alpha}{2}(r^2 - 2z^2) \tag{2-3}$$

where $\alpha = \Phi_o/r_o^2$. The electric field components are (from $\boldsymbol{E} = -\nabla\Phi$):

$$E_r = -\alpha r \tag{2-4a}$$
$$E_\theta = 0 \tag{2-4b}$$
$$E_z = 2\alpha z \tag{2-4c}$$

The corresponding electrode configuration for the ion trap is shown in figure 2-1. It consists of a ring electrode, with radius r_o, between two endcap electrodes, with spacing $2z_o$. All three electrodes are rotationally symmetric about the z-axis with hyperbolic cross-sections following:

$$\frac{r^2}{r_o^2} - \frac{z^2}{z_o^2} = \pm 1 \tag{2-5}$$

where the right hand side of the equation is negative for the ring and positive for the endcaps. The ratio of r_o^2 to z_o^2 is 2 for hyperbolic electrodes forming a pure quadrupole field. Knight [KNI] has explored other electrode manifestations for ion confinement.

In order to contain ions, a potential $\Phi_o = U + V\cos\Omega t$ is applied between the ring and endcaps as shown in figure 2-1. This potential restores the ions towards the trap center along the radial and axial directions alternately. The trap is tuned for a particular mass by selection of the applied voltage and frequency. This dynamic, mass selective instrument bears the name of its creator, Wolfgang Paul. Penning traps use the same electrode configuration but, unlike Paul traps, operate in a static environment. A DC voltage between the ring and endcaps of the Penning trap contains ions in the axial direction and a static, axial magnetic field accomplishes this in the radial direction by constraining particle motion to small helical paths about the z-axis.

The above equations indicate how a charged particle may be confined in space. The quadrupole potential accomplishes this in the most simple way. A dipole only acts along one axis and it is practically impossible to combine dipoles in any way to confine ions in three dimensions. Higher order approaches (sextupole, octupole, etc.,) are possible but the electrode manifestations become quite unwieldy. Furthermore, they introduce aberrations. Other trapping implementations have been discussed by Todd *et al.* [TLA]. Alternate forms of applied potential have also been addressed by Richards *et al.* [RHH].

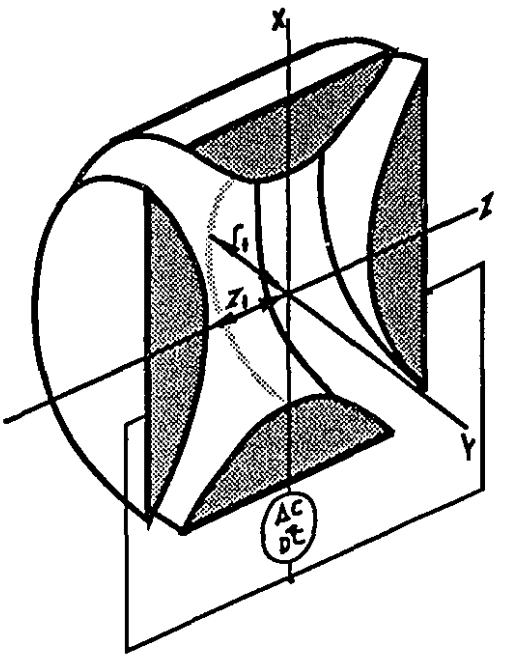

Figure 2-1: Cross-sectional view of a Paul trap. The potential is applied between the ring and endcap electrodes as shown. It is also possible to operate the trap with the endcaps grounded.

Description of the ion motion in traps is initiated with the Lorentz equation:

$$F = e[v \times B + E] \qquad (2\text{-}6)$$

where F is the force acting on a particle of mass m, charge e, velocity v, in a magnetic field B and electric field E. The motion of this particle is then determined from Newton's law ($\mathbf{F} = m\mathbf{a}$). We are concerned with the axial component of motion in a Paul trap (within which B is zero):

$$eE_z = m\frac{d^2z}{dt^2} \tag{2-7}$$

Substituting equation 2-4c and rearranging yields:

$$\frac{d^2z}{dt^2} - \frac{e}{mz_0^2}(U + V\cos\Omega t)\,z = 0 \tag{2-8a}$$

which is a differential equation of the Mathieu† type that has the canonical form:

$$\frac{d^2z}{d\xi^2} - (a_z + 2q_z\cos\Omega t)\,z = 0 \tag{2-8b}$$

having substituted $\xi = \Omega t/2$ and made the following additional change of variables:

$$a_z = \frac{4eU}{mz_0^2\Omega^2} \qquad q_z = \frac{2eV}{mz_0^2\Omega^2} \tag{2-9}$$

These two dimensionless, governing parameters of the Mathieu equation, called the *Mathieu parameters*, combine the operating parameters of the trap. The relationships to the corresponding Mathieu parameters in the radial dimension are: $a_r = -a_z/2$ and $q_r = -q_z/2$ which follow from the Laplace equation. General solutions to the Mathieu equation take the form of an infinite trigonometric series which represents a frequency spectrum of trapped ion motion.§

The actual motion that is represented by this spectrum is characterized by a fundamental oscillation, known as *macromotion*, which is modulated by the RF, or *micromotion*. In an ideal quadrupole field the radial and axial ion motions are uncoupled. The ratio of macro- to micromotion frequencies in each dimension is determined by the so-called β parameter that is defined by:

---

† after the French mathematical physicist Émile Léonard Mathieu (1835-1890) who developed the equation and functions bearing his name for the solution of elliptical membrane motion in 1868. The Mathieu equation is a special case of the Hill equation, developed later by the American mathematician Gordon William Hill (1838-1914) in 1877 for the description of the motion of the lunar perigree. The Hill equation uses functions that are periodic but not necessarily sinusoidal.

§ Volumes have been written about the solution to the Mathieu equation [DAW, LTB, MHU] so there is no need to enlarge upon the subject here. In any case, chapter 3 describes how the equations of motion were solved numerically in this work.

$$\beta_{r;z} = 2\frac{\omega_{r;z}}{\Omega} \tag{2-10}$$

The β term is generally a tortuous, recursive function of the Mathieu parameters but can be approximated (for $q < 0.5$) by:

$$\beta = \sqrt{a + \frac{q^2}{2}} \tag{2-11}$$

Ions oscillating at characteristic frequencies in each dimension can be described as bound by a pseudopotential well D, described by:

$$D(r,z) = \frac{1}{2} m \left(\omega_r^2 r^2 + \omega_z^2 z^2\right) \tag{2-12}$$

The well depths in each dimension are designated as follows: $D_r = D(r = r_o, z = 0)$ and $D_z = D(r = 0, z = z_o)$. In general, this well is ellipsoidal but can be made spherical by judicious choice of a and q such that the macromotion frequencies are the same in each dimension, or $\omega_r = \omega_z$. In this case, from equation 2-12, the total depths in each dimension (at r_o and z_o, respectively) will be such that $D_r = 2D_z$ since $r_o^2 = 2z_o^2$. So the pseudopotential well distribution is controlled by the DC voltage for without it, $a = 0$, $D_r = \frac{1}{2} D_z$ and $\omega_r = \frac{1}{2} \omega_z$.

Stable solutions to the Mathieu equations in each dimension are superimposed to form an overall stability diagram, with a and q as axes, which is shown in figure 2-2. The boundaries are determined by the β parameters and β must fall between the values of zero and one in both radial and axial dimensions for stable (i.e., trapped) ion trajectories. The design of a Paul trap and its drive parameters is accomplished by selecting a target mass (or mass range) for a certain trap size and then computing a and q such that they fall inside the stability diagram. The choice of trap size is usually determined by the number of ions required because smaller traps have a smaller capacity. Sample operating parameter combinations are listed in table 2-1 with the corresponding Mathieu parameters, β's and well depths. The first entries give round number examples to illustrate the order of magnitudes of each parameter. Note that in cases where $\beta_r = \beta_z$ the well depths are such that $D_r = 2D_z$ (spherical well).

Figure 2-3 shows some examples of the axial motion of a ^{133}Cs ion inside a Paul trap computed by the simulation program described in chapter 3. Different values of β illustrate the relative components of macro- and micromotion. One example of an unstable solution is also shown. A kinetic energy plot accompanies the displacement plot for the case of $\beta = 0.4$ illustrating the enormous contribution and fluctuation of the micromotion component. The

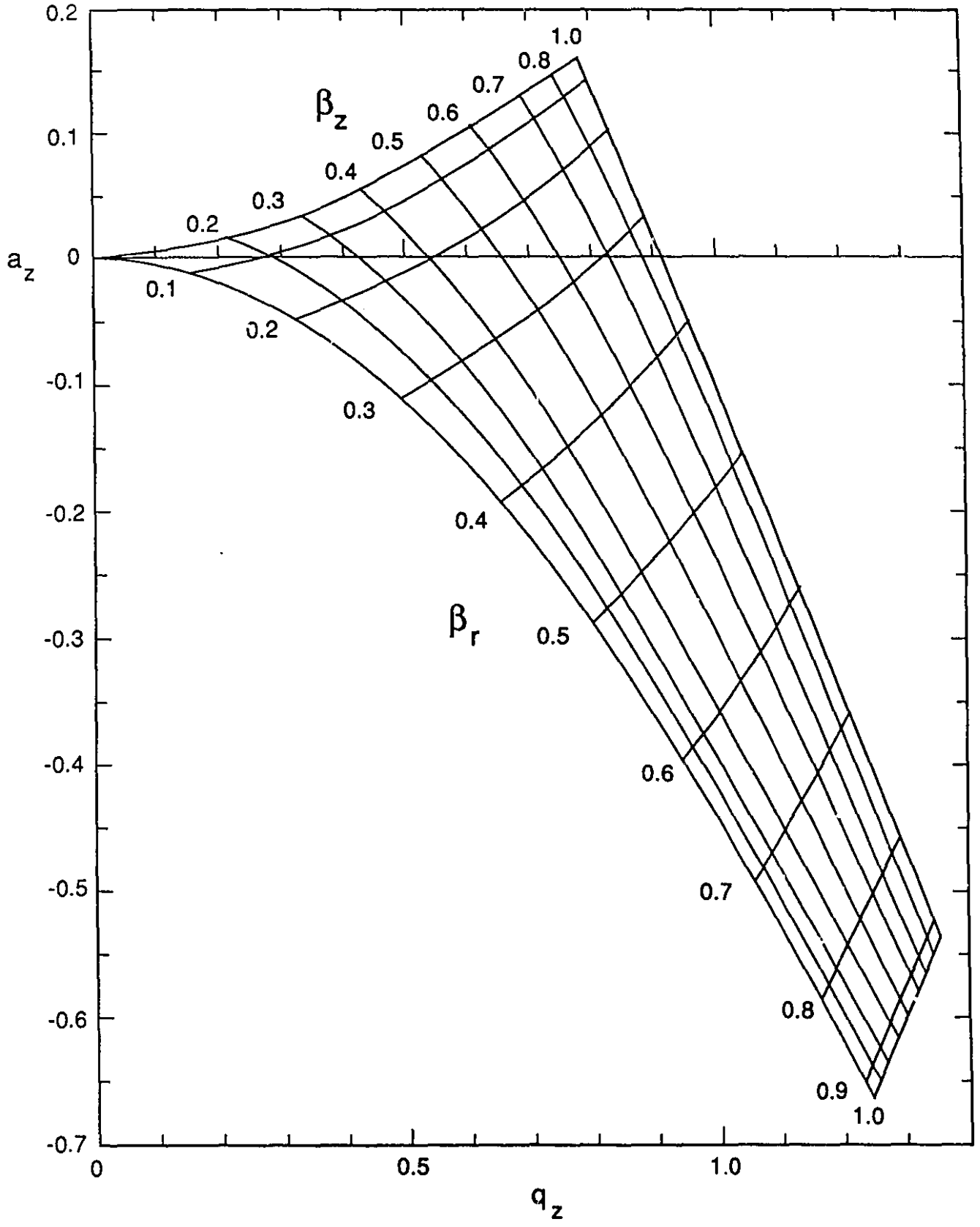

Figure 2-2: Mathieu stability diagram for the ion trap operating parameters. Iso-β lines for stable solutions to the Mathieu equation are plotted as a function of the Mathieu parameters, a and q for the axial dimension.

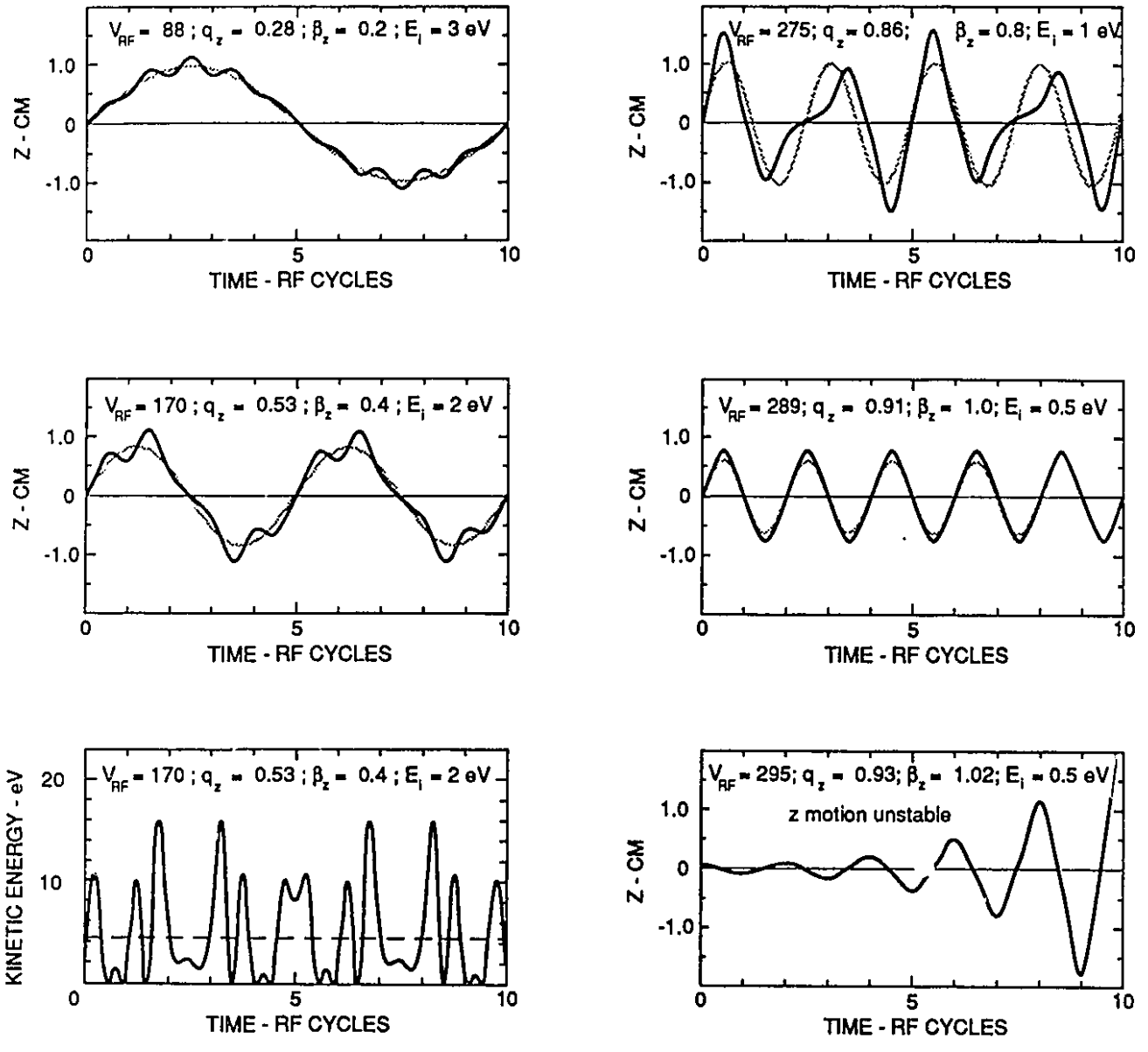

Figure 2-3: Different examples of axial ion motion inside a Paul trap. The endcap spacing is 28 mm and applied RF frequency is 238 kHz for a mass of 133 with no DC voltage ($a = 0$). The RF voltage, q, β, and initial ion energy are shown for each diagram. The shaded lines represent simple harmonic motion in the absence of RF micromotion for comparison. Also shown, at bottom left, is a plot of micromotion kinetic energy versus time for the trajectory immediately above it. The kinetic energy associated with the macromotion is shown as a dotted line. These motions were computed by the simulation program described in chapter 3.

energy contained in the macromotion is plotted as a dotted line. This energy is simply the kinetic energy of a harmonic oscillator given by equation 2-29.

Table 2-1: Various combinations of Paul trap operating parameters and the corresponding Mathieu parameters. Also tabulated are the stability parameter β and the well depth D in each coordinate. Note: $q_z = -2q_r$ and $a_z = -2a_r$.

m (amu)	z_o (mm)	U (V)	V (V)	Ω (kHz)	a_z	q_z	β_r	β_z	D_r (eV)	D_z (eV)
100	10	0	1000	1000	0	0.50	0.18	0.36	30	60
100	10	30	1000	1000	-0.03	0.50	0.20	0.30	45	45
100	10	60	1000	1000	-0.06	0.50	0.25	0.25	60	30
39	14	0	200	650	0	0.30	0.11	0.22	4	8
39	14	-6	200	650	0.02	0.30	0.05	0.25	1	10
39	14	8	200	650	-0.02	0.30	0.15	0.15	8	4
23	14	0	200	650	0	0.50	0.18	0.36	6	12
23	14	0	400	920	0	0.50	0.18	0.36	12	24
23	1.4	0	115	5000	0	0.50	0.18	0.36	4	8
23	14	0	300	650	0	†0.72	0.30	0.60	19	38
39	14	0	500	650	0	†0.72	0.30	0.60	32	64

† note for $q > 0.5$ the approximate solution (equation 2-10) gives: $\beta_r = 0.25$ and $\beta_z = 0.50$

An important consequence of the quadrupole field is the independence of the radial and axial dimensions which leads to uncoupled motion in the trap so that ions trace out Lissajous-like trajectories. It is this uncoupled characteristic which allows the use of the Mathieu equation to describe the ion motion. However, if the trapping field is not a perfect quadrupole, higher order components contribute mixed terms to the equation which couples the motion of the two dimensions. For example, the sextupole potential contains a mixed r and z term:

$$\Phi = \frac{a}{2}(3r^2z - 2z^3) \qquad (2\text{-}13)$$

In this instance the Mathieu equation is no longer valid and ion motion must be calculated numerically. The introduction of higher order multipoles can result from electrode misalignment, deviation of the electrode shape from hyperbolic form and holes in the electrodes. The trap used for this work has been analyzed using a finite element procedure [LWM] and found not to deviate significantly from a pure quadrupole. However, the extraction of ions from the trap is accomplished by applying a pulse to one of the endcap electrodes. Since there is no closed form for such a potential, a multipole expression was constructed to provide the electric field contribution to equation 2-6. The details of this technique have been published by the author [LMO]. This reference is appended to the thesis.

B: PHASE SPACE VOLUME

We have shown that ions oscillate periodically inside the Paul trap and now make the assumption that trapped ion dynamics may be sufficiently approximated by the simple harmonic oscillator macromotion. The effects of the RF micromotion are discussed later. The state of motion of an oscillator at time, t is completely specified if two quantities: displacement, x(t) and velocity, $\dot{x}(t)$* are known. Since the Lorentz equation (2-6) is *second* order, *two* quantities are needed. These quantites are considered to be the two coordinates of a point in *phase space*, $(x,\dot{x})$. For a Paul trap with three degrees of freedom, the phase space is, therefore, six dimensional. For different initial conditions, the oscillator motion is described in time by different phase paths. The totality of all possible phase paths constitutes the *phase space volume.*

Mathematical description of the collection and manipulation of ion beams can only be accomplished in the context of phase space because all the laws regarding this manipulation are derived from phase space arguments. The concept of phase space is elegantly derived from the equations of Hamiltonian† mechanics (shown here in canonical form):

$$\dot{q}_i = \frac{\partial H}{\partial p_i} \qquad (2\text{-}14a)$$

$$\dot{p}_i = -\frac{\partial H}{\partial q_i} \qquad (2\text{-}14b)$$

where q is the *generalized position*, p the *generalized momentum* and H the *Hamiltonian*, or total energy of the *collection* of particles, i = 1,2,3... If, at a given instant of time, the initial positions and momenta of all the particles in a collection are known, then the subsequent motion of the collection is completely determined.‡

Returning to the oscillator§ model for trapped ions, we can define (as functions of time) the axial position $z(t)$ and momentum $p_z(t)$ of an ion of mass m, oscillating in the trap at amplitude A, with frequency ω, as:

$$z(t) = A\cos\omega t \qquad (2\text{-}15)$$

$$p_z(t) = m\dot{z}(t) = -m\omega A\sin\omega t \qquad (2\text{-}16)$$

---

* We now adopt the convention of representing the first derivative with time of, for example, x, by $\dot{x}$.

† after Sir William Rowan Hamilton (1805-1865), Scottish mathematician and astronomer who first derived the equations in 1834 from a variational principle and made them the basis for a far-reaching theory of dynamics.

‡ An excellent discussion of Hamiltonian mechanics and phase space is presented by Marion [MAR]. Another good reference is Goldstein [GOL].

§ Phase space considerations are by no means restricted to oscillating systems.

Eliminating t from these equations gives:

$$\frac{z^2}{A^2} + \frac{p_z^2}{m^2\omega^2 A^2} = 1 \qquad (2\text{-}17)$$

This equation represents a family of ellipses which constitute the axial phase space of the trapped ion cloud as shown in figure 2-4. This area is the axial projection of the entire phase space volume. The angular motion around each ellipse, at frequency ω, is clockwise because when $z < 0$ the velocity is always increasing (and vice versa) as shown by equations 2-15 and 2-16. No two phase paths of the diagram can cross as the solution of the governing differential equation is unique for given initial conditions. The momentum axis can be scaled such that the maximum momentum $m\omega a$, corresponds to the maximum displacement a. This way the ellipses are conveniently represented as circles.

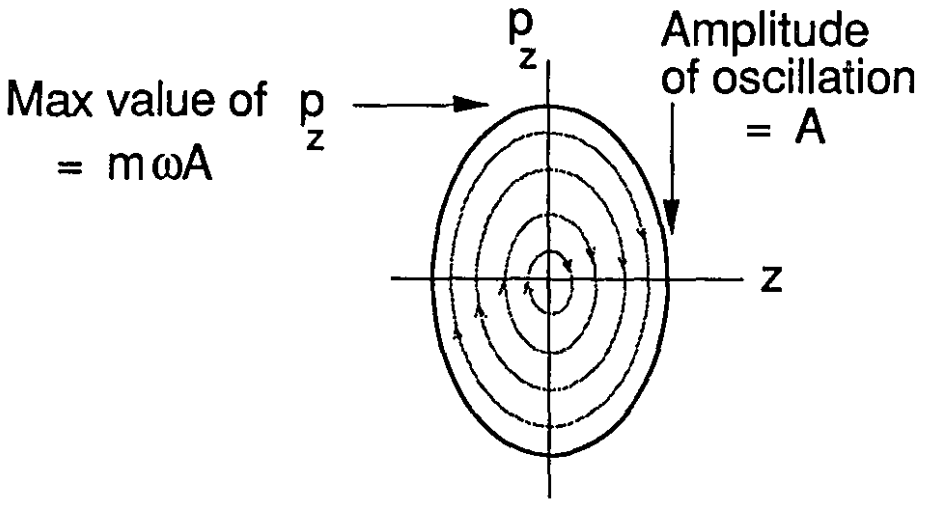

Figure 2-4: The family of ellipses constituting the axial phase space of an oscillating trapped ion cloud.

The total phase space volume S can be defined as the product of the phase space area in each dimension:

$$S = S_x S_y S_z = \int dx\, dp_x \quad \int dy\, dp_y \quad \int dz\, dp_z \qquad (2\text{-}18)$$

From beam optics comes an important quantity called *emittance*, ξ_u which is defined as:

$$\xi_u = \int \theta\, du \qquad (2\text{-}19)$$

where θ is the angle of the beam with the corresponding axis, or beam *divergence* and u is the corresponding spatial coordinate. Emittance is usually described by two components: transverse and longitudinal. An *emittance diagram* is generally used to characterize the transverse component of the beam. The emittance is plotted as $\dot{u}$ versus u so the emittance is the area represented by this phase space diagram. The emittance is related to the transverse phase space components by:

$$S_x = p_0 \xi_x \;\; ; \;\; S_y = p_0 \xi_y \qquad (2\text{-}20)$$

where p_0 is the central momentum of the beam.

For complex collections of numerous particles, such as an ion beam, it is clearly a practical impossiblility to determine the initial conditions for each constituent ion. Since we cannot identify any particular point in phase space as representing the actual conditions at any given time, we must turn to the field of *statistical mechanics* and introduce the representation of the ion collection by an *ensemble of systems*.†

The phase space is a collection of points where each point represents a particular system of the ensemble. Each system in an ensemble is comprised of any number of constituents *e.g.*, particles. The ensemble has a *phase space density* that determines the number of points inside an infinitesmal hypervolume element of the six-dimensional phase space. An important result from Hamiltonian mechanics is that the phase space density of the ensemble remains constant as it moves through phase space in time. This result is known as *Liouville's theorem*.§

The geometrical consequence of Liouville's theorem is that the phase space volume will behave like an incompressible liquid drop that, if squeezed one way, will bulge out the other conserving both the density and the volume. Furthermore, for linear forces acting on the ensemble (forces which do not couple the different motions) the various projections of the phase space volume, (p_x vs x, p_y vs y, p_z vs z) will also behave as incompressible areas. (For non-linear forces, coupling can occur between dimensions resulting in the projections changing area.) A similar theorem does not exist for three-dimensional configuration space.

An example of Liouville's theorem at work is illustrated by figure 2-5 (page 22). A phase space diagram representing the beam in the transverse direction is shown at position 1. As the beam drifts to position 2 at a constant momentum spread, the displacement spread increases but the overall phase space area is the same. When the beam goes through the lens, the phase space

† See, for example, Landau and Lifshitz [LLI].

§ Published in 1838 by the French mathematician Joseph Liouville (1809-1882). Liouville's theorem is proved and discussed at length by Goldstein [GOL], Marion [MAR] and Landau and Lifshitz [LLI].

diagram is transformed at position 3 resulting in an increased momentum spread for the same displacement spread but the area is still the same. When the beam reaches the focus at postion 4, it has the same momentum spread as position 3 but the beam width is dramatically reduced so as to conserve the overall area. This figure illustrates how a tight geometric focus can only come at the expense of a large spread in momentum because of Liouville's theorem.

For continuous beams, the longitudinal phase space component is often ignored. For pulsed beams, however, it assumes much greater importance. The longitudinal, or axial phase space area is expressed as:

$$S_z = \Delta p_z \, \Delta z \tag{2-21}$$

where Δz is the length of the beam pulse along the beam axis. The total phase space *volume* of such a beam is then given by the product of the transverse phase space components in equation 2-20 and the longitudinal component in equation 2-21.

In a trap, before considering the effect of the RF micromotion, the ions oscillate with simple harmonic motion. The axial phase space area for a Paul trap is therefore given by the area of figure 2-4 with $A = z_{max}$:

$$S_z = \pi m \, \omega_z \, z_{max}^2 \tag{2-22a}$$

Similarly, the transverse phase space areas are expressed as:

$$S_x = \pi m \, \omega_x \, x_{max}^2 \qquad S_y = \pi m \, \omega_y \, y_{max}^2 \tag{2-22b}$$

In the transverse plane of the ring electrode, $x_{max} = y_{max} = \frac{1}{\sqrt{2}} r_{max}$ and $\omega_x = \omega_y = \omega_r$ so that:

$$S_x \, S_y = \tfrac{1}{4} (\pi m)^2 \, \omega_r^2 \, r_{max}^4 \tag{2-23}$$

When the trap is operated with no DC voltage recall that $D_r = \frac{1}{2} D_z$ so that $\omega_r = \frac{1}{2} \omega_z$ and from equation (2-12): $r_{max} = \sqrt{2} z_{max}$. From equation 2-18 the trapped ion phase space *volume* is therefore given by:

$$S = S_x \, S_y \, S_z = (\pi m)^3 \, \omega_z^3 \, z_{max}^6 \tag{2-24}$$

Referring back to the Hamiltonian equations (2-14), the product of generalized position and momentum has the dimension of *action*. Such a dimension is also described by energy × time. Quantities yielding the dimension of action are said to be *canonically conjugate*. Another set of

generalized coordinates that are canonically conjugate is energy and time. Using these coordinates, the axial phase space area can be rewritten as:

$$S_z = \Delta p_z \Delta z = m\Delta v \; v \Delta t = \Delta E \, \Delta t \qquad (2\text{-}25)$$

A particularly useful unit for phase space is the eV-μs which equals 1.6×10^{-25} kg-m^2/s. The eV-μs is more manageable and better lends itself to phase space described according to equation 2-25. Lenses and voltage pedestals are always controlled by *voltage* and pulsed system operation is always controlled by *time* so the eV-μs is a more intuitive unit. The corresponding unit for momentum in this system is the eV-μs/mm from the relation $p = 2E/\omega a$.

If the frequency is expressed in MHz, the mass in atomic mass units and the amplitude in mm, the phase space volume in (eV-μs)^3 can be calculated using:

$$S = 0.0022 m^3 f_z^3 z_{max}^6 \qquad (2\text{-}26)$$

If the trap is not operated in zero-DC mode, the phase space components are computed using equations 2-22a and 2-22b and the phase space volume by multiplying these two results. A trapped ^{39}K ion cloud of radius 2 mm oscillating at 0.15 MHz would therefore have a kinetic energy of 0.72 eV, an axial momentum of 0.76 eV-μs/mm, an axial phase space component of 4.7 eV-μs and a phase space volume of 26 (eV-μs)^3. Some comparative phase space volumes are discussed in chapter 4.

The phase space volume is expressed in terms of emittances by:

$$S = 2 \times 10^{-7} m \; \xi_x \xi_y \; E \; \Delta E \; \Delta t \qquad (2\text{-}27)$$

where m is in atomic mass units, the emittances are expressed in π-mm-mrad, E is the central beam energy in eV, ΔE the energy spread in eV and Δt the time spread in μs.

In a Paul trap, the simple elliptical phase space diagram of figure 2-4 is distorted by the RF micromotion. While the RF micromotion is coherent and does not change the periodic collective oscillation of the ion cloud, it does dramatically distort its phase space. The effect of the RF field is to dynamically squeeze the phase space diagram (without changing its volume) and extend its displacement beyond the circular limit. Because the RF is coherent, the distortion repeats with each RF cycle. An example is shown in figure 2-6. Figure 2-6a shows the initial distortion at a particular RF phase of 0° superimposed on the original circular (scaled elliptical) phase space diagram. Figure 2-6b shows how the distortion behaves over one RF cycle before returning the same shape as figure 2-6a. This distortion is calculated by assuming several sets of initial conditions and computing the amplitude and phase of the macromotion until a distorted shape was found which repeated for each RF cycle. A similar calculation was performed by Baril and

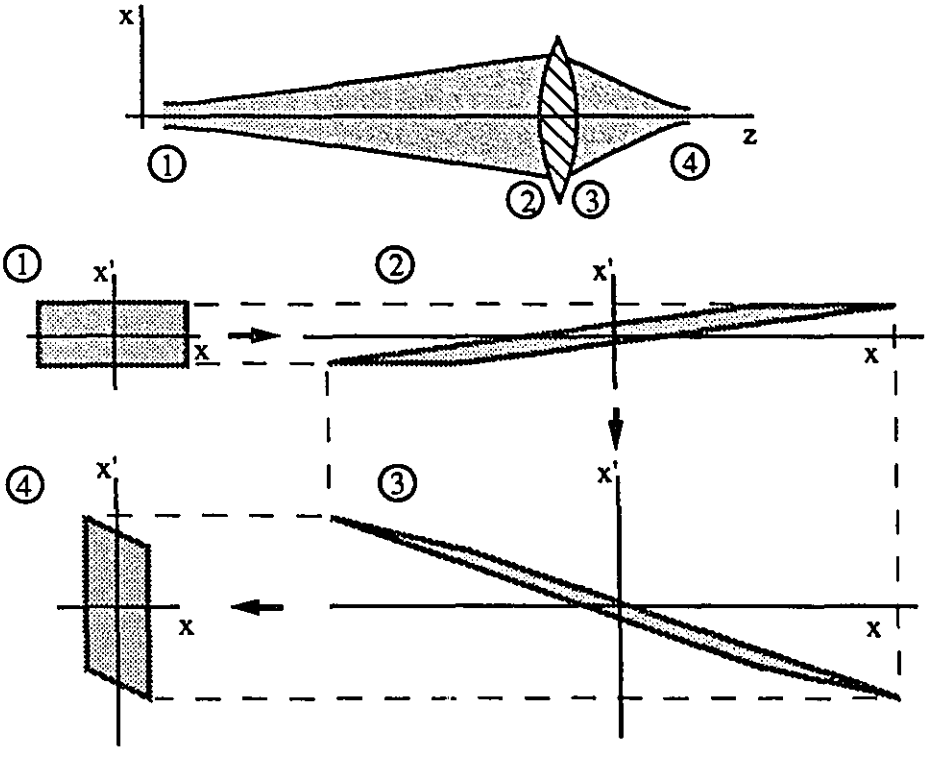

Figure 2-5: Geometric and transverse phase space representation of the focusing of a beam by a lens. A detailed description of each step is given the text.

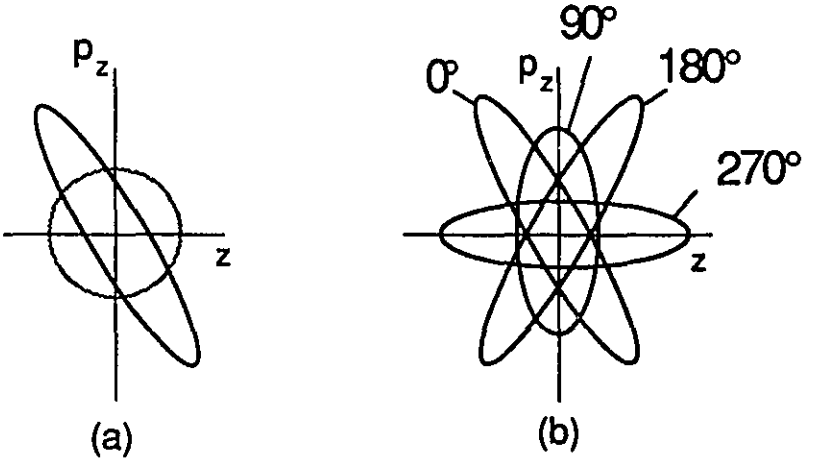

Figure 2-6: RF distortion of the trapped-ion phase space diagram. (a) RF distortion at phase of 0° superimposed on the equilibrium phase space diagram; (b) RF distortion as a function of RF phase. At 360° the ellipse is the same as at 0°.

Septier [BSE] from which some helpful information was gleaned. RF distortion is important because the usable phase space volume of a trap is reduced since the distorted displacement component can exceed the trap dimensions.

For a given set of trap parameters the phase space volume of a trap relative to that of a collected ion cloud can be increased by dissipatively cooling the trapped ion energy. Liouville's theorem is only valid for non-dissipative systems so that once a cooled equilibrium is reached then phase space density is again conserved. Once the ions are in equilibrium then the concept of ion temperature can be introduced. This is a favorable concept since a given temperature governs both the velocity and spatial distributions of ions occupying a given phase space volume.

C: TEMPERATURE OF A TRAPPED ION CLOUD

The original model for the temperature of ions in a Paul trap is presented by Dehmelt [DEHb]. Ideally, trapped ions reach a steady state where the inter-ion space charge repulsion and the trapping potential balance. Ions fill the trap potential well at a constant density to a level dependent upon the number of ions; rather like rum filling a punch bowl. In an electrically and geometrically perfect trap in a perfect vacuum, the cold ion density would remain constant inside this level and would be zero outside. The ion macromotion would be completely damped out and only the perfectly coherent "synchronous breathing" of the cloud at the RF frequency would be present in this ideal world. Electrode imperfections and collisions with background gas will disturb this coherence, however, and the ions will absorb energy from the inhomogeneous RF field. The net effect is to *heat up* the ion cloud. For larger ion clouds this RF heating mechanism leads to a loss of ions from the trap. This is because the RF field strength increases from the trap center and the micromotion becomes large enough that ions hit the electrodes. This "boiling" of ions from the trap rids the trap of hot ions and is actually referred to as *evaporative cooling*. One analog for evaporative cooling is pouring beer. If poured too quickly, a head is created with overflows the glass. Ion boiled out of a trap by the RF can be thought of as the head.

While heating is caused by collisions of background gas, the same process can effect a temperature *loss*. When trapped ions collide with much *lighter* masses, the trapped ion *loses* energy and becomes *cooler*. This mechanism, called *buffer gas cooling*, is frequently used to reduce the kinetic energy of a trapped ion cloud (which evaporative cooling does *not*, for the same number of ions). Buffer gas is a light, neutral variety such as H_2 or He. Ions cooled in this way approach the constant density scenario mentioned earlier but the collisions with the buffer gas introduce friction between the gas and the ion cloud and cause a loss of ion motion coherence. This friction results from the space charge repulsion of the ions in the cloud that extends the cloud boundary into regions of higher RF field.

In modeling the dynamics of an ion cloud in a trap, one fundamental assumption must be made: that the cooled ions are in equilibrium. If this is the case, we can again turn to the field of statistical mechanics where the ions can be described by a distribution. Several observations of trapped ion clouds have reported Gaussian velocity and spatial distributions [KPR, SSW, BZH]. The Gaussian distribution can be cast in the same mathematical form as the Gibbs† distribution in statistical mechanics from which the concept of an ion temperature can be introduced.‡

Gibbs developed the idea of statistical mechanics as a departure from the kinetic theory of gases. It treats bodies of arbitrary complexity moving according to the laws of mechanics but investigates the motion statistically. Problems treated by statistical mechanics consist of a large number of systems similar in all ways but with initial conditions which vary from system to system. The fundamental formulation describes the evolution in time of the phase space density (Liouville's theorem) based on the work of Maxwell and Boltzmann that dealt with the theory of probability. The main point about the Gibbs distribution is that, unlike the Boltzmann distribution which applies to an ideal gas or the Maxwellian distribution which applies only to velocities, the formulation describes the dynamic and thermal properties of bodies with no hypothesis regarding molecular constitution. Because the characterization of a trapped ion cloud is unlike that of an ideal gas, the generality of the Gibbs distribution is important.

The Gibbs distribution tells us that trapped ions will arrange themselves into the possible energy levels of each state of macromotion according to:

$$\frac{dN(E)}{dE} = \frac{N}{kT}\, e^{-\frac{E}{kT}} \tag{2-28}$$

where N is the total number of ions and kT the mean temperature. Considering an ion in the circular phase space diagram at radius a and momentum $m\omega a$, the energy E of the ion is:

$$E = \frac{1}{2} m(\omega a)^2 \tag{2-29}$$

The spread of energy in an annular band of width da is therefore:

$$dE = m\omega^2 a\, da \tag{2-30}$$

and from equation 2-28 the number of particles in the band is:

$$dN(E) = \frac{N}{kT}\, e^{-\frac{E}{kT}} m\omega^2 a\, da \tag{2-31}$$

---

† Josiah Willard Gibbs (1839-1903), an American mathematical physicist, earned a doctorate in engineering before contributing hugely to the fields of thermodynamics and statistical mechanics.

‡ See, for example, Huang [HUA].

In a statistical distribution, the particles in this energy band will be uniformly distributed in phase of oscillation, meaning that they are uniformly distributed around the band. Using equation 2-29 for E, the density per unit area of the phase space diagram will therefore be $dN(E)$ divided by the band area $dS_a = 2\pi a\, da$:

$$\frac{dN(E)}{dS_a} = \frac{N}{2\pi kT} m\omega^2 e^{-\frac{m\omega^2}{2kT}a^2} \qquad (2\text{-}32)$$

which gives us the Gaussian form of the distribution. Thus, only the temperature is required to determine the momentum and spatial distributions of the ion cloud. Implicit in this model is the assumption of equipartition of energy. This means that the temperature that describes the axial phase space component will also apply to the radial component. Since the trapped ion dynamics are uncoupled in each dimension, the radial distributions can be described in the same fashion. The equivalence of energy in each normal mode of the system follows from the definition of temperature as an equilibrium.

The axial phase space density distribution can be visualized as shown in figure 2-7. The height of the distribution is determined by N and the cross-section follows the Gaussian form of equation 2-32. The distribution projects onto the scaled phase space circle shown in figure 2-6a. This circle is represented (discretized) by an ensemble which is weighted according to the $N(E)$ at that particular point. At this point, the RF distortion correction is applied and then the ensemble dynamics are numerically computed through the trapping, extraction and transport processes. This procedure is described in more detail in chapter 3. It is still necessary to decide on how well the phase space density is represented by the discrete ensemble.

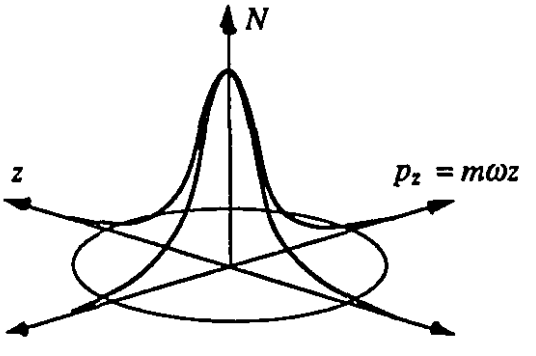

Figure 2-7: Distribution of the trapped ion cloud over the axial phase space area. This distribution is projected onto the scaled phase space circle of figure 2-6a.

The number of particles N_a that are inside an amplitude a in the phase space diagram is given by the integral of equation 2-28:

$$N_a = \frac{N}{kT} \int_0^{E_a} e^{-\frac{E}{kT}} dE = N\,(1 - e^{-\frac{E_a}{kT}}) \qquad (2\text{-}33)$$

where E_a is the energy of an oscillation at amplitude a. Thus, 1 - 1/e or 63% of the particles have amplitudes of oscillation less than that of particles at the mean energy kT. About 95% will have amplitudes less than that for particles of energy $3kT$ or of amplitude $\sqrt{3}$ times the amplitude for particles at the mean energy. For the analysis presented in chapter 4, the ion cloud was represented with an ensemble spanning an energy of $3kT$. For larger N, more points are required in the discretization.

The use of equation 2-28 to describe the trapped ion cloud phase space is, of course, not ideal. For low trap loadings, the ion density should approach the constant density model of Dehmelt [DEHb]. However, smaller, cooler ion clouds have a higher ion density which causes a shift in the macromotion frequency due to space charge. In this case, the simple phase space diagram of figure 2-4 becomes distorted and the oscillation frequency varies with radius. The effect of space charge has been addressed by Meis *et al.* [MDJ] and is discussed further in chapter 4. For larger clouds the Gibbs description should be sufficiently accurate. In this work, the minimum possible trap loading was about 1000 ions which, due to RF heating, is believed to be well beyond the point at which space charge affects the ion motion.

CHAPTER 3: APPARATUS

Arthur: Now what happens?
Bedevere: Well now, Lancelot, Galahad and I wait until nightfall and then leap out of the rabbit and take the French, not only by surprise, but totally unarmed!
Arthur: Who... who leaps out?
Bedevere: Er... Lancelot, Galahad and I... er... leap out and... um... well look, perhaps if we built this large wooden badger...

Monty Python and the Holy Grail

A: TIME OF FLIGHT SYSTEM

The technique used in this work to study the phase space volume of a cloud of ions in a Paul trap is to extract them through an adjustable but well defined transport system and observe the time structure of the detected pulse. By numerical calculation of individual trajectories based on knowledge of the transport system, the beam pulse from an assumed distribution of ions at the trap center can be computed and compared with measurements. The ion distribution in the trap is governed by a temperature as explained in chapter 2. The extraction parameters can be adjusted to enhance the effect of either the spatial extent of the ion cloud or its velocity distribution in the observed beam pulse. This is essentially a refinement of the techniques used by Mosburg *et al.* [MVZ], Brincourt *et al.* [BCZ] and Champeau *et al.* [CCL] for time-of-flight measurements.

Shown in figure 3-1 is a general schematic diagram of the entire apparatus which is a two meter beamline of standard 4-inch (10.16 cm) *HVE Dependex* vacuum components pumped by two *CVC* 250 l/s oil diffusion pumps and an *Alcatel* mechanical pump. Pressures of 10^{-5} torr (1.3 mPa) were obtained as measured by *CVC GPH-320C* Penning vacuum gauges. When trapping, helium buffer gas at pressures up to 2×10^{-4} torr (27 mPa) is introduced to the system through a needle valve. At one end of the beamline is a chamber which houses the ion source and Paul trap. The mounting and service flange for the ion source and ion trap is isolated and can be floated up to 5 kV. The cavities are biased using *BNC MHV* vacuum feedthroughs along the beamline. A detailed schematic diagram of the ion source, ion trap and cavity system is shown in figure 3-2.

The ion source is a surface ionization type which is commonly used to produce positive ions of the alkali metals, all of which have relatively low ionization potentials. The alkali atom is adsorbed onto a surface which has a high work function (*e.g.*, tungsten). The loosely bound electron of the adsorbed atom is lost to the surface which is heated so an ion is thermally desorbed. The ion source consists of a Na_2CO_3 reservoir plugged with tungsten wire and covered with a thin alumina sleeve which provides electrical isolation and good thermal conductivity. The reservoir and plug are heated using 0.1 mm diameter Nichrome heating wire of about 10 Ω resistance wrapped around the alumina. Typically, a heating current of 1.0 A

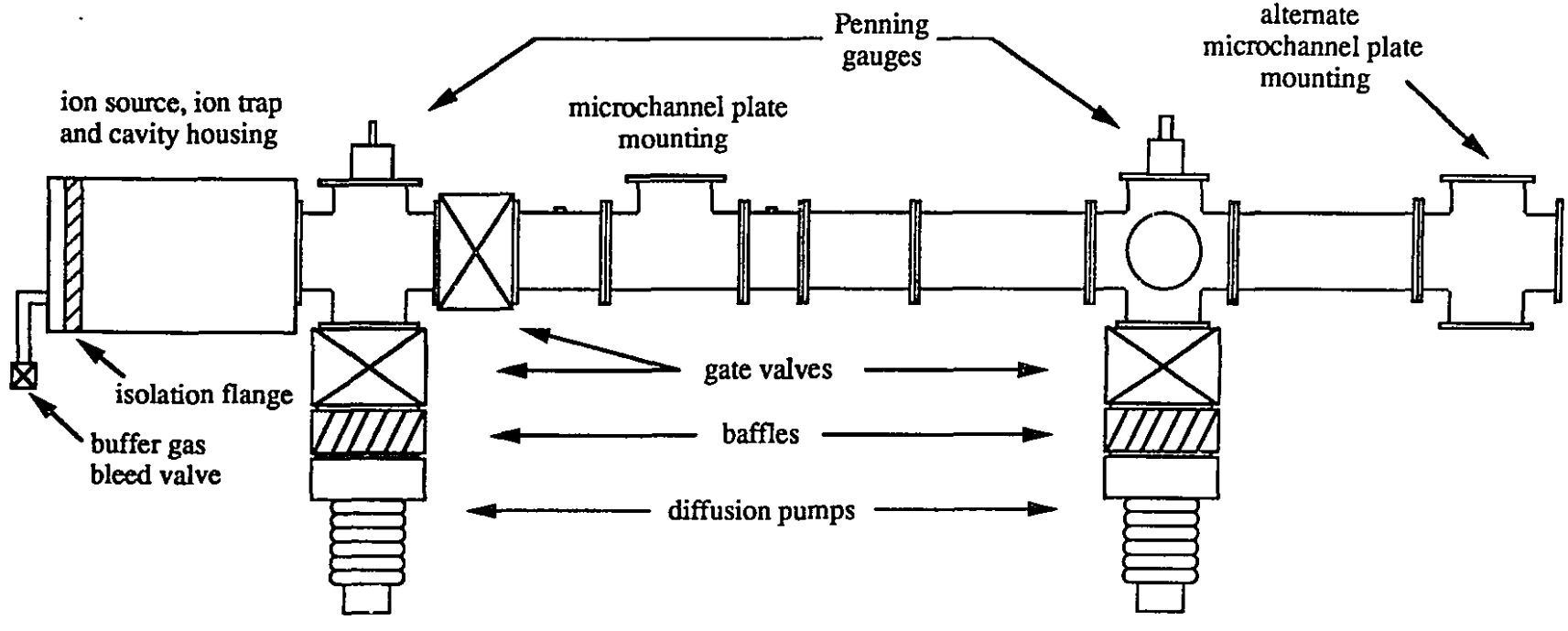

Figure 3-1: Schematic diagram of the time of flight beamline used for observation of the phase space volume of extracted ion beams. The overall length of the beamline is 2 meters.

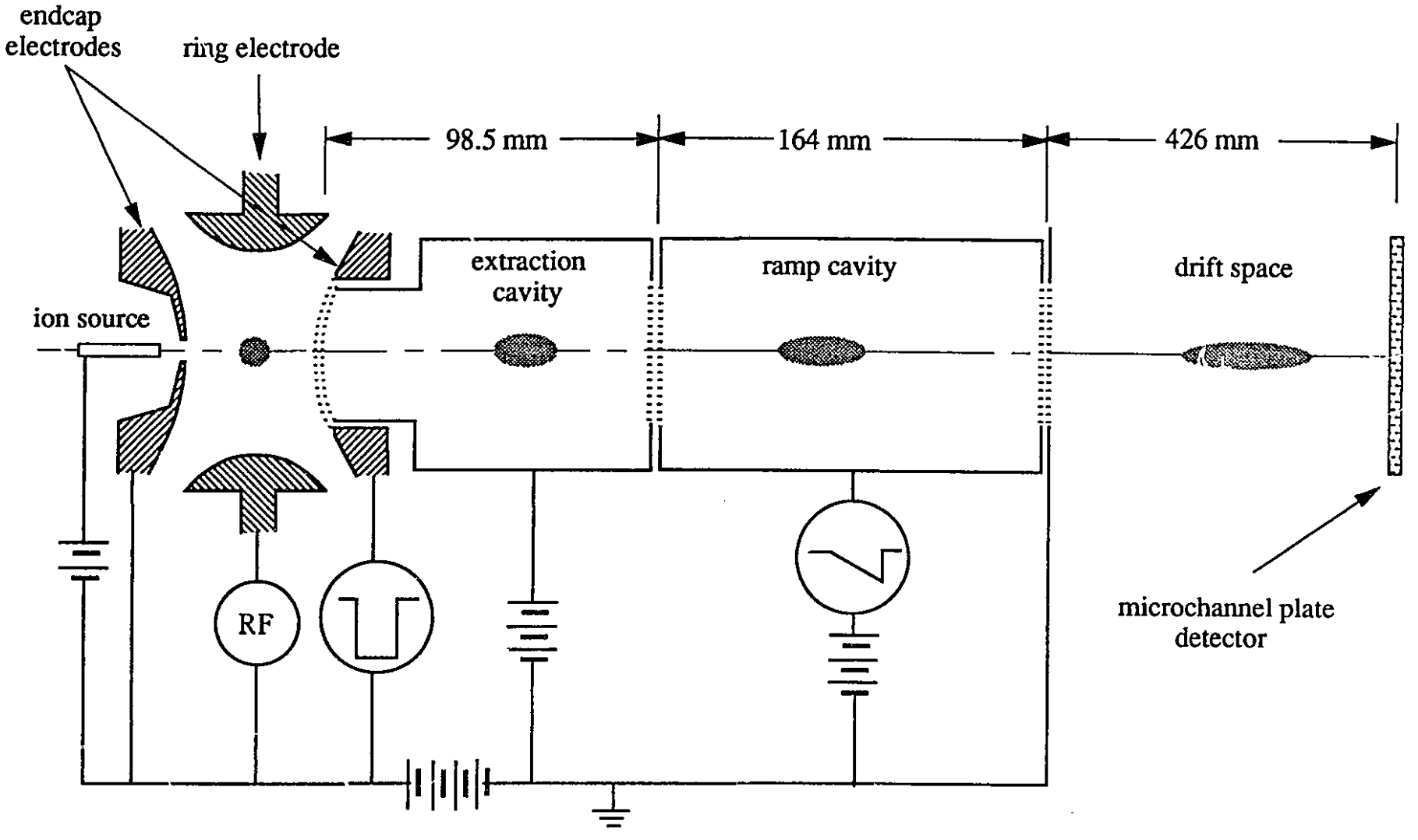

Figure 3-2: Detailed schematic diagram of the ion source, ion trap and cavity electrodes used in the time of flight system.

produces a weak potassium beam of a few pA. (At low heating the source favors adsorption of potassium over sodium even though sodium has a lower ionization potential.) Increasing the source heating to about 20 W yields a sodium beam of a few nA. Further details concerning the ion source construction are given by Nantel [NAN].

The ion trap used for these experiments is of the same design used in previous work at McGill [LUN, GUL, MGU]. It consists of aluminum hyperbolic electrodes with an endcap spacing of 28 mm. The extraction endcap is formed from a steel mesh with openings of about 1 mm^2. Ions are continuously injected through a 7 mm hole in the other endcap which is held at trap ground. The ion source can be biased relative to the trap to control the ion injection energy which is typically 15 V. The trap is driven at 650 kHz using a *Hewlett Packard 8656A* signal generator, an *ENI 325LA* RF power amplifier and a high-Q resonant LC circuit. The RF drive voltage is about 300-350 V_{op} for ^{23}Na and 400-500 V_{op} for ^{39}K. These trap settings yield a Mathieu q-parameter value of about 0.75 and a potential well depth of about 60 eV. No DC bias was used on the ring.

The cavity system was designed using rough energy retardation and time-of-flight measurements for achieving a time focus. Planar mesh windows are used on the cavities to avoid ion-optic aberrations and focusing effects which would be caused by large apertures. By making the mesh separation as small as possible, most of the cavity system is field-free so that the drift times can be accurately determined. For this reason, one of the extraction cavity windows is contoured to the endcap hyperboloid shape as seen in figure 3-2. The length and potential of the extraction cavity was chosen to allow a time spread to develop in the ion bunch as the ions are extracted in a very narrow time window (less than 200 ns). Following the extraction cavity is the ramp cavity which is designed to convert a large energy spread into a time spread as explained in chapter 4. The ramp cavity can also be floated at high voltage. Finally, the ions see the ground cavity where they obtain their full transport energy and drift 43 cm to a *Galileo Electro-Optics* B-25 microchannel-plate detector.

The microchannel-plate is a large area, extremely sensitive single ion detector. It is essentially a thin (0.5 mm) semiconducting sieve which detects impinging particles by secondary electron emission along the channels in the plate. This is the same idea as an electron multiplier tube but with the dynode chain replaced by thousands of cylindrical channels. The channel diameters are 10 μm and the center spacing is 12 μm. The active area of the plate is about 6.7 cm^2. Two plates are used in tandem and a bias of 1000 V across each plate provides a gain of about 10^6. The electron signal is collected on a floating conductor mounted behind the channel plates. The transit time for gain pulses is less than 2 ns with almost zero recovery time; unlike an electron multiplier tube which has long recovery and risetimes. This makes the channel plate extremely useful for measuring the time distribution of incoming ion bunches typically having

100-1000 ns widths. Details concerning the mounting and biasing of the channel plates are given by Nantel [NAN].

A cloud of trapped ions is extracted using a fast negative square pulse applied to the endcap. This pulse is produced by a *Nikkinen HVS* high voltage switch which has a risetime of 20 ns and amplitude of 100 to 300 V below trap ground. These somewhat stringent specifications are required to extract the ions cleanly. The fast risetime is important because of the large swing of the RF voltage (1 kV in 2 μs). The timing of the extraction pulse is derived from an electronic module that counts RF cycles so the extraction period can be varied. This module was also designed to insure that each ion bunch is extracted at the same RF phase. The RF phase at extraction is varied using an *Ortec 416A* gate and delay generator which then triggers the high voltage switch. Another gate and delay generator is used to derive the ramp trigger. The RF and extraction trigger are sent through a *Nikkinen Cheaplink* fiber optic transmitter/receiver system to a Faraday cage which houses the resonant LC circuit, RF power amplifier and high voltage switch. The ramp trigger is also sent through a fiber optic *Cheaplink* to an isolated 100 V/μs *Nikkinen HVR* high voltage ramp generator which is in a separate Faraday cage. The ramp voltage is adjustable between ±100 V and the duration can be varied from 1-10 μs. A schematic diagram of the electronics system is shown in figure 3-3.

To record the detected ion pulse time distributions, a *Hewlett Packard 54501A* digitizing oscilloscope was used with an *IEEE-488* computer interface. A *Philarche* software package was used to interface the oscilloscope to an *IBM PC*. However, due to the limited sampling frequency of this oscilloscope (10 Msamples/s), the recorded ion signals sometimes contain small artifacts resembling peaks. Several ion signals were averaged on the oscilloscope to avoid this problem. The signals are then captured in the computer memory and stored on disk. The oscilloscope is triggered using the output from the gate and delay generator.

B: PHASE SPACE MODELING PROGRAM

The modeling program was developed to interactively follow the dynamics of an ensemble of ions inside a Paul trap before, during and after the extraction process. The trapped ion pnase space density is characterized by an ensemble weighted by a Gibbs energy distribution as described in chapter 2. This requires an input temperature and collective ion oscillation frequency. Alternately, the initial momentum and spatial distributions in each coordinate can be specified by the user at run time (or read from a file). The RF distortion can also be specified at this stage. The distortion is parametrized by a coefficient, with which the ion phase space circle is squeezed, and a slope, to which the diagram is rotated. The drive parameters of the ion trap and the transport system voltages are also specified by the user (or read from a file) when running the program. The input parameters to the program are listed in table 3-1.

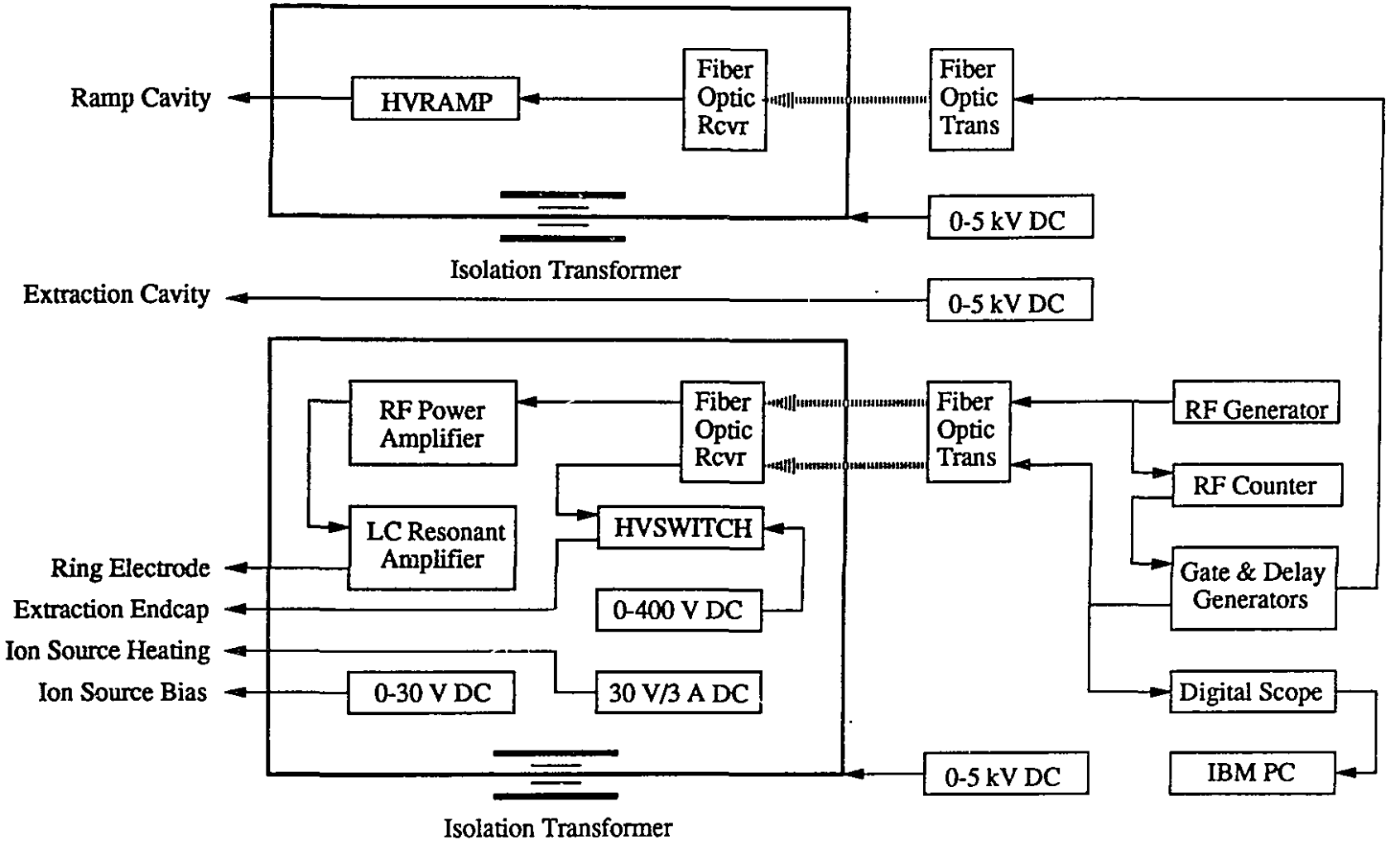

Figure 3-3: Schematic diagram of the electronics used in the time of flight system.

Table 3-1: Input parameters to the trapped ion phase space simulation and transport program.

Particle parameters

charge (e) -	1	1	0
masses(amu) -	1	39	0
start time (μs) -	1	0	0
initial x (mm) -	1	0	0
initial y (mm) -	1	0	0
initial z (mm) -	13	-2.24	4.48
initial E_x (eV) -	1	1	0
initial E_y (eV) -	1	0	0
initial E_z (eV) -	13	-0.75	1.5

Runge-Kutta algorithm parameters

Initial trial step size (μs)	= 0.05
4th order error tolerated (ppm)	= 1
Error scale for distance (mm)	= 10
Error scale for speed (mm/μs)	= 10
Power factor for increasing dt	= -0.2
Power factor for decreasing dt	= -0.25

System parameters

number of parameters	= 22	z range (mm)	= 8
sep. of end el. (mm)	= 28.74	mom. range (eV-μs/mm)	= 4.6
RF (kHz)	= 650	plot ext. t range (μs)	= 1
RF-V (ring above end)	= 380	ext. energy range (eV)	= 100
RF phase at t_0 (deg)	= 0	ion cloud temp. (eV)	= 0.25
DC-V (ring above end)	= 0	RF z expansion factor	= 1.1
extraction pulse (V)	= -200	RF p_z slope (eV-μs/mm^2)	= -0.6
extraction phase (deg)	= 196	trap potential (V)	= 800
axial osc. freq. (kHz)	= 137	extr. cavity potential (V)	= 600
plot int. (μs)	= 0.1538	ramp cavity potential (V)	= 0
plot time range (μs)	= 20	ramp rate (V/μs)	= 0
energy range (eV)	= 100		

The phase space of the ion ensemble is displayed at each requested plot interval up to the time the ions leave the trap and then at each cavity interface thereafter. At the detector position, the weighted ion ensemble is interpolated to construct an ion pulse which can be compared to measured pulses.

The entire program comprises over 6000 lines of *C* source code and runs on the *Macintosh* series of *Apple* computers. It was developed using the *Lightspeed C* compiler. A similar program was developed in parallel to verify the results of the *C* version. This check program was written in *BASIC* and *FORTRAN* to run on an *IBM PC* computer under *MS-DOS*. It uses a simpler version of the Runge-Kutta algorithm and does not include RF distortion but otherwise performs the same computations with the exception of the final pulse shape interpolation. These two independently developed programs produced identical phase space plots for the same initial conditions. The *C* program is significantly faster than the *BASIC/FORTRAN* program and has a better user interface. The extraction of a typical ensemble of 49 ions takes about 2 minutes on a *Macintosh IIci* using the *C* version and about 15 minutes on an *IBM PS/2 55SX* using *BASIC/FORTRAN*.

The quadrupole trapping field is calculated analytically and the extraction field, which has no closed form, is calculated from a multipole model as outlined by Lunney and Moore [LMO] in the appendix. To integrate the equations of motion for ions in an electric field the *C* program uses a sixth-order, Runge-Kutta algorithm with adaptive step size error-correction provided by Press *et al.* [PFT] in *Numerical Recipes*. The integration is used until all the ions have been extracted from the trap at which point the phase space is represented as energy versus time. The ions are then transported at a uniform velocity derived from the potential difference between adjacent cavities excepting, of course, the ramp voltage. All coordinates and velocities for each member of the ion ensemble are calculated in parallel for each step. Trajectories of spatial coordinates versus time can also be displayed though they provide less information. Each ion in the ensemble is displayed with a uniquely coded symbol so the user can monitor the evolution of not only the phase space outline but also the migration of ions inside it. Finally, file utility routines have been included to save the generated data.

To illustrate the capabilities of the program a simulation is shown in figure 3-4 for the ion cloud phase space inside the trap before application of the extraction pulse. Each square in the ion ensemble is coded so the migration of the ions in the phase space diagram can be observed. The original circular phase space diagram is RF distorted as shown in figure 2-6a and returns to its original shape after each RF cycle as discussed in chapter 2. After one macro-oscillation cycle the ions return to the same position in the diagram as also illustrated by figure 2-4. The calculation was made for $m = 39$, $V = 550$, $\Omega/2\pi = 650$ kHz and the collective oscillation is 217 kHz which is one third the RF frequency. Note how the ions rotate clockwise as determined by equations 2-15 and 2-16.

Figure 3-5 shows an axial phase space plot displayed as energy versus time and momentum versus displacement. This simulation was run for a 0.5 eV (5800 °K) temperature, 75 ion ensemble extracted with 200 V at an RF phase of 197°. The RF voltage was 420 V and frequency 0.65 MHz giving a macromotion frequency of 151 kHz. As the ion motion is integrated until the last ion reaches $z = z_0$ (the adaptive step size routine allows this), the energy versus time plot is a picture of the beam as it passes through this point. The momentum versus displacement plot represents the beams spatial extent at the time when the last ion reaches z_0 (about 1.06 μs for a z_0 of 14.36 mm). From figure 3-5, the length of the beam at this time is about 15 mm and the time taken for the beam to pass the endcap is about 0.44 μs.

Figure 3-6 shows the phase space diagrams of ion ensembles extracted at different RF phases. Figure 3-6a shows the original, circular phase space distribution before applying the RF distortion. Figure 3-6b shows the axial phase space diagram for the ion ensemble extracted at the RF phase for which the time-of-flight was minimized. The ensemble of figure 3-6c was extracted at an earlier RF phase illustrating the contribution of the momentum spread. The

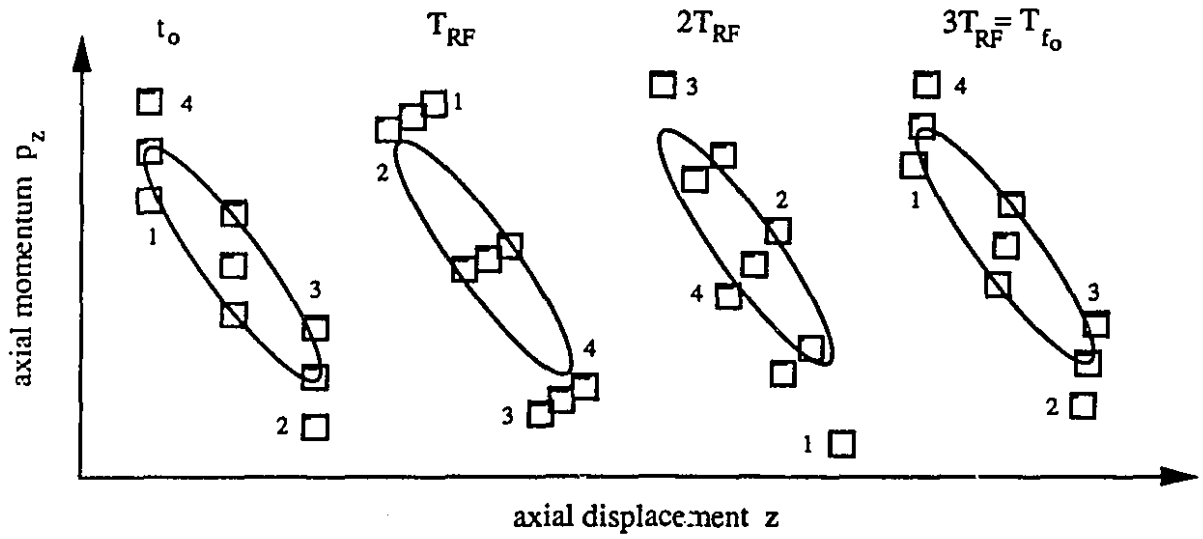

Figure 3-4: Phase space diagrams (momentum versus displacement) for successive times inside the Paul trap. The original cloud is RF distorted as in figure 2-6a. Ions in the ensemble are coded to illustrate the phase space oscillation shown in figure 2-4. After one complete macromotion cycle, the ensemble returns to its original phase space configuration at time zero.

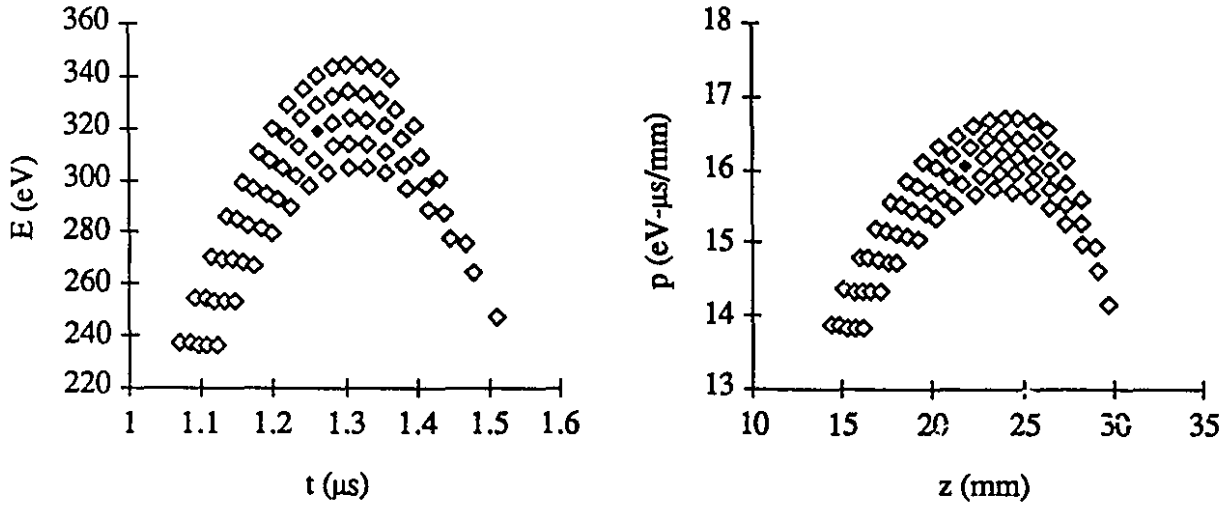

Figure 3-5: Axial phase space diagram for an extracted 0.5 eV ion ensemble plotted as energy versus time and momentum versus displacement. The central particle in the ensemble is shaded.

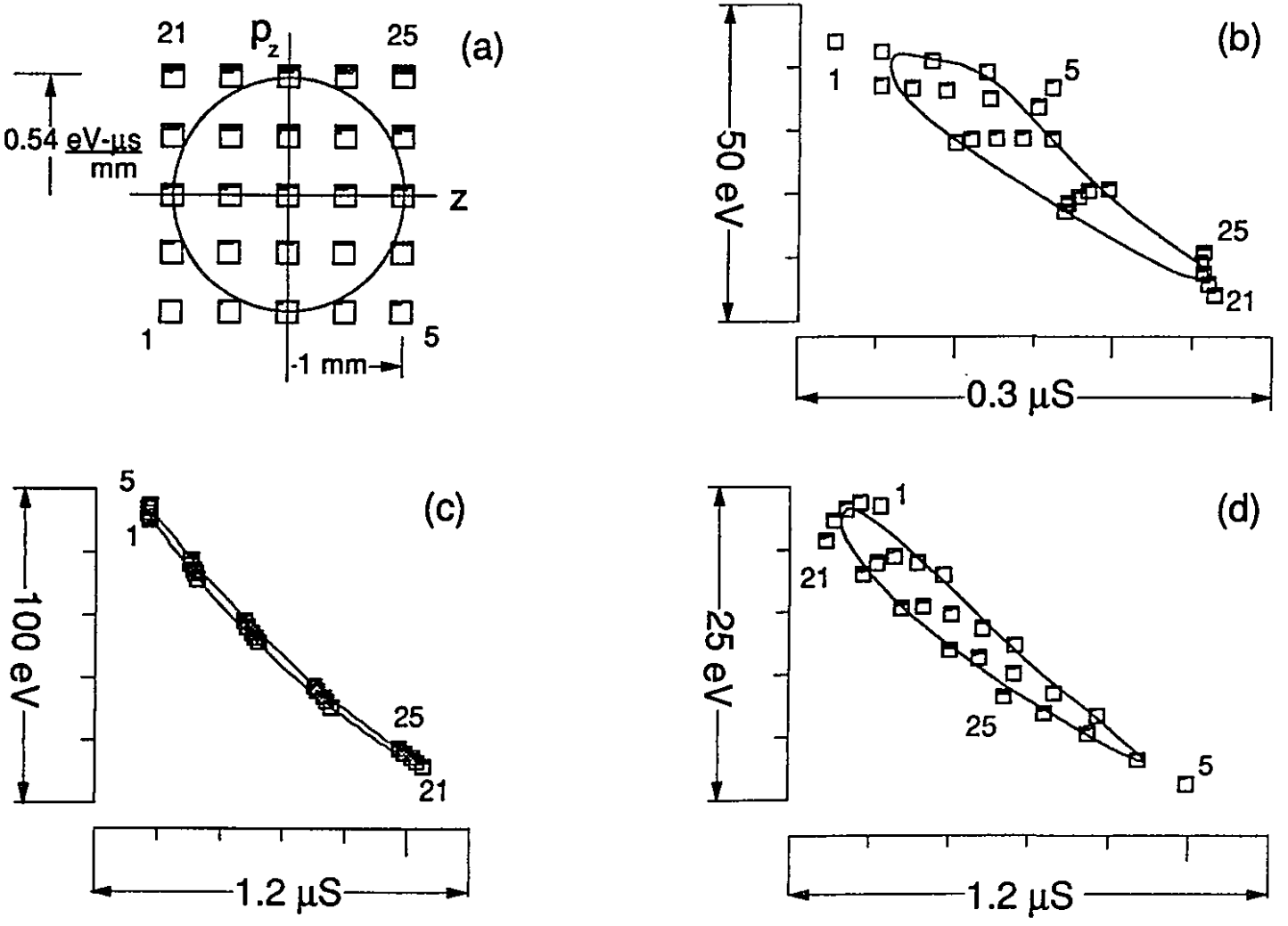

Figure 3-6: Phase space diagrams of simulated ion ensembles at the detector position extracted from the trap at different RF phases. (a) Initial equilibrium ensemble in the center of the trap; (b) extracted for minimum time of flight; (c) early extraction; (d) late extraction

ensemble of figure 3-6d was extracted at a later RF phase illustrating the contribution of the spatial spread. Note that the area of each ellipse in figure 3-6 is the same in accordance with Liouville's theorem.

Because the individual points in the ensemble are coded, the orientation of the original phase space diagram can be divined from the extracted ion phase space diagram. That this orientation changes with RF phase is evident from figure 3-5. This illustrates the idea of reconstructing the original phase space diagram from its various projections which is discussed in Appendix 3.

CHAPTER 4: RESULTS AND DISCUSSION

Mon centre cède, ma droite récule, situation excellente, J'attaque

Maréchal Foch

As explained in chapter 2, the phase space of a collection of trapped ions has components of time and energy which are folded together. The complications of systematically separating these components was also mentioned. In order to extract the ions efficiently, they must be extracted with fairly large kinetic energy which, in turn, results in an extremely narrow time distribution. Consequently, any attempts at time-gating the ion pulse are impossible. Energy analyzing measurements are not as accurate because too much of the signal is lost in the process. On the other hand, a complete time profile of the extracted beam can be obtained very accurately with the multichannel plate detector described in chapter 3. In general, time measurements are more accurate than other quantities. By varying the time profile by changing the extraction conditions, a good sampling of the phase space distribution can be obtained.

The aim of this experimental work is to match the measured extracted-ion pulse shapes and times with the correct ion temperature parameter of the thermodynamic model presented in chapter 2. The combination of the generality of the Gibbs distribution and the directness of numerical integration yield quite a powerful computational model for the ion extraction process as described in chapter 3. This model is used with a single parameter, the temperature, to fit the measured curves over a systematic variation of RF phase. All of the following measurements are made for the axial component only. Measurement the transverse time and energy components of the beam bunch would be nearly impossible. In any case, since the extraction is done in the axial direction, it is the axial phase space component which is most profoundly affected. Because of the general definition of temperature and equipartition of energy, the temperature is the same in each dimension so having determined the temperature by axial measurements, the radial phase space component may be calculated.

A: INITIAL CONDITIONS

The application of the Gibbs phase space model involves one crucial assumption: the trapped ion cloud is in a symmetric, thermal equilibrium. This establishes the validity of the temperature argument and provides a firm starting point from which the temperature evaluation process can be initiated. The first data to be presented, therefore, relate to the ion capture and cooling process which establish the initial conditions of the trapped ion cloud.

Shown in figure 4-1 are several curves which represent the number of ions extracted plotted versus extraction period (time between successive extracted ion clouds). The various curves represent ion bunches extracted at different buffer gas pressures. At long extraction periods

(figure 4-1a), a saturation effect is evident with the total number of ions reaching a maximum which depends, inversely, on the buffer gas pressure. At shorter extraction periods, the number of ions trapped is higher for higher pressure. It appears that buffer gas cooling abets the initial capture of the injected ions but also hinders their long term storage. This is due to the energy loss mechanism of the collision of the ions with the buffer gas molecules. Initially, energetic ions must lose energy to stay in the trap and take up the characteristic collective oscillation. When they are cool, further collisions cause a dephasing of the collective ion orbits and subsequent loss of the ions. When the extraction curves are examined more closely at fast extraction (figure 4-1b), interesting features can be discerned. At higher gas pressure, the extraction curve increases linearly with a steep slope indicating that the ions are cool. At lower gas pressure, the curve increases exponentially which indicates that the ions have not yet achieved cool equilibrium. From these curves, the cooling time is estimated to be about 10 ms. Cutler *et al.* have measured the cooling rate of buffer gas collisions and report a result of about 30 ms [CGM]. Subsequent measurements were made at a pressure of 2×10^{-4} torr (27 mPa) and with extraction periods of 10-100 ms, well into the linear, cooled region of extraction for which we assume the ions are in thermal equilibrium.

To provide evidence for a symmetric equilibrium, we turn to figure 4-2 which shows three extracted ion pulses versus time differing in buffer gas pressure and extraction period. While the high pressure/slow extraction pulse is much wider and flatter, the centroid of the pulse is essentially the same as the low pressure/slow extraction and low pressure/fast extraction pulses. Figure 4-3 shows two extracted ion pulses differing in the energy with which the ions were injected into the trap. Again, the centroid positions are unchanged indicating that, although the ions entered the trap with different kinetic energies, they were cooled to symmetric equilibrium.

B: TEMPERATURE MEASUREMENTS

Having established arguments for symmetric thermal equilibrium, the remaining results will concentrate on the study of the dependence of ion temperature on ion bunch size. Results are presented for two masses: potassium (m=39) and sodium (m=23). For each case, the measurements were done mainly with one set of transport parameters. To demonstrate the validity of the phase space program fits, some variations from these parameters will also be presented. Also, the effect of a voltage ramp on the ion cloud phase space will be discussed.

The fitting procedure is performed by entering the known operating parameters into the phase space program which was described in chapter 3. The single most important parameter affecting the phase space of the extracted beam at a certain temperature is the RF phase at extraction. There is a strongly preferred RF phase where the ion signal is maximized which depends on the

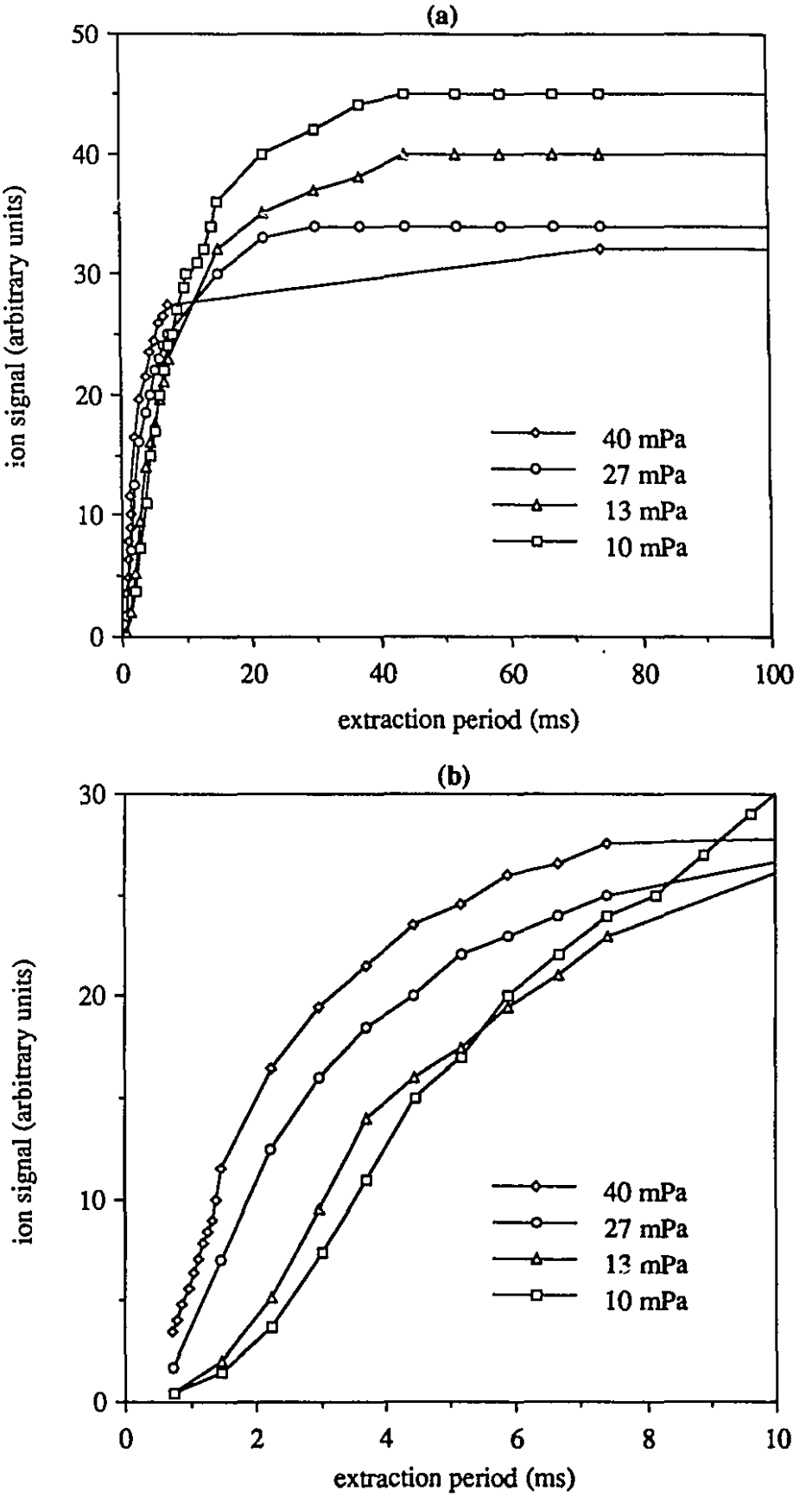

Figure 4-1: Ion signal versus extraction period as a function of buffer gas pressure. (a) long extraction periods (b) short extraction period blown up from (a).

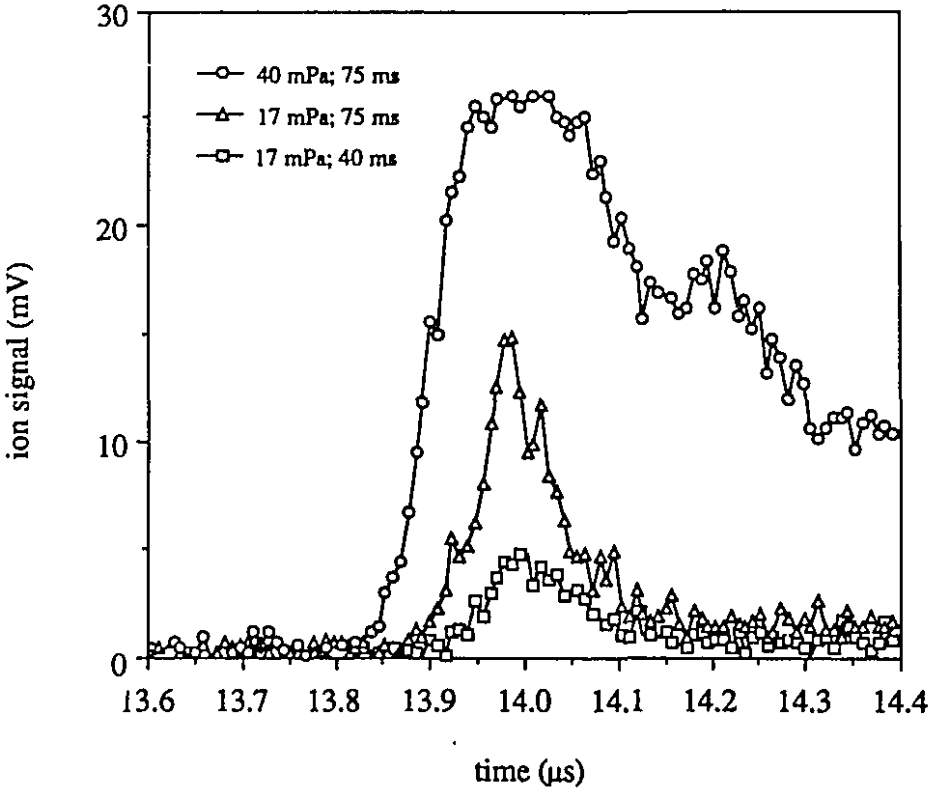

Figure 4-2: Detected ion signals for different buffer gas pressures and extraction periods.

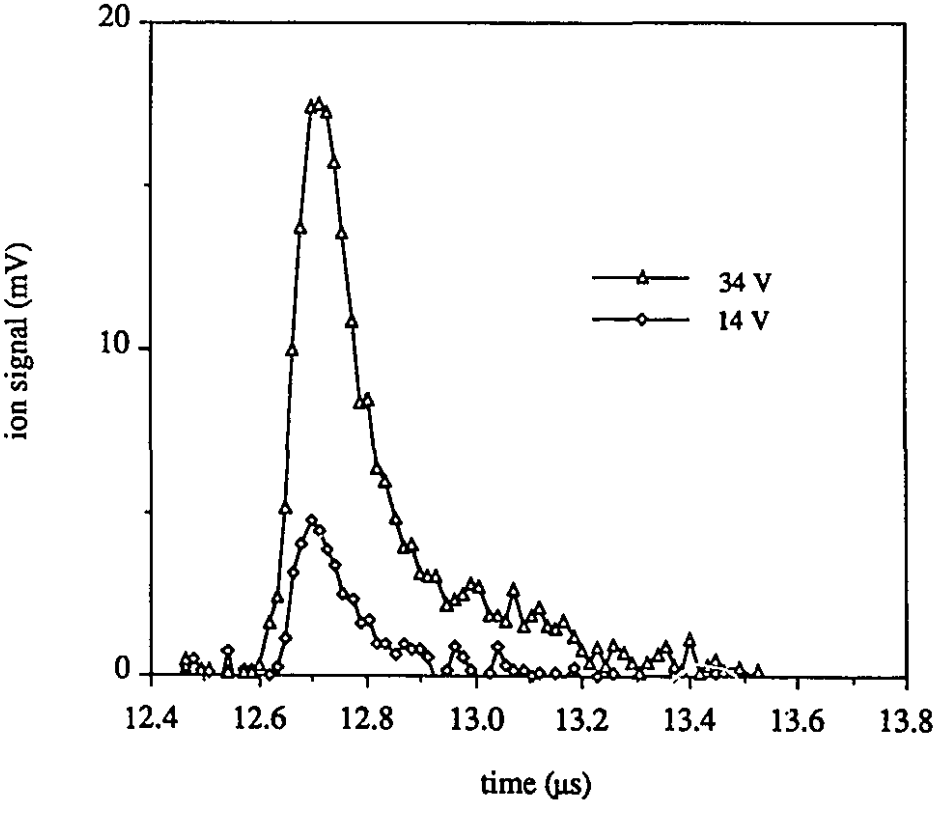

Figure 4-3: Detected ion signals for different injection energies.

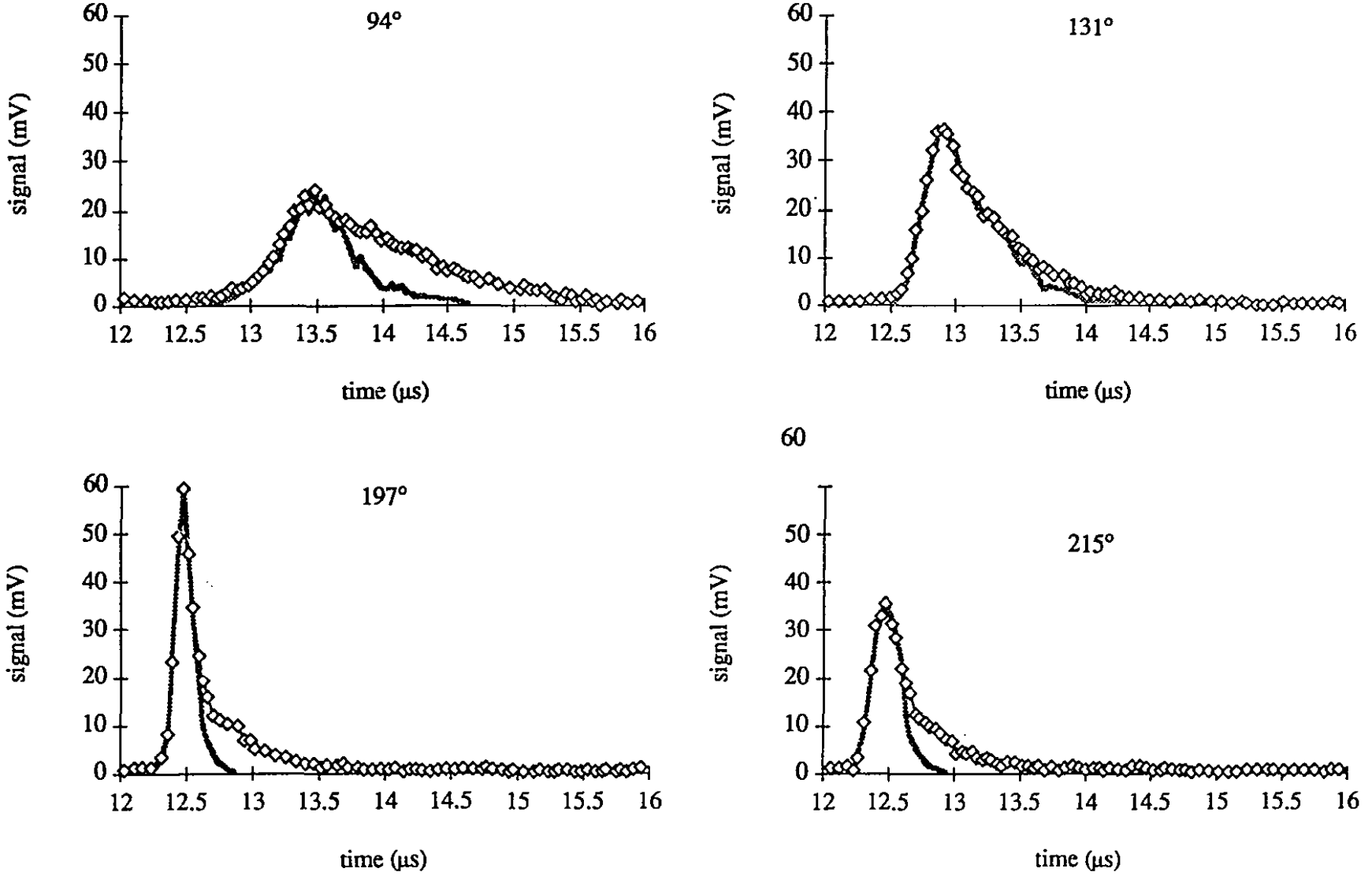

Figure 4-4: Intensity versus time signals for 500 K ions fit with a temperature of 0.25 eV.

extraction electric field. The detected ion signal has a dramatically narrow width at this preferred phase which, in beam optics terminology, is referred to as a time focus.

In figure 4-4 (page 42), extracted potassium (mass 39) ion signals are shown, for a 200 V extraction pulse, at four RF phases. At 197° the time focus is obvious with its narrow, high peak. Superimposed on the data are fits generated by the phase space program. These fits correspond to transported initial ion distributions with a temperature of 0.25 eV.‡ The number of ions in the signal (as determined by comparison with single ion signals) is about 500±100. The fits are quite good with the asymmetric shape of the ion signal reproduced. The time of arrival (TOA) of each pulse is calculated to within 0.12 μs on a 13 μs total flight time which is less than 1%. The time focus is also reproduced. Besides temperature, the only other fitting parameter adjusted is the pulse amplitude which is simply scaled to the data. To test the sensitivity of the fit, the ion temperature was varied from 0.15 to 0.35 eV and the corresponding pulse reconstructions at the time focus plotted in figure 4-5. It is quite obvious from this figure that the temperature falls between these values so, conservatively, kT (500±100) = 0.25±0.10 eV. The parameters of this fit are summarized in table 4-1.

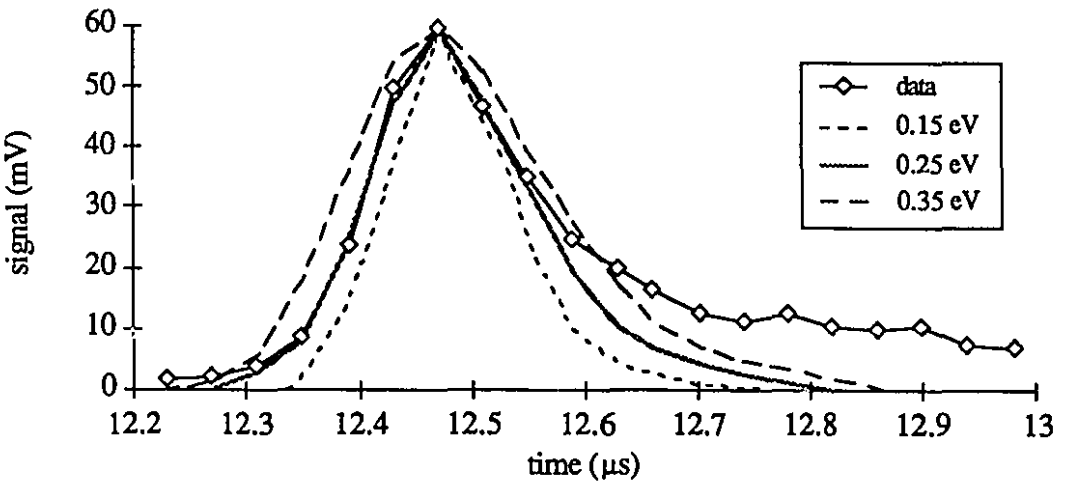

Figure 4-5: Sensitivity of the 0.25 eV temperature fit to the measured ion intensity signal.

An obvious feature of figure 4-4 is the tail present in the data but not reproduced by the fit. This is somewhat expected as a simulation will generally not include processes such as scattering

‡Temperature is fundamentally defined in terms of the change of entropy with energy. Since entropy is dimensionless, temperature has the units of energy. Customarily it is measured in its own absolute units °K. In beam optics, temperature is usually measured in eV which are related to degrees by Boltzmann's constant such that 1 eV = 11606 °K.

Table 4-1: Fit parameters for $^{39}K^{+}$ ions extracted at 200 V. In all cases RF frequency is 0.65 MHz with no DC voltage on ring.

ion temp. (eV)	0.75 ± 0.1	0.25 ± 0.1	0.20 ± 0.1	0.125 ± 0.04	0.125 ± 0.04	0.06 ± 0.02	0.05 ± 0.02
number of ions	2300 ± 300	500 ± 100	400 ± 50	120 ± 30	80 ± 30	20 ± 10	15 ± 5
initial z (mm)	± 2.77	± 2.24	± 1.38	± 1.44	± 1.46	± 0.99	± 0.91
initial E (eV)	± 2.25	± 0.75	± 0.6	± 0.375	± 0.375	± 0.18	± 0.15
$z \times E$ array	7 × 21	9 × 9	13 × 13	13 × 9	11 × 11	11 × 11	9 × 15
RF-V (V_{op})	500	380	512.5	420	420	420	420
f_o (kHz)	192	137	198	151	151	151	151
q parameter	0.72	0.55	0.74	0.60	0.60	0.60	0.60
well depth D (eV)	60	31	64	37	37	37	37
RFD (coef/slope)	1.05/-0.725	1.1/-0.6	1.2/-0.75	1.15/-0.65	1.15/-0.65	1.15/-0.65	1.15/-0.65
trap potential (V)	800	800	800	800	800	800	800
ext. cav. pot. (V)	600	600	600	600	600	600	600
ramp cav. pot. (V)	0	0	200	200	0	200	200
tof agreement (%)	0.3	0.1	0.9	0.1	0.3	0.1	0.4
S_z (eV-μs)	11.5	5.4	2.9	2.4	2.4	1.2	1.0
figure	4-9	4-4	4-14	4-16	4-11	4-15	4-12

that can cause a loss of energy. As the ions wend their way through the cavity system, they transit several meshes which cause a certain amount of small deflection, or scattering due to the local deviation of the mesh from a plane. This will convert a certain fraction of the ion axial velocity to radial velocity. This makes the ion travel further to get to the detector and therefore appear later in the time distribution, *i.e.*, to form a tail. The first ions to arrive at the detector are those that have lost only a minimal amount of their axial velocity due to scattering. Therefore, the leading edge of the data should be well reproduced by the simulation, which it is.

Another possible contribution to the deviation of the fit is the coupling of axial motion to radial motion due to the sextupole term in the extraction field. The sextupole contribution to the field near the endcap electrode is less than 10% of the total axial field.† Simulations were run to check extraction field effects by introducing a large amount of radial energy to the ion ensemble and then checking the variation in axial time-of-arrival but no significant variation (larger than experimental error) was observed.

A corresponding set of phase space diagrams (energy versus time) for each of the fits in figure 4-4 is given in figure 4-6. Because the ion ensemble is weighted, a complete correspondence of the reconstructed pulses to the phase space diagrams is not apparent. Also, since the initial ensemble is rectangular, rather than elliptical, the corners tend to extend the diagram slightly. In any case, these corners have little weight in the distribution and consequently contribute little to the reconstructed pulse. What is important is the relative energy and time spreads at the different phases and the fact that the area of each diagram is the same, in accordance with Liouville's theorem.

To determine the effect of the RF distortion a fit was made with and without the distortion parameters. At the time focus, the difference in the fits was not as pronounced but at other phases there was a more significant change in width and TOA as shown in figure 4-7 for the 103° phase of figure 4-4. The corresponding phase space diagrams with and without RF distortion are shown in figure 4-8. While the reconstructed ion signal is only moderately altered, the energy-time structure is dramatically different for the two situations. This indicates the importance of handling the RF distortion properly.

Figure 4-9 illustrates a second data set measured under the same transport conditions but with a much higher trap loading of about 2300 ions. The tails are a little more pronounced and the fits a little noisier due to the large ion cloud (about 8 mm in diameter). The parameters for this and the remaining fits are summarized in table 4-1. The accompanying sensitivity plot in figure 4-10 shows the choice of temperature to be less sensitive but still certainly within the illustrated bounds, hence, kT (2300±300) = 0.75±0.10 eV.

---

† The extraction field components and their relative contributions are described in the appended reference.

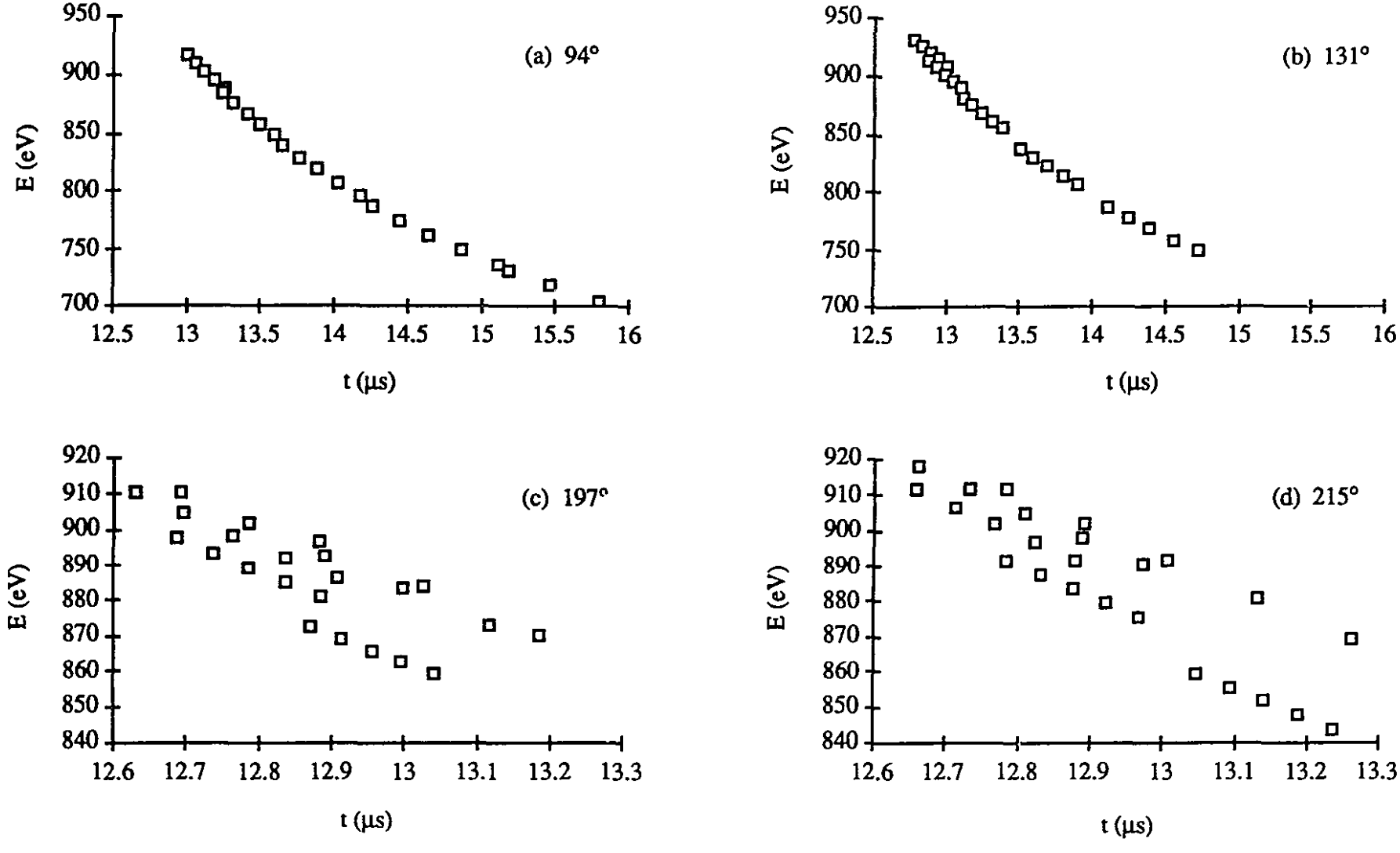

Figure 4-6: Axial phase space diagrams (energy versus time) for 0.25 eV temperature ion clouds extracted at 200 V. (a) 94°; (b) 131°; (c) 197° (time focus; (d) 215°. (Continued on next page).

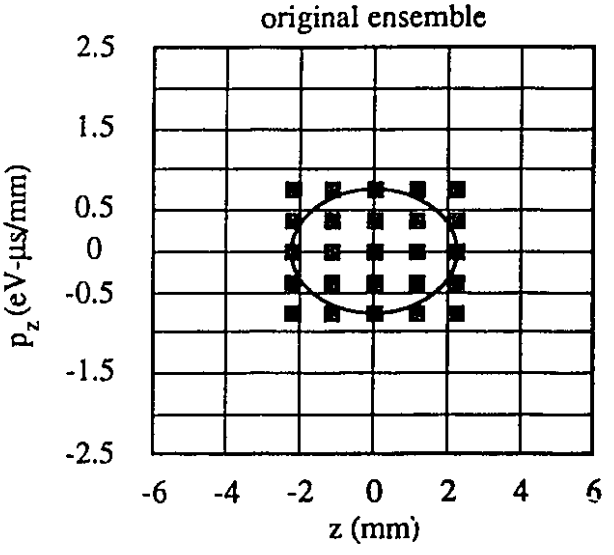

(e)

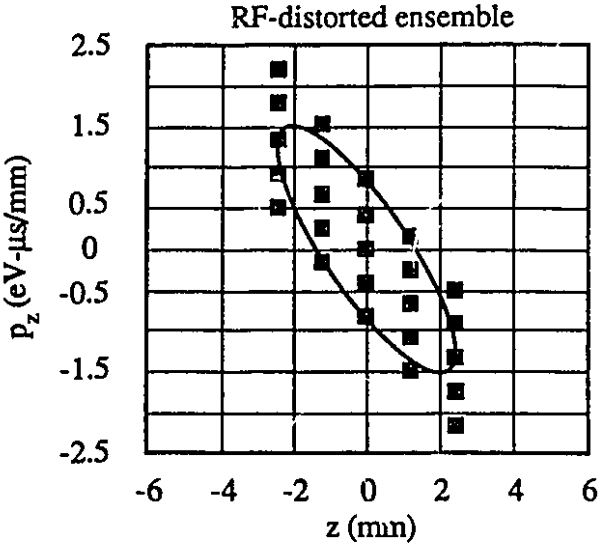

(f)

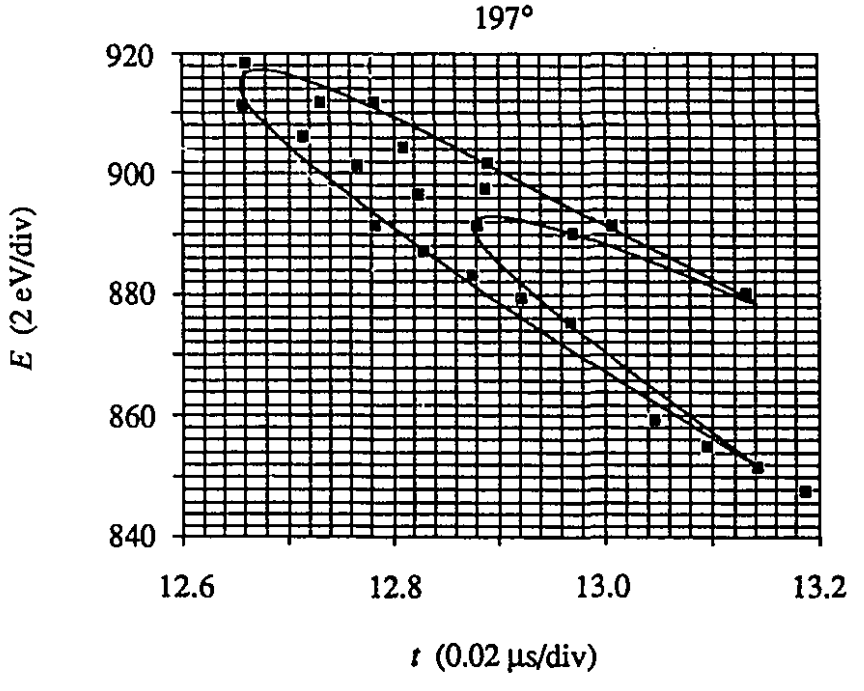

(g)

Figure 4-6 (continued): (e) shows the original ion ensemble representation of the axial phase space and (f) illustrates the correction for the rf-distortion of the original ensemble. (g) is a subdivided plot of the axial phase space diagram of (c). Each square in this diagram represents a phase space area of 0.04 eV-μs. the number of squares enclosed by the ellipse fit to the ensemble is roughly 135 giving a total phase space area of about 5.2 eV-μs.

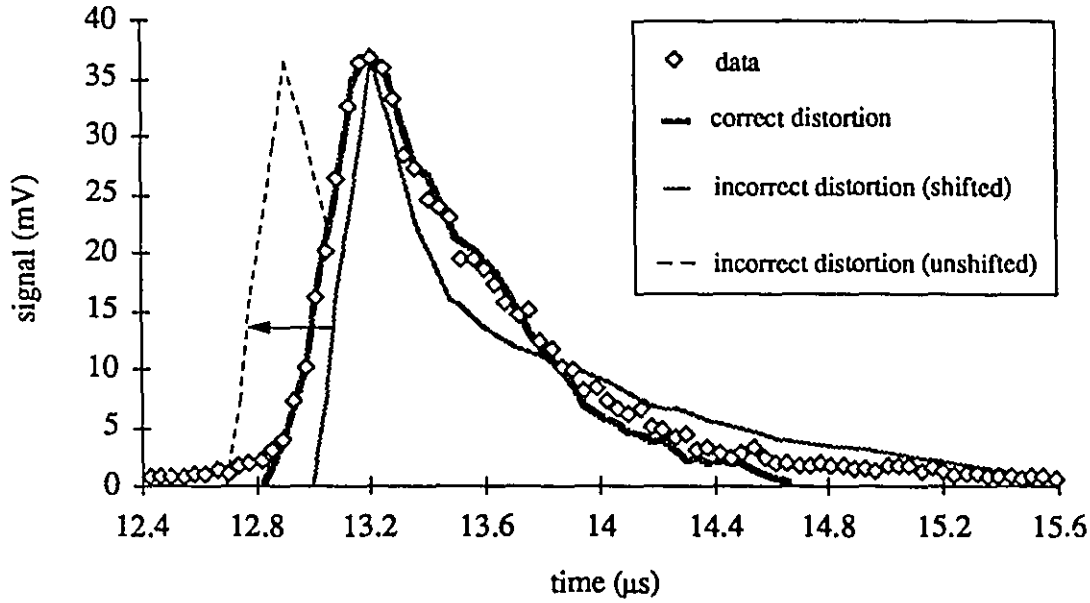

Figure 4-7: The effect of RF distortion of the 0.25 eV temperature fit.

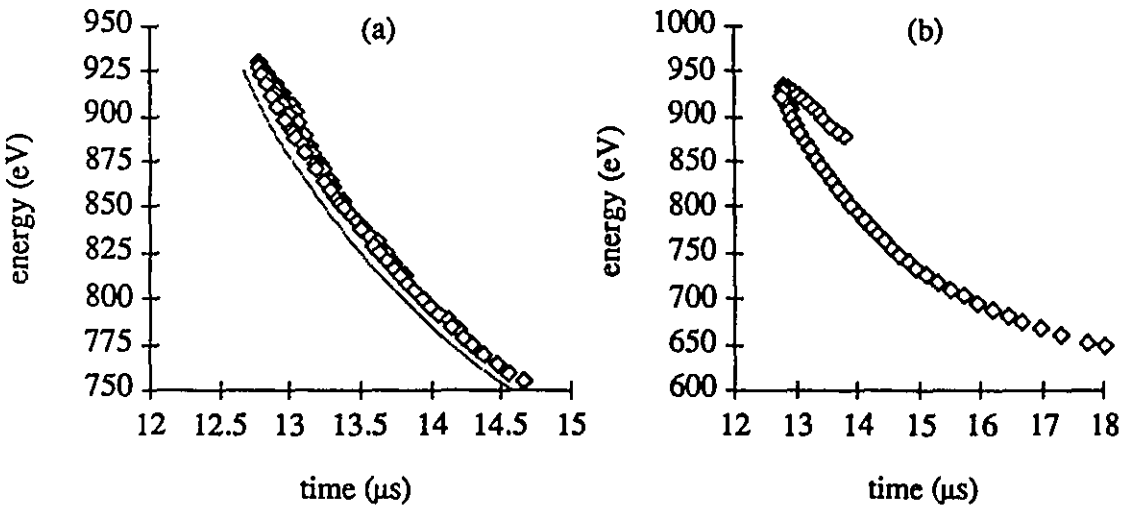

Figure 4-8: The effect of RF distortion on the phase space diagrams of the pulses shown in figure 4-7. (a) correct RF-distortion; (b) incorrect RF-distortion.

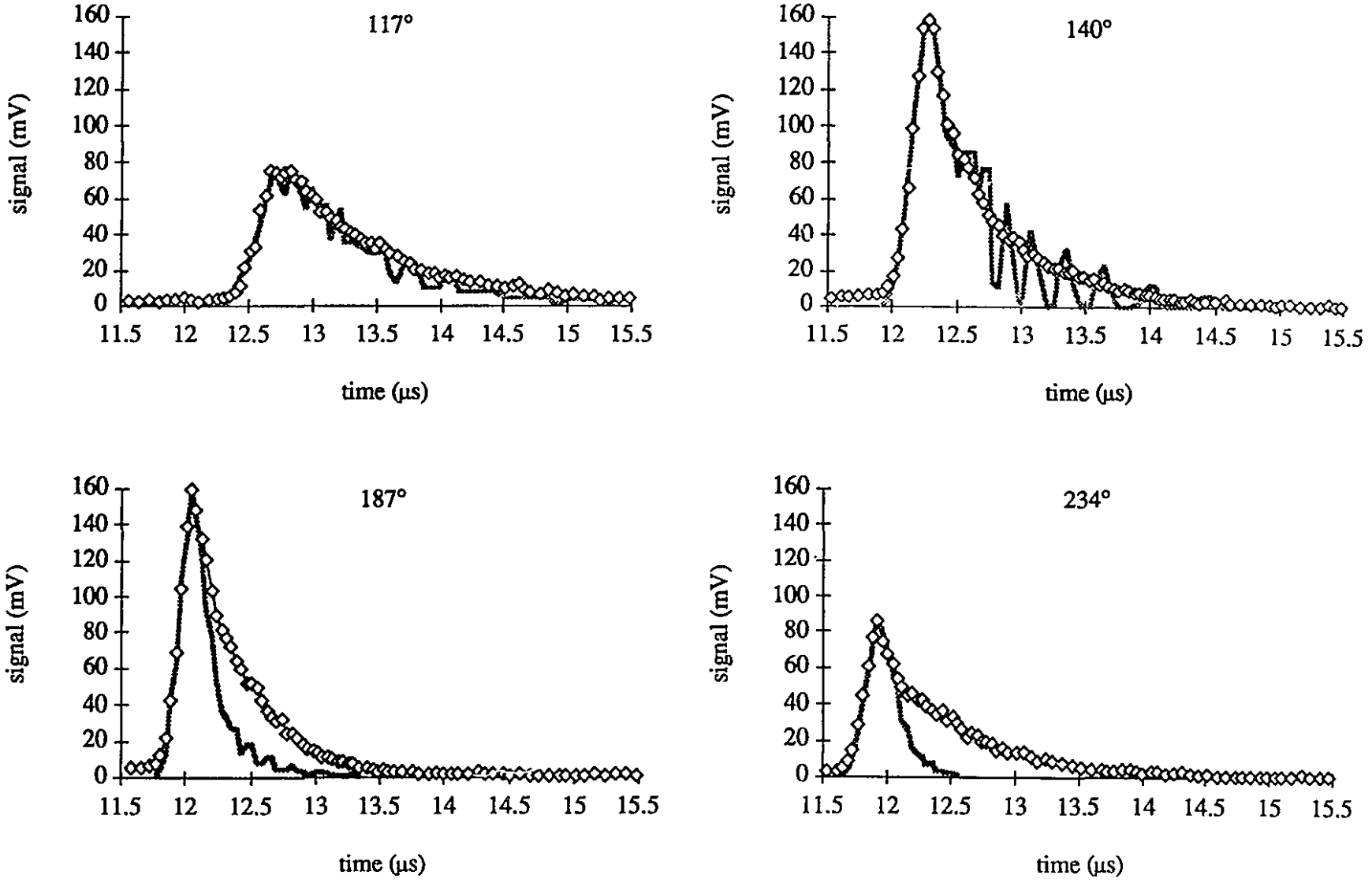

Figure 4-9: Intensity versus time signals for 2300 K ions fit with a temperature of 0.75 eV.

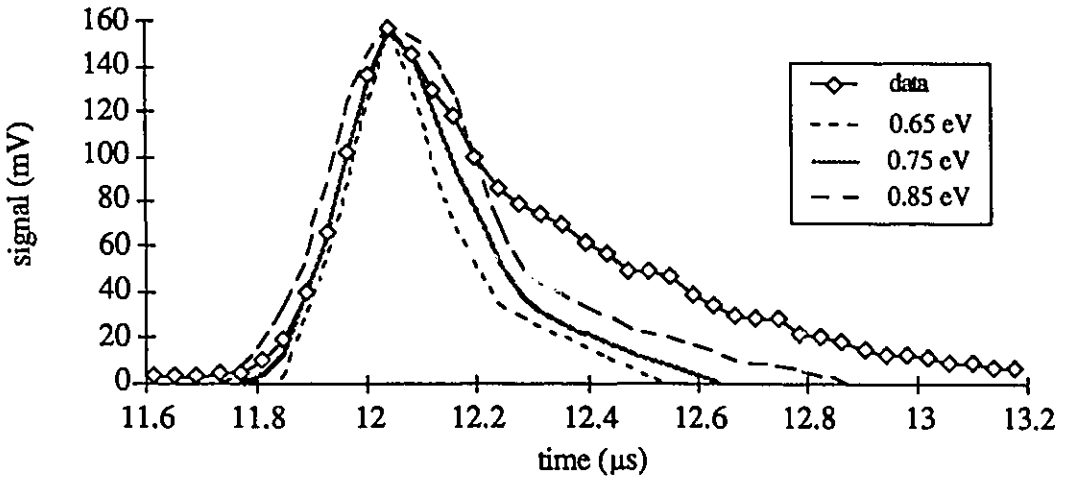

Figure 4-10: Sensitivity of the 0.75 eV temperature fit to the measured ion intensity signal.

Figure 4-11 (page 51) illustrates a data set with a much lower trap loading of about 80 ions. The temperature used for this fit was kT (80±30) = 0.125±0.04. Figure 4-12 (page 52) shows a data set measured for the lowest possible detected ion signal. Though the data are quite noisy away from the time focus, a good fit of kT (15±5) = 0.05±0.02 eV was obtained with the limits shown by the sensitivity curves of figure 4-13.

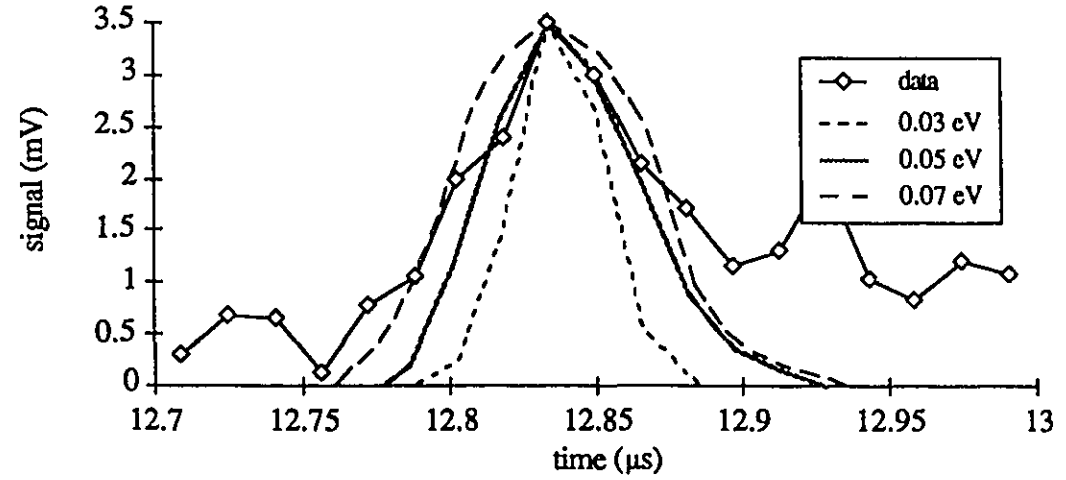

Figure 4-13: Sensitivity of the 0.05 eV temperature fit to the measured ion intensity signal.

Another data set for a moderate trap loading of about 400 ions is presented figure 4-14 (page 53). In this case, we get kT (400±100) = 0.20±0.10 eV with TOA agreement also less than 1%. One aspect of the fits common to each case is the slightly poorer fit at later extractions, *i.e.*, after

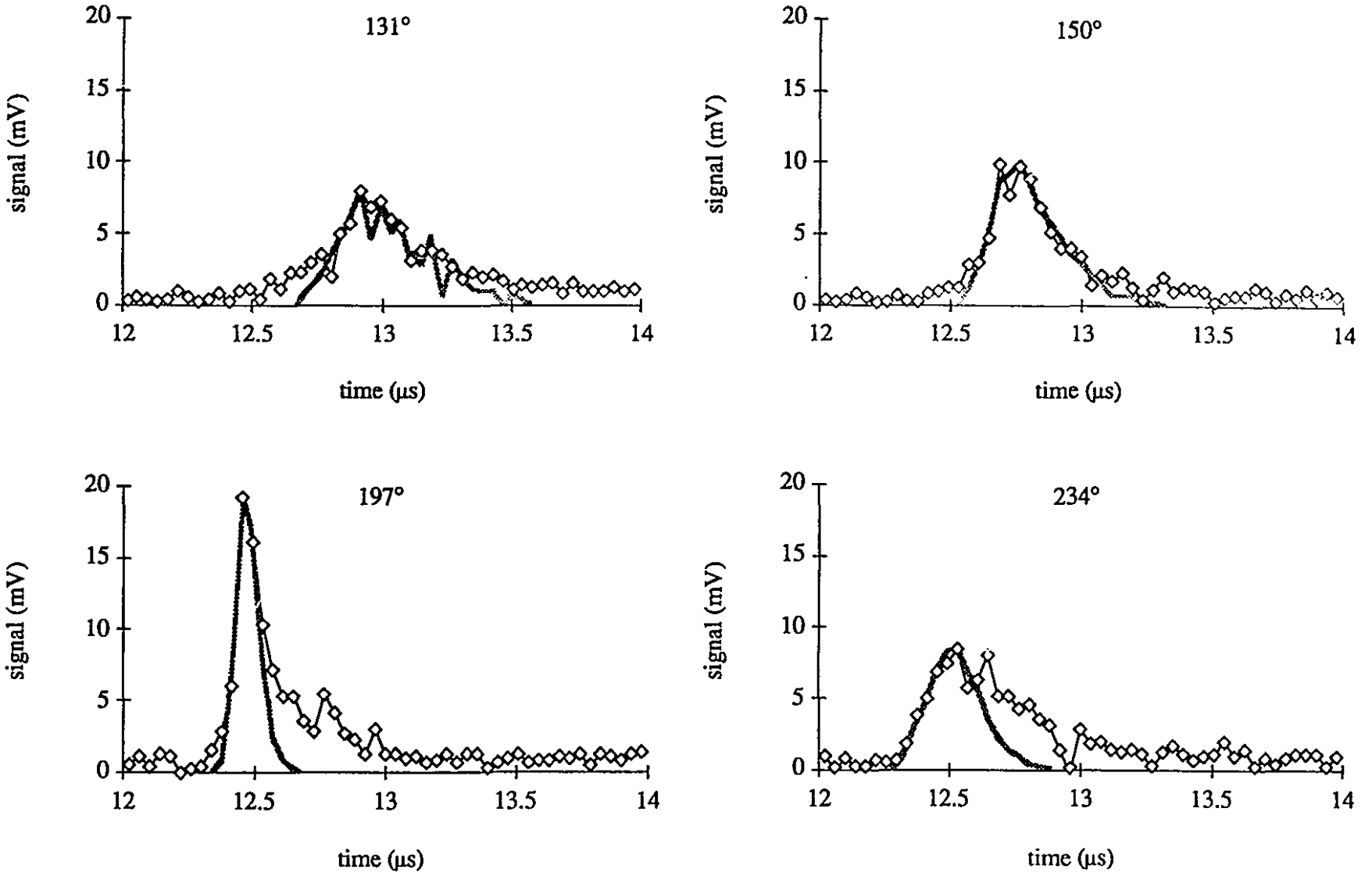

Figure 4-11: Intensity versus time signals for 80 K ions fit with a temperature of 0.125 eV.

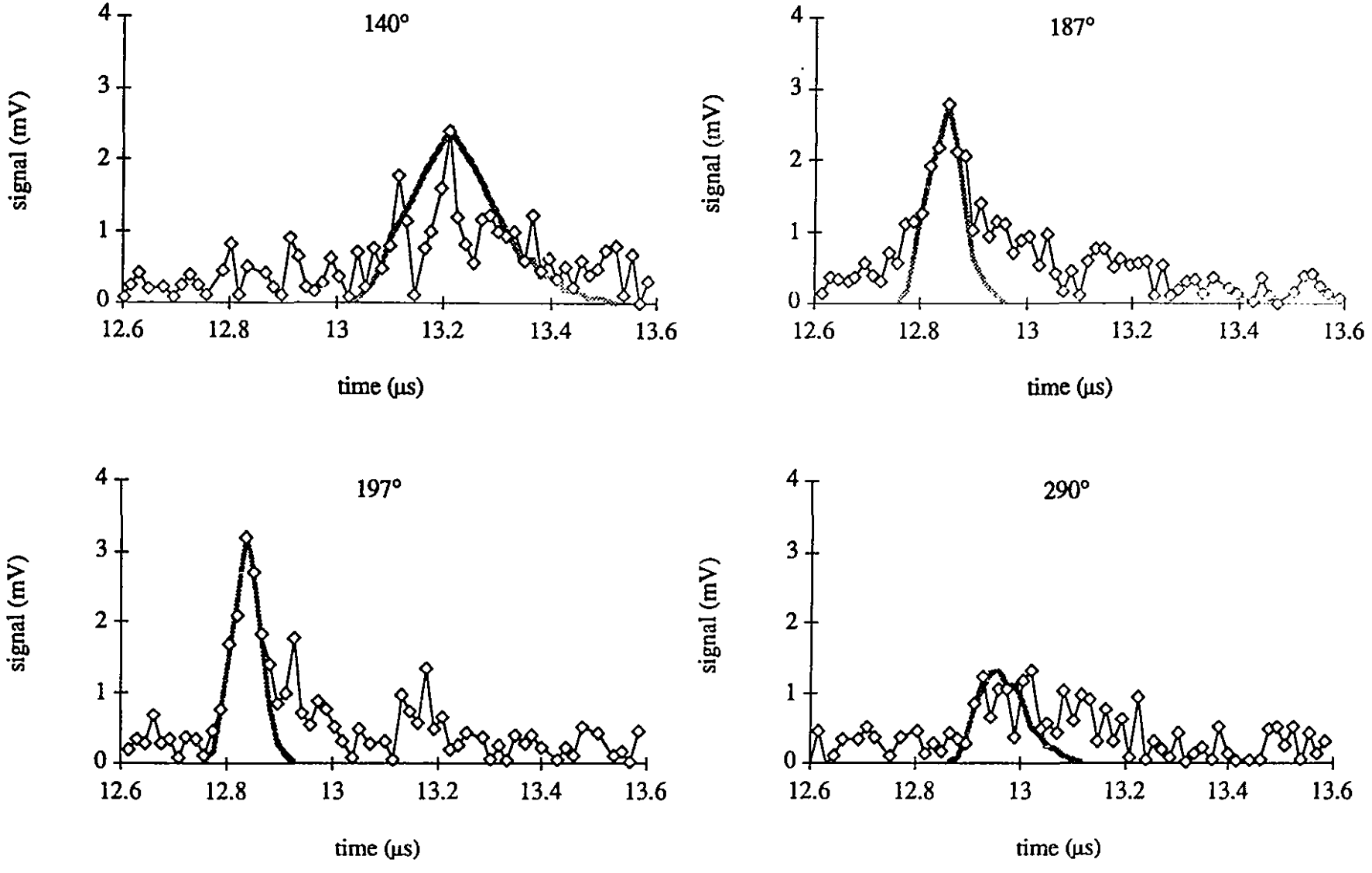

Figure 4-12: Intensity versus time signals for 15 K ions fit with a temperature of 0.05 eV.

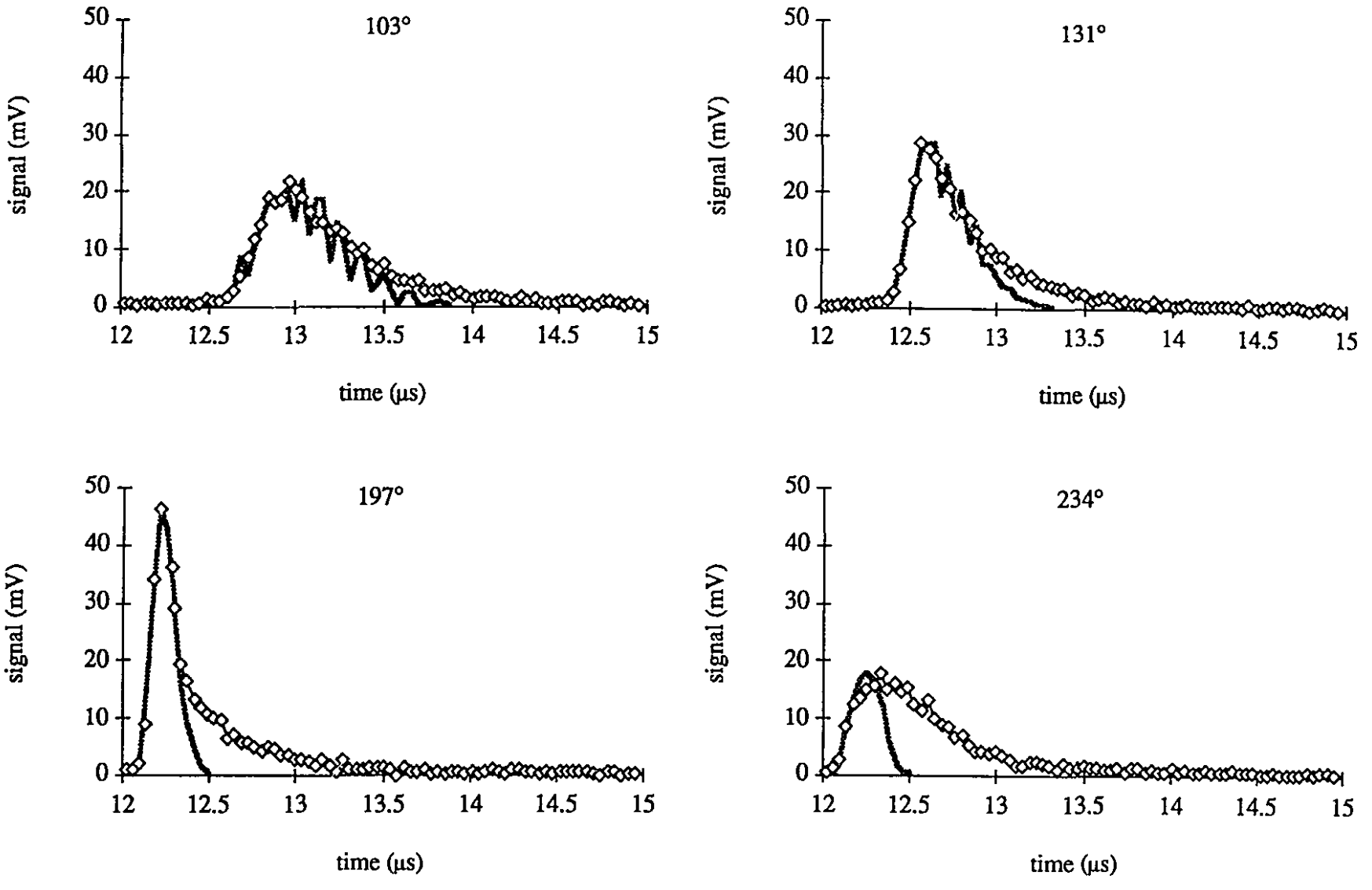

Figure 4-14: Intensity versus time signals for 400 K ions fit with a temperature of 0.20 eV.

the time focus. This is explained by the mesh aberration problem mentioned above which is exacerbated at late-phase extractions due to the axial defocusing effect of the RF field. At this instant the electric field is pointing from the endcaps to the ring, *i.e.*, away from the axis.

Two other data sets for mass 39 extracted at 200 V are shown in figures 4-15 and 4-16. These two signals correspond to the equilibrium curves presented earlier in the chapter. They were extracted at 197° only and were fit with temperatures of 0.125±0.04 eV and 0.06±0.02 eV for ion clouds numbering 120±30 and 20±10, respectively.

Having presented ion cloud temperature measurements for several trap loadings, the systematic variation of temperature versus number of ions can be explored. As discussed in chapter 2, the buffer gas, while cooling the ion cloud, also introduces friction that makes the macromotion incoherent. Vedel [VED] has pointed out that, in principle, trapped ions should be cooled to the temperature of the buffer gas itself but only in the absence of RF heating in which case the ion temperature is increased. RF heating arises from the space charge repulsion of the ion cloud that causes larger clouds to oscillate in regions of higher RF field. The larger velocities resulting from the higher field increase the chance of collision with buffer gas atoms, destroying the coherent motion and thermalizing the cloud. Therefore, the increase in the ion cloud temperature above the buffer gas temperature should depend on the amount of heat absorbed from the RF field. For this reason, the temperature of the buffer gas (assumed to be at room temperature of 0.025 eV) must first be subtracted from the measured temperatures.

The fit temperatures of the above seven cases with the buffer gas temperature subtracted off are plotted versus ion number in figure 4-17 on a log-log plot. A simple linear fit was made to the data that produced a slope of 0.63. The temperature error bars were estimated from the fit variations such as illustrated by figure 4-5. The ion number error bars are estimated from the integration of the measured peaks as compared to single ion signals. Some allowance was made for the tail produced by large ion signals and the error estimation is conservative.

Certainly, there is a lingering question concerning the absolute number of trapped ions versus the number detected. The transport system has a somewhat low transmission which is difficult to measure for pulsed beams. From DC beam measurements the transmission was found to be about 5% but it is difficult to extrapolate from well behaved DC beam emittances to the distorted and dynamic emittances of trapped ion beams. A transmission of 1% would yield an ion cloud numbering about 250,000 for the largest signal that could be obtained (the 0.75 eV case). This number of ions closely corresponds to an experimentally observed maximum by Moore and Gulick [MGU] who worked with the same ion trap.

Four data sets are now presented for 200 V extraction of sodium (mass 23) ions. These figures are accompanied by a fitting parameter summary in table 4-2 (page 58). In these cases an RF voltage of 300-350 V was used that, for the lighter mass, gives roughly the same Mathieu

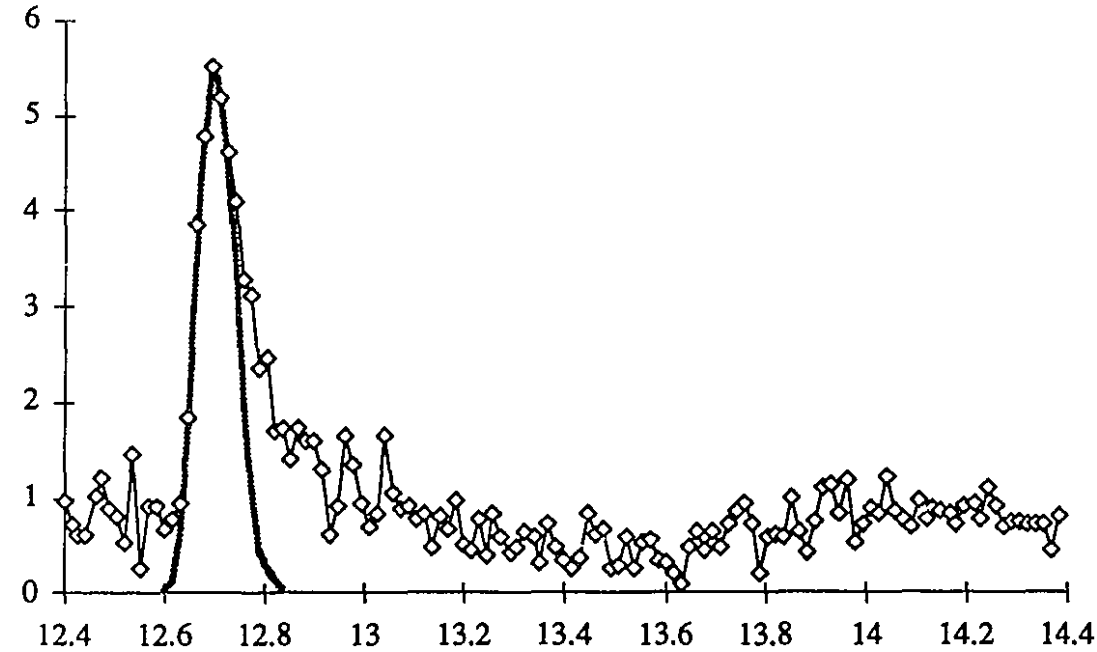

Figure 4-15: Intensity versus time signal for 20 K ions fit with a temperature of 0.06 eV.

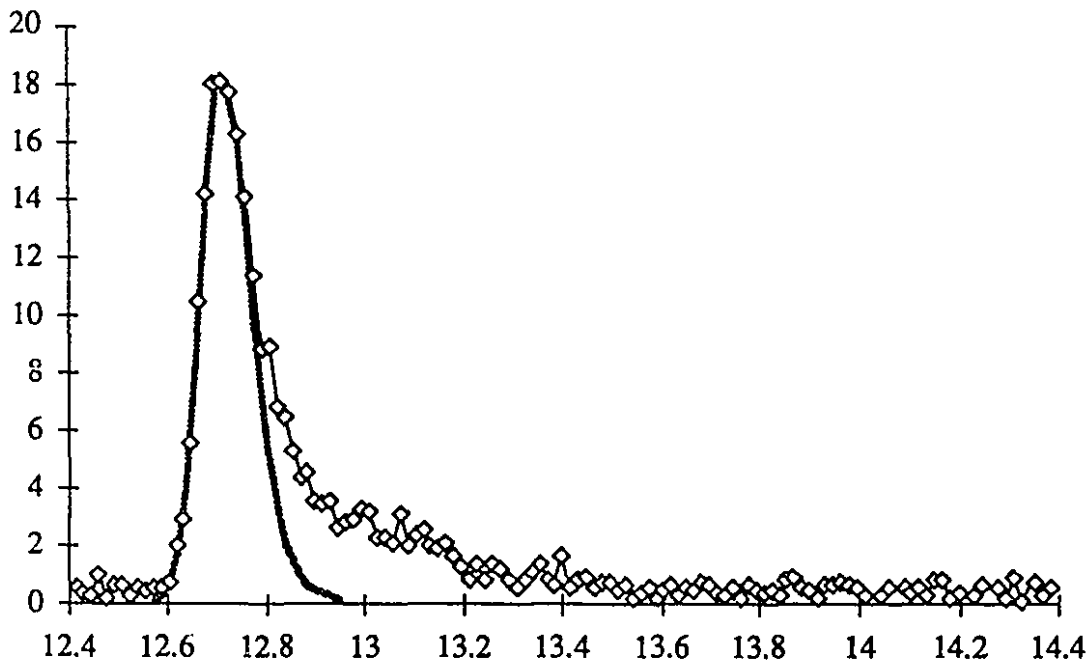

Figure 4-16: Intensity versus time signals for 120 K ions fit with a temperature of 0.125 eV.

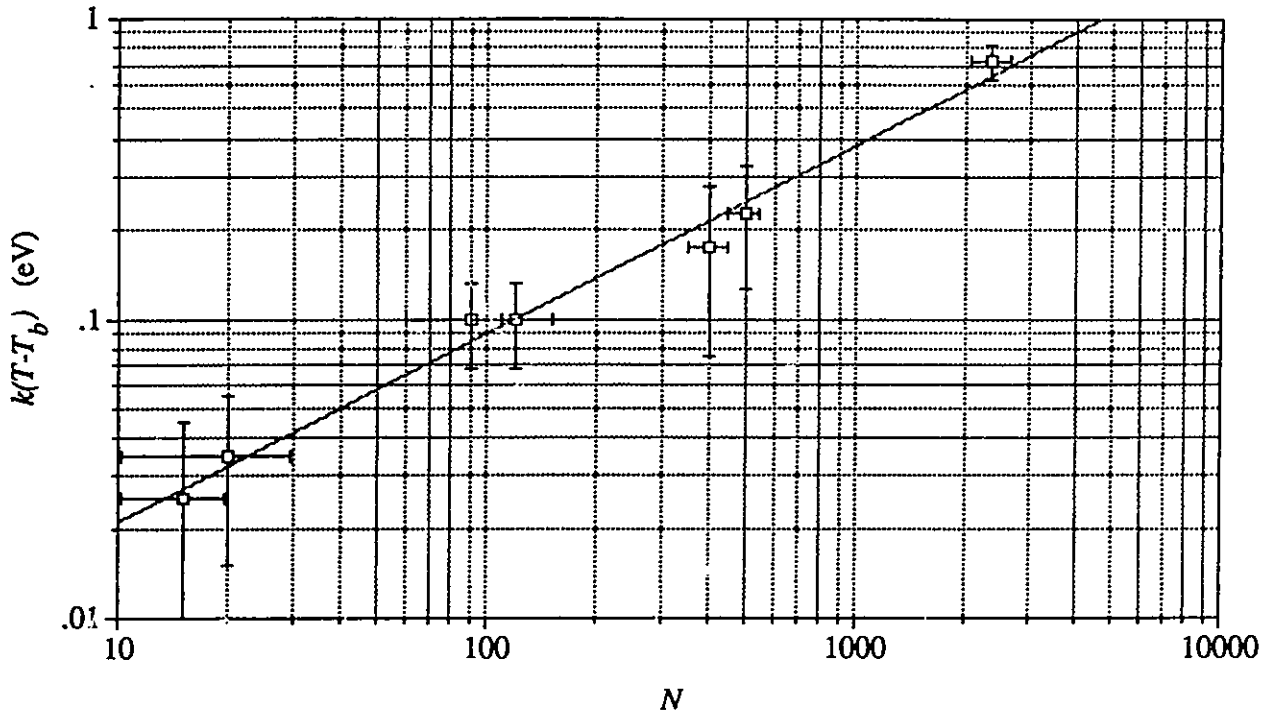

Figure 4-17: Log-log plot of ion temperature above buffer gas temperature versus ion number for potassium ion clouds extracted at 200 V. The linear fit to the data has a slope of 0.63.

q-parameter as for mass 39 with an RF voltage of 400-500 V. The various TOAs are noticeably shorter for the lighter mass which is expected. Also the phase at which a time focus is obtained has shifted which is also expected due to the different mass. Figure 4-18 illustrates four phases for a cloud of 5000±500 ions fit with a temperature of 0.60±0.10 eV. Figure 4-19 shows four phases fit such that kT (1200±200) = 0.25±0.10. The remaining two cases for mass 23 are shown in figure 4-20, for which kT (180±30) = 0.10±0.04 and figure 4-21, for which kT (25±10) = 0.05±0.02. For each trap loading and for each extraction phase, the time-of-flight measurement is reproduced by the simulation to within 2%.

The ion cloud-buffer gas temperature difference is plotted versus ion number on a log-log scale for the mass 23 case in figure 4-22. The straight line fit to the data in this case produced a slope of 0.59. The absolute position of the curve is slightly different from the mass 39 case due to the different transmission of the lighter mass however, the slope is roughly the same.

For the temperature versus ion number experiments, the transmission parameters were kept constant so the different loadings could be directly compared.. In order to further verify the agreement of the simulation program with experimental measurements, the extraction voltage was also varied. Illustrated in figure 4-23 (page 65) are the measurements and fits (at four extraction phases) for an extraction voltage of 300 V (all previous cases were extracted at 200 V). One notices that the phase at which a time focus occurs has shifted from 196° to 229°. In figure 4-24 (page 66), measurements and fits are plotted for four RF phases extracted at 100 V. In this case, a different time focus phase of 328° is observed. The fit parameters for these cases are listed in table 4-3. Due to the different transmission caused by varying the extraction voltage, it is difficult to compare the ion temperatures for these trials.

Table 4-3: Fit parameters for $^{39}K^+$ ions for three extraction voltages. The 200 V extraction case has been reproduced from table 4-1 for comparison. In each case the RF frequency is 0.65 MHz with no DC voltage on the ring and the RF amplitude is 512.5 V yielding a macromotion frequency of 198 kHz, a Mathieu q-parameter of 0.74 and a well depth of 64 eV. The RF distortion parameters are 1.2/-0.5. The trap potential is 800 V and the ramp cavity potential is 200 V in each case.

ext. voltage (V)	100	200	300
ion temp. (eV)	0.1	0.2	0.2
number of ions	350	400	250
initial z (mm)	± 0.98	± 1.38	± 1.38
initial E (eV)	± 0.3	± 0.6	± 0.6
$z \times E$ array	9 × 15	13 × 13	7 × 17
ext. cav. pot. (V)	700	600	500
tof agreement (%)	0.9	0.9	1.3
figure	4-24	4-14	4-23

Though the phase at which ions are extracted changes with extraction voltage, the time taken for the ions to leave the trap (t_e) also changes. This implies that the ion cloud experiences

Table 4-2: Fit parameters for $^{23}Na^+$ ions extracted at 200 V. In all cases RF frequency is 0.65 MHz with no DC voltage on ring.

ion temp. (eV)	0.60 ± 0.1	0.25 ± 0.1	0.10 ± 0.04	0.05 ± 0.2
number of ions	5000 ± 500	1200 ± 200	180 ± 30	25 ± 10
initial z (mm)	$\pm$ 1.88	$\pm$ 1.21	$\pm$ 0.57	$\pm$ 0.40
initial E (eV)	$\pm$ 1.8	$\pm$ 0.75	$\pm$ 0.30	$\pm$ 0.15
$z \times E$ array	11×11	11×11	9×9	9×9
RF-V (V_{op})	300	300	350	350
f_o (kHz)	195	195	262	262
q parameter	0.73	0.73	0.86	0.86
well depth D (eV)	37	37	67	67
RFD (coef/slope)	1.2/-0.5	1.2/-0.5	1.3/-0.55	1.3/-0.55
trap potential (V)	800	800	800	800
ext. cav. pot. (V)	600	600	600	600
ramp cav. pot. (V)	200	0	200	200
tof agreement (%)	1.2	2.8	0.5	0.2
S_z (eV-μs)	5.3	2.2	0.4	0.1
figure	4-18	4-19	4-20	4-21

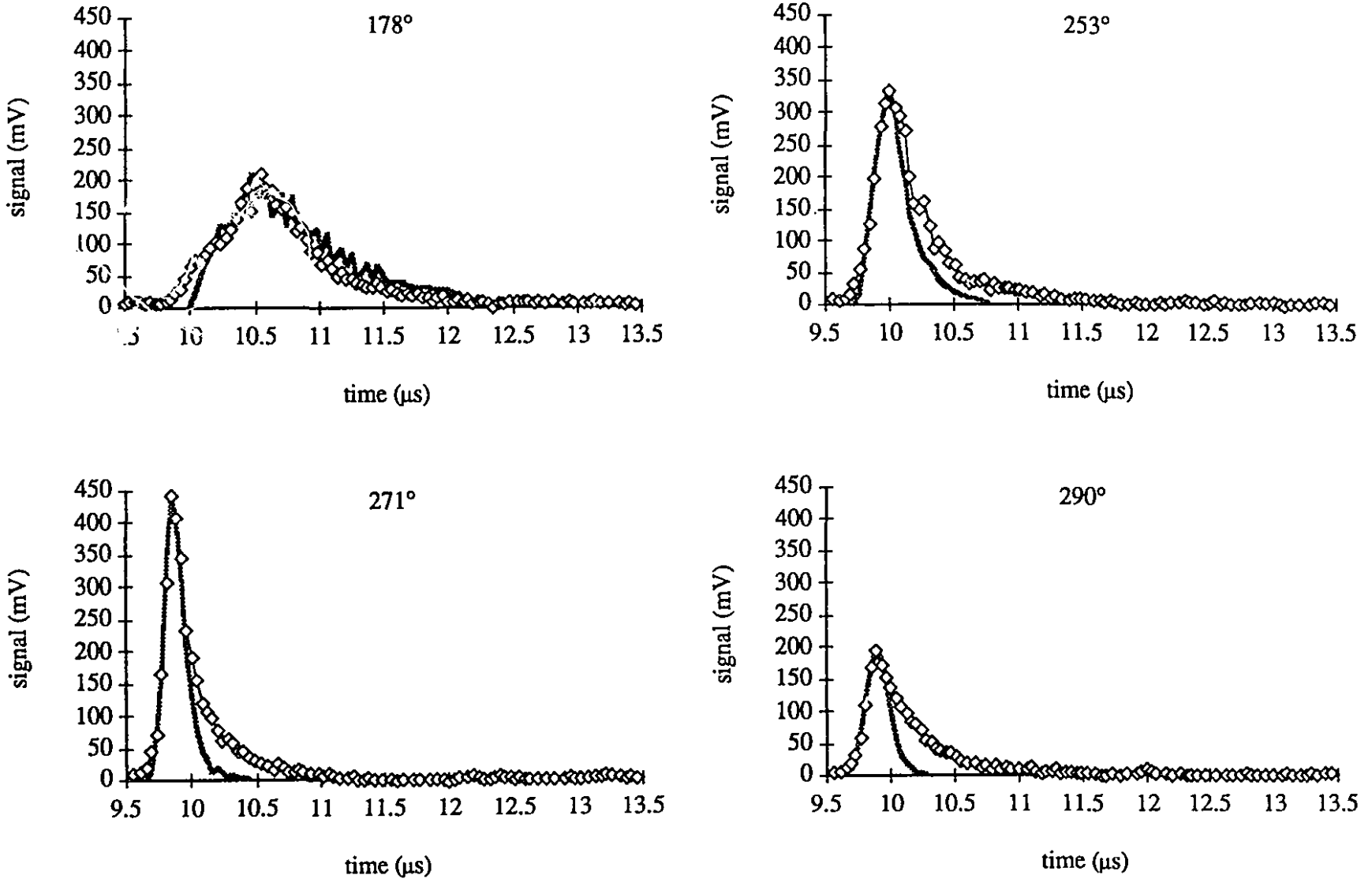

Figure 4-18: Intensity versus time signals for 5000 Na ions fit with a temperature of 0.6 eV.

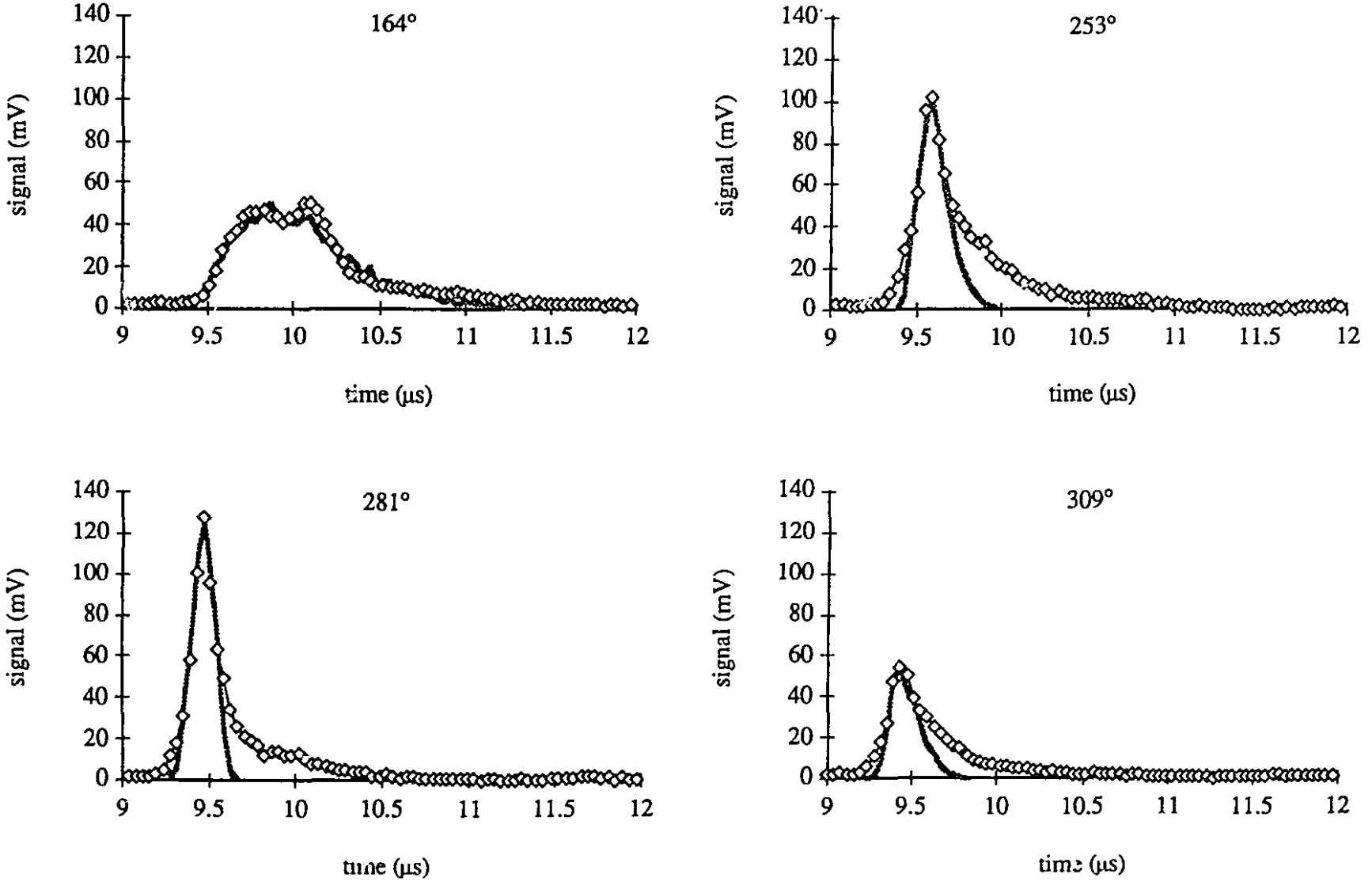

Figure 4-19: Intensity versus time signals for 1200 Na ions fit with a temperature of 0.25 eV.

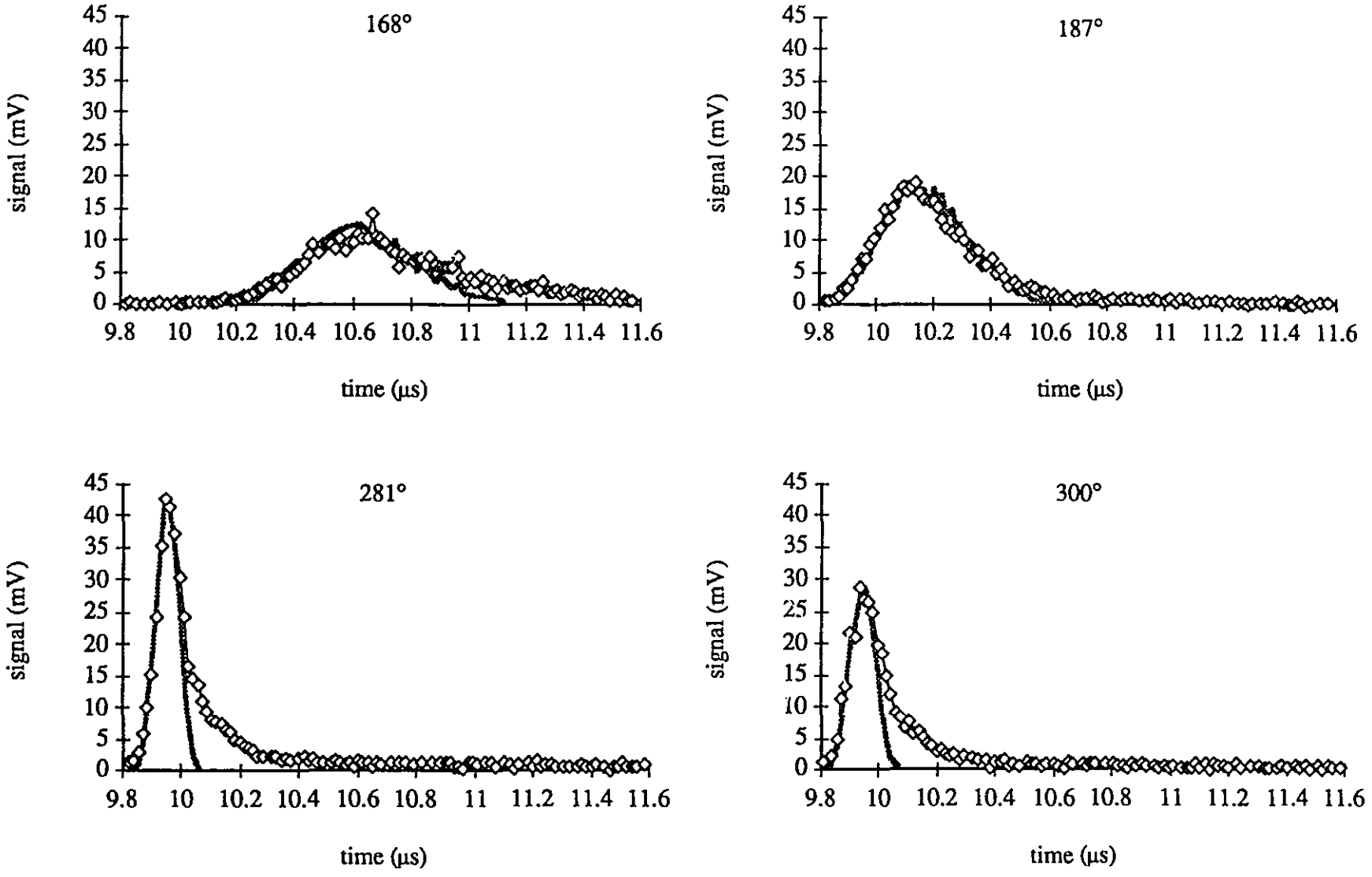

Figure 4-20: Intensity versus time signals for 150 Na ions fit with a temperature of 0.06 eV.

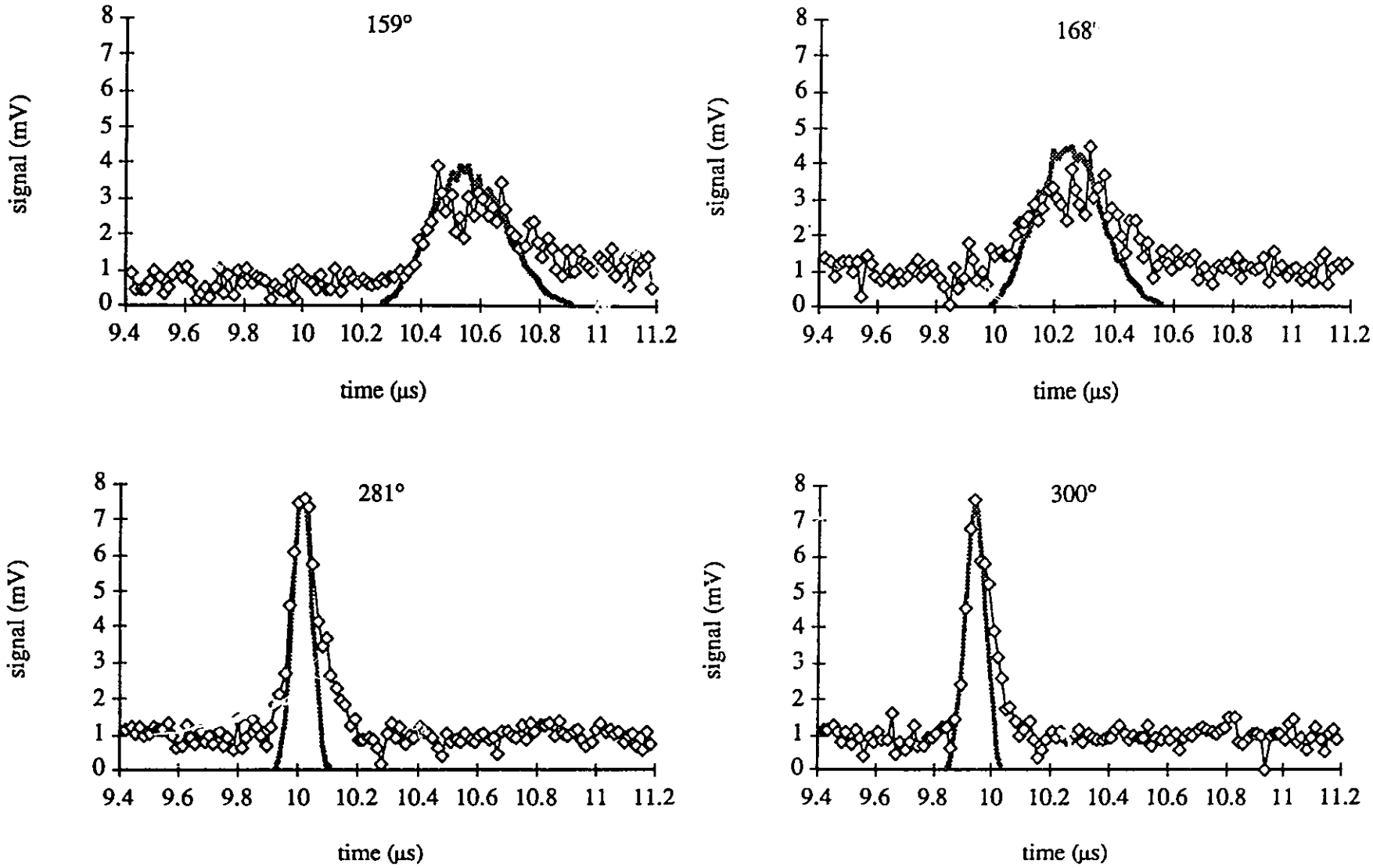

Figure 4-21: Intensity versus time signals for 25 Na ions fit with a temperature of 0.05 eV.

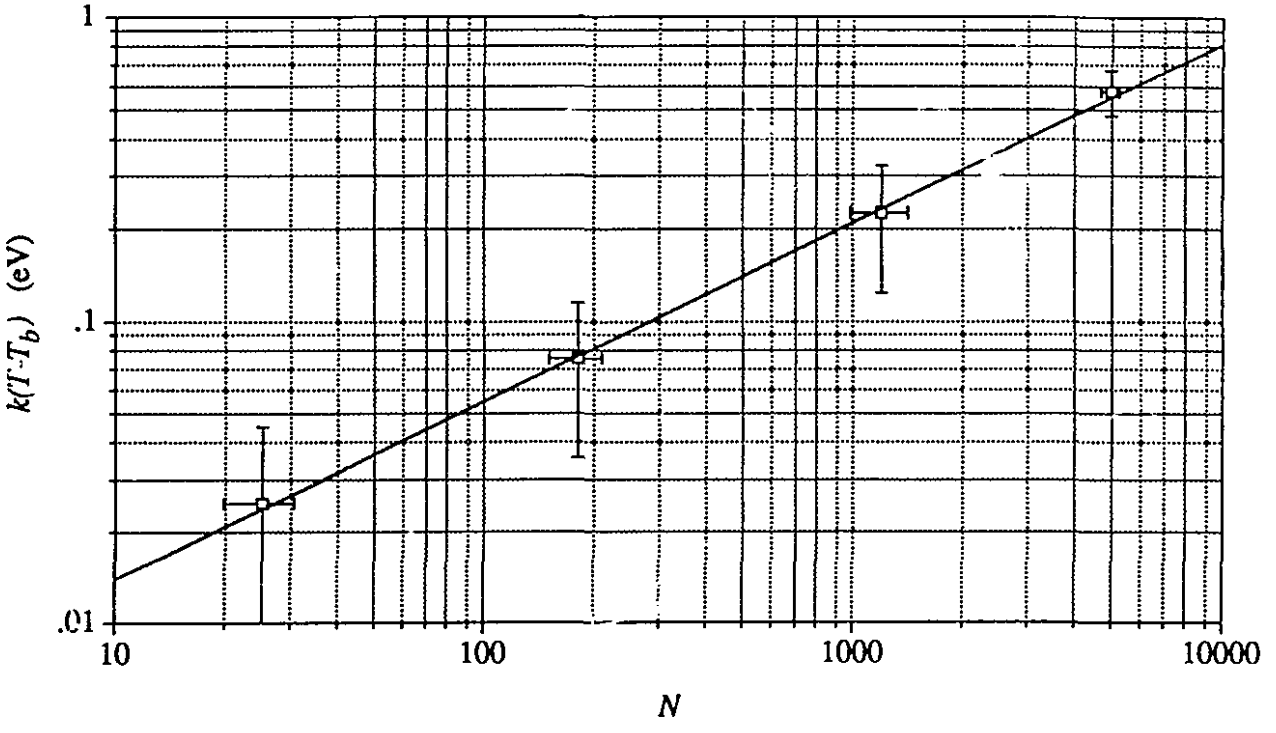

Figure 4-22: Log-log plot of ion temperature above buffer gas temperature versus ion number for sodium ion clouds extracted at 200 V. The linear fit to the data has a slope of 0.59.

the same RF field as it reaches the trap endcap. Listed in table 4-4 are the ion extraction durations (time taken to extract the ions from the trap) t_{ext} as calculated by the simulation program for the three extraction voltages V_{ext}. These times are also converted to degrees of RF phase (at 650 kHz, 360° = 1.5385 μs). The results show that for a time focus the ions reach the endcap at roughly the same phase of the RF field for each extraction voltage used. This is established by adding the RF extraction phase (ϕ_{ext}) to the extraction duration (t_{ext}) in degrees for each extraction voltage. As seen in the last column of table 4-4, the ions reach the endcap on the same part of the RF cycle for all three extraction voltages indicating the preferred RF phase for a time focus.

Table 4-4: Extraction voltage, corresponding RF phase, and extraction duration. The trap driving frequency is 0.65 MHz giving a period of 1.5385 μs.

V_{ext} (V)	ϕ_{ext} (°)	t_{ext} (μs)	t_{ext} (°)	$[t_{ext}+\phi_{ext}]$ mod 360
100	328	2.25	525	133
200	197	1.26	295	132
300	281	0.96	225	146

Another interesting phenomenon is evident from the 100 V extraction pulses in figure 4-24. For earlier extraction phases, multiple peaks can be seen in the ion signals. This behavior only occurred at an extraction voltage of 100 V. This is due to the ions not all being extracted during the same RF cycle. Note from the extra bumps in the fit that the simulation program also picks up some of the ions not fortunate enough to have escaped the trap at the first opportunity. Thus, two (or more) ion "sub-clouds" are detected for each extraction cycle.

Mather and Todd [MTO] hypothesized that, for complete extraction, an extraction voltage of 4 times the well depth would be needed. This is because of the superposition of the (mostly) dipole extraction potential on the parabolic pseudopotential well of the trap. For the parabolic well to be completely open at one endcap, an applied dipole extraction potential would have to be four times the well depth. This idea is illustrated in figure 4-25.

In practice, Mather and Todd found that only a voltage of between 2.5 and 3 times the well depth was needed, a conclusion reached in this work also. The well depth in our case is about 65 eV, thus requiring about 180 V of extraction voltage. Certainly, at 200 V extraction, all the ions were extracted cleanly. This is due to the extra "boost" the RF voltage gives the cloud on its way out of the trap. If the ion cloud feels the RF field at the right phase, it can actually be extracted from the trap with greater energy than the applied extraction field. Simulations indicate that for a 200 V extraction voltage and 500 V of RF field, ions are extracted with up to 350 V of

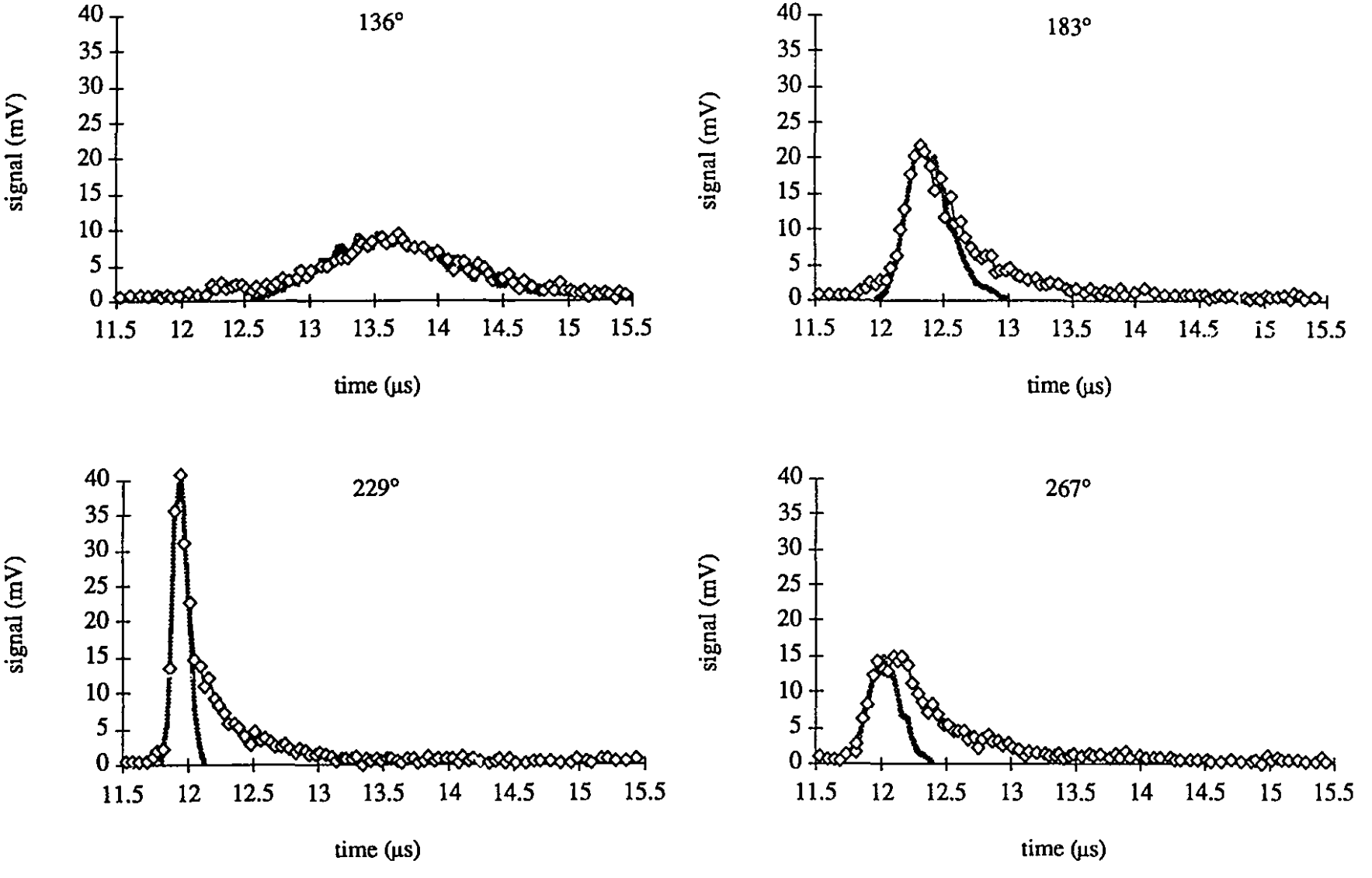

Figure 4-23: Intensity versus time signals for ions extracted with a voltage of 300 V.

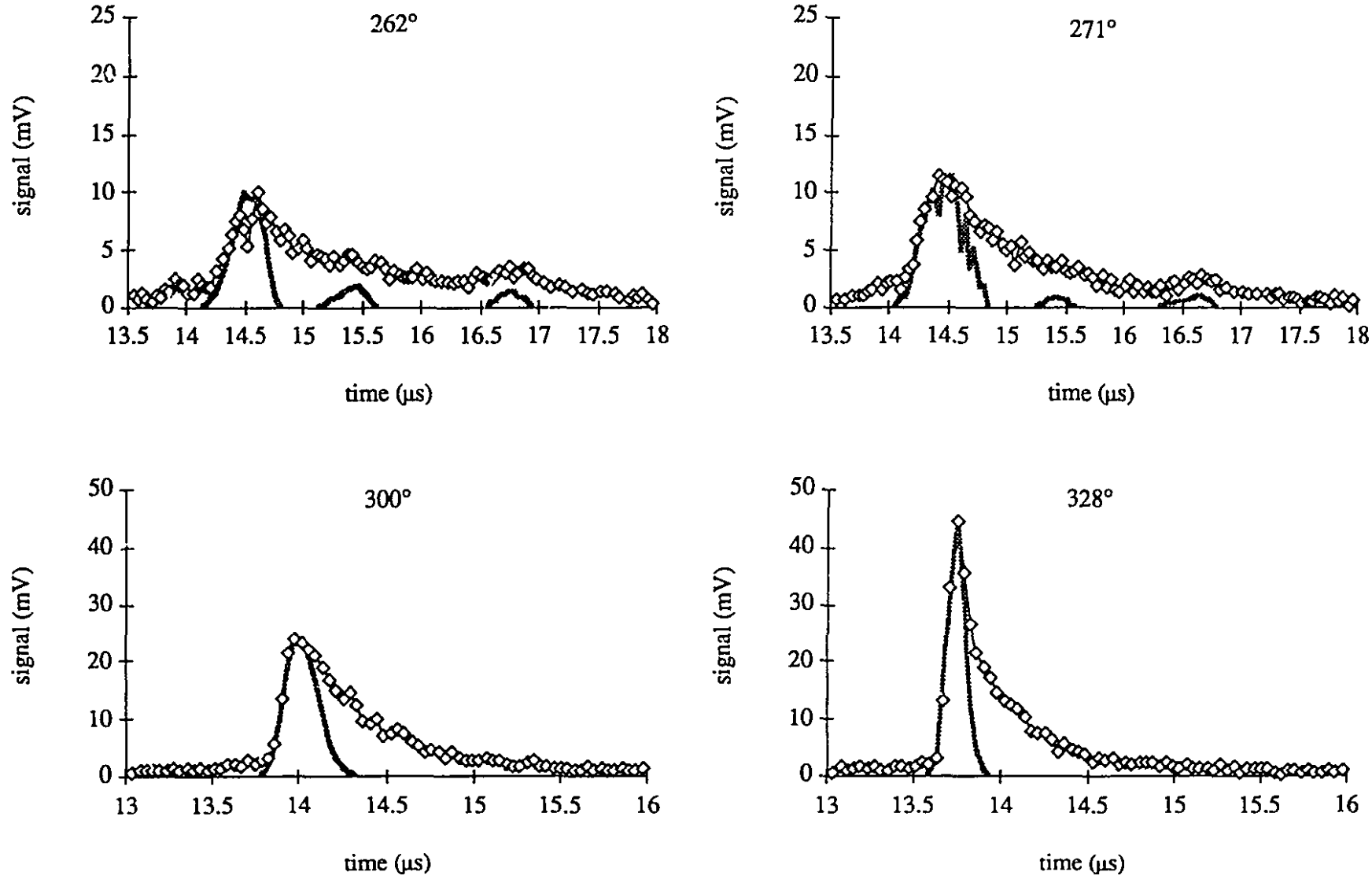

Figure 4-24: Intensity versus time signals for ions extracted at 100 V.

kinetic energy. This phase-dependent RF boost can also eject the ions the opposite directions [WTO]. This can cause uncertainty in the kinetic energy of the extracted beam which could possibly be avoided by switching off the RF voltage during extraction. This option has not been pursued due to the intention of building larger traps and operating them at much higher RF voltages (10 kV_{pp}). In such cases, the trap capacitance becomes such that switching high voltages in the required time (less than 100 ns) is impossible. Though severe, the effect of the RF on the extracted ion phase space volume can be modeled fairly accurately however.

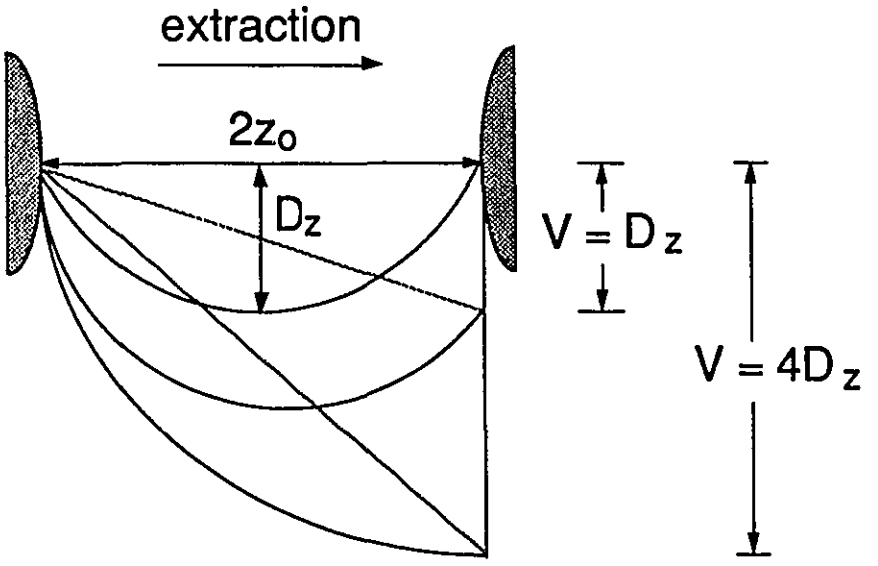

Figure 4-25: Axial potential distribution in a trap with well depth D when a pulse of amplitude V is applied to one endcap. Reproduced from [MTO].

C: DYNAMIC MANIPULATION OF PHASE SPACE

The Gibbs phase space model has provided excellent agreement with the measured time profiles and time of arrivals of extracted ion beams over the whole RF phase range for various extraction conditions and for different ion masses. The governing parameter of this model, the ion temperature, has systematically fit the measurements for ion clouds of various numbers. It is reasonable to assume, therefore, that the computed energy distributions arising from a particular choice of temperature, correspond to those actually present in the extracted ion cloud.

As it stands, the extracted cloud is not in a useful form; that is, its axial phase space is not suitable for transport to other apparatus. This is because of the large energy spread which: (1) makes injection into a mass-measuring Penning trap inefficient due to the long time spread that develops after transporting the cloud and (2) makes laser spectroscopy impossible due to the consequent doppler width

Injecting an extracted beam into a Penning trap is complicated by the phase space volume of the trap which renders the exercise similar to stuffing a letter inside an envelope: the letter must be folded in order to fit. This requires refocusing the beam in time so that it arrives at the Penning trap all at once. In order to ameliorate the second situation, the large energy spread of the extracted beam must be eliminated. Both of these feats may be realized by applying time-varying acceleration voltages as shown in figure 4-26.†

The phase space diagram of figure 4-26a will resemble figure 4-26b after drifting some distance as ions having a *higher* kinetic energy arrive at a given point *sooner* in time. By accelerating the high energy (early arrival) ions a little, and the low energy (late arrival) ions a lot, as in figure 4-26c, the phase space diagram is inverted (4-26d) and an axial time focus is effected after another drift segment as shown in figure 4-26e. (This is analogous to the transverse focusing example in figure 2-5.) By applying a less severe ramp voltage as in figure 4-26f, the same time-varying acceleration principle gives ions at different times a more uniform energy as in 4-26g. The ions then spread in time as in 4-26b but at a much lower rate as seen by 4-26h. Here, the large energy spread is transformed into a well-defined time spread in accordance with Liouville's theorem. Because real phase space diagrams are more complicated than in figure 4-26, the use of more complicated voltage-time waveforms may be necessary.

To demonstrate these effects, time of flight measurements were made with a voltage ramp applied to the ramp cavity (figure 3-2) as the ion bunch drifted through. The extraction cavity allowed the bunch to acquire some time spread so a ramp of feasible duration could be applied. Energy spreads of roughly 100 eV were predicted, but a ramp generator of 100 V in anything less than 1 μs was extremely difficult to build. Therefore, the ions had to be transported through the extraction cavity at such an energy as would yield a time spread of not less than 1 μs. This was difficult to do as the overall transmission was compromised by this requirement. A trade-off had to be made which rather lessened the effect of the voltage ramp on the measured time profile.

Results of this experiment are shown in figures 4-27 and 4-28. Figure 4-27 shows the measured pulses with the corresponding fits for voltage ramps of -100, 0 and +100 V/μs. There is a small bump in the measured signal due to the fact that the width of the pulse was actually wider than that of the ramp. The leading edges and TOAs of these measurements are all fit extremely well. The fit parameters are listed in table 4-5a. In these studies the ion transmission was quite poor which explains the rather large temperature required to fit the detected ion clouds of relatively small number. The measurement is difficult because the ramp must be triggered such that the center of the ion pulse crosses the cavity gap at roughly the midpoint of the ramp.

---

† Again, the discussion is restricted to the axial phase space component since it is mostly this component affected by the extraction process.

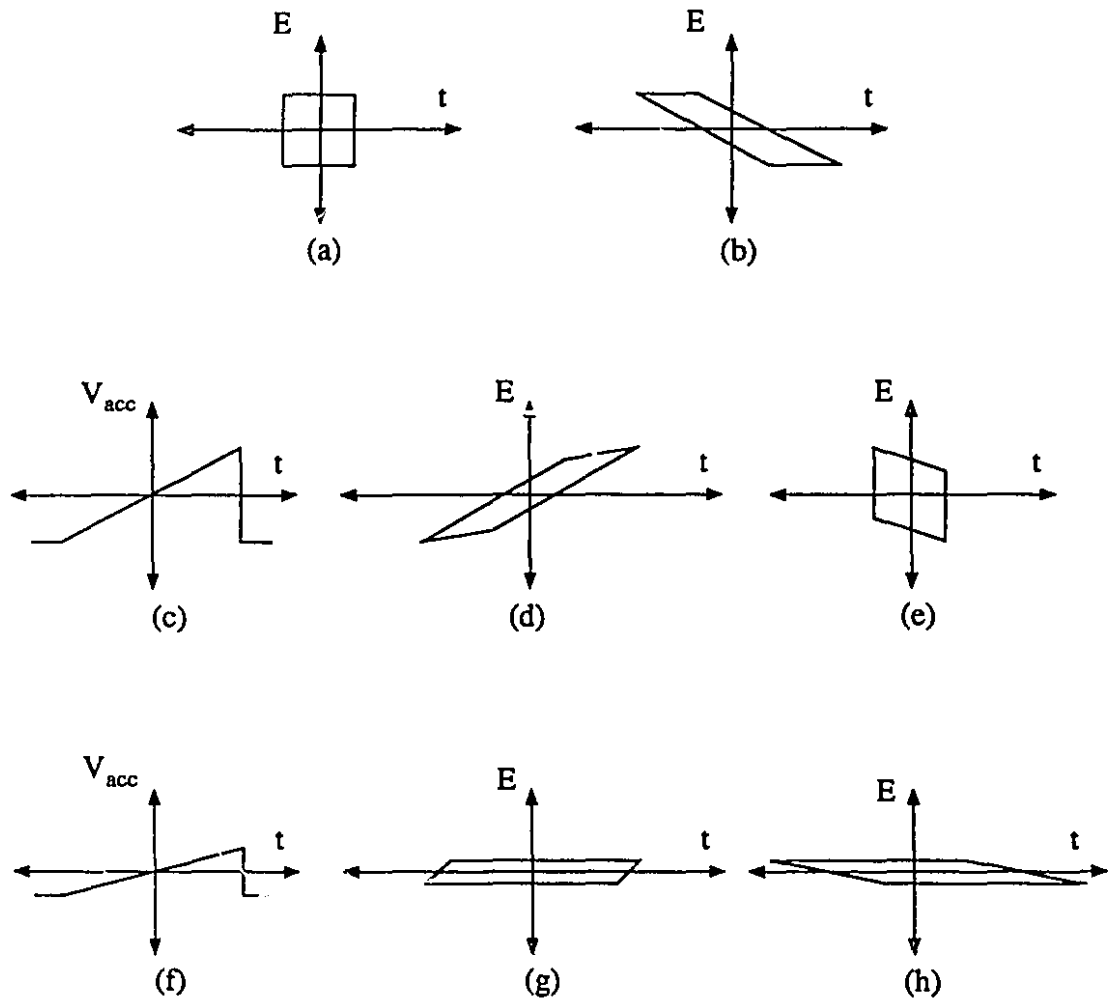

Figure 4-26: Illustration of phase space manipulation using a voltage ramp. Details are discussed in the text.

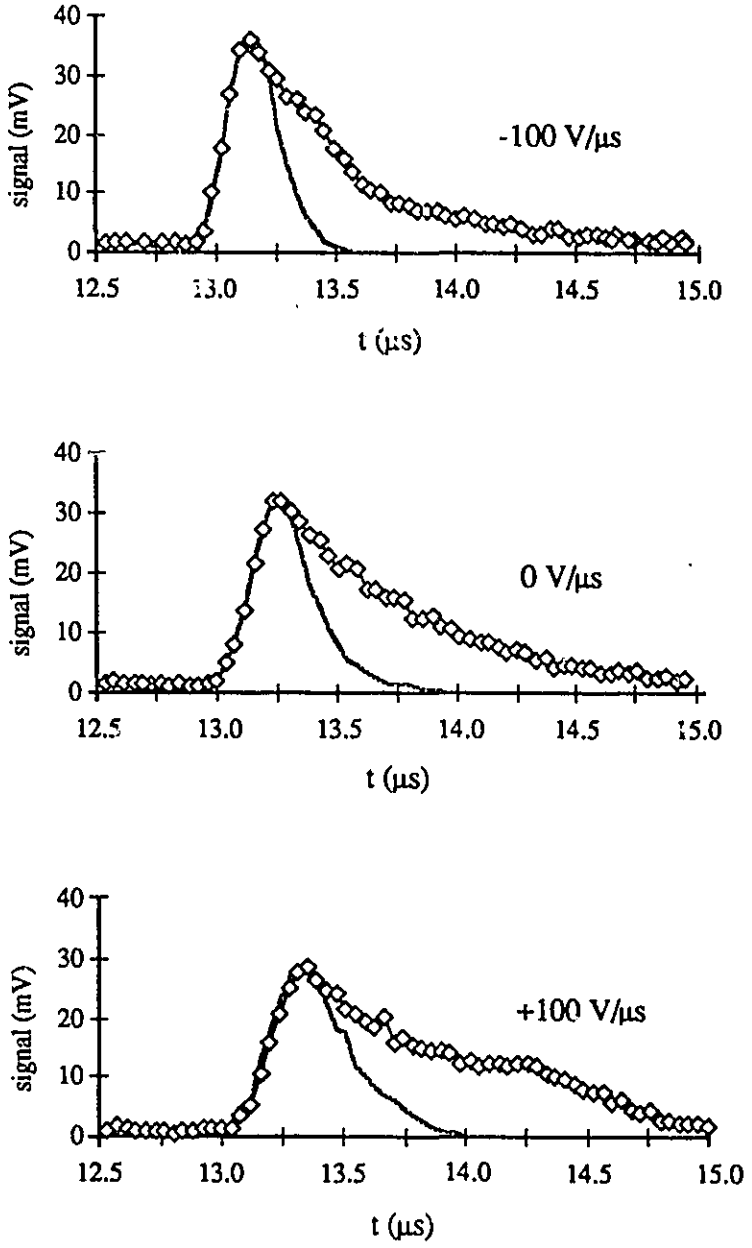

Figure 4-27: Measured time distributions of extracted ion clouds for different voltage ramp rates. Shaded line is the fit generated by the phase space program.

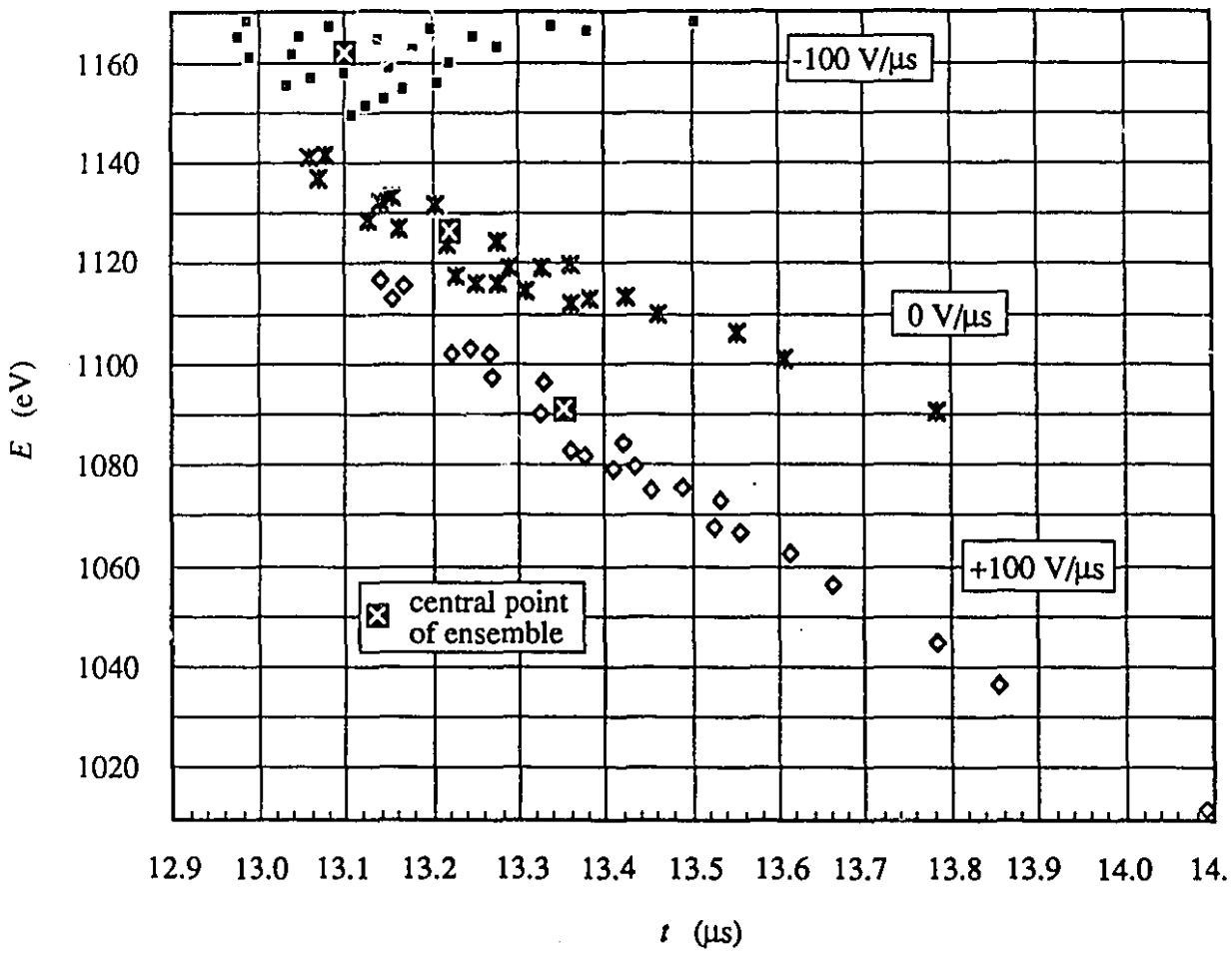

Figure 4-28: Phase space diagrams (energy versus time) for ion signals subjected to a voltage ramp.

The trigger, which is derived from the ion extraction pulse, is adjusted by observing the time of flight which changes according to how much accelerating voltage the ion pulse is experiencing. The trigger is set at the midpoint of the time of flight shift and the delay is recorded and input to the simulation program.

Table 4-5a: Fit parameters for $^{39}K^+$ ion clouds experiencing voltage ramps of -100, 0 and +100 V/μs. These parameters correspond to the measured time-of-flight profiles in figure 4-28. In all cases the RF frequency is 0.65 MHz with no DC voltage on ring.

ion temp. (eV)	0.6	well depth (eV)	72
number of ions	500	S_z (eV-μs)	2.8
initial z (mm)	±1.31	RFD (coef/slope)	1.2/-0.8
initial E (eV)	±1.8	trap potential (V)	1000
$z \times E$ array	5×17	ext. voltage (V)	100
RF-V (V_{op})	525	ext. cav. pot. (V)	920
f_o (kHz)	209	ramp cav. pot. (V)	0
q-parameter	0.76	tof agreement (%)	1.8

Since only the time distribution is measured, and well downstream from the ramp region, the effects of the ramp are not obvious from the measured pulses. Because of the good fit, the computed simulations for these ramped ion ensembles before and after the ramp give a fairly good idea of what the effects on the energy spread really are. These computed phase space diagrams, shown in figure 4-28, nicely illustrate the improved and exacerbated energy spreads for the negative and positive ramps, respectively. (As a negative ramp should reduce the energy spread, so a positive ramp should increase it.†) There is a definite measured effect of the voltage ramp on the time distribution which is satisfactorily accounted for in the simulation as evident if figure 4-27. A summary of the computed phase space parameters of the ensembles of figure 4-28 is shown in table 4-5b.

The effect of the ramp is more complex than illustrated by figure 4-26 due to the "boomerang" shape of the phase space diagram.

Indicated in figure 4-28 are the central points of the ensemble for each case. These points correspond to an ion having zero kinetic energy at the center of the trap. In the zero ramp case, the central point has a final energy of 1127 eV. The other center points have energies about 35 eV higher and lower in spite of the fact that the overall transport voltage, 1000 V to ground, is the same in each case. This is because after experiencing an accelerating field in the gap between the extraction and ramp cavities, the ramp cavity potential returns to the pre-ramp level

† In figure 4-26, the voltage ramp is shown as positive. For the measurement, the ions are created at high voltage and accelerated to ground. Therefore a negative ramp voltage is actually a positive accelerating voltage with respect to the trap voltage.

(in this case, ground) while the ion bunch is inside the cavity. Therefore the ions transit the last gap unaccelerated. By changing the potential while the ions are inside the conducting cavity they do not experience the same overall acceleration. This measurement demonstrates the feasibility of the manipulation of extracted beams by time-varying voltages and has potentially far-reaching ramifications for the transport of such beams.

Table 4-5b: Computed phase space parameters for ramped $^{39}K^+$ ion clouds at the detector. These parameters are derived from the same simulation as table 4-5a.

V_{rr} (V/μs)	dE (eV)	dt (μs)	dp (eV-μs/mm)	dz (mm)	S_z (eV-μs)†
-100	20	0.30	0.25	23	~3
0	30	0.37	0.40	27	~3
+100	61	0.52	0.83	38	~3

†Determined by estimating the area of each ensemble in figure 4-28.

D: DISCUSSION

It remains to discuss the above results in the context of published work concerning the temperature of ions in Paul traps. A recent review by Fernande Vedel [VED] included some such discussion. In that paper, a table was presented which summed up all published work in which optical measurements of the mean kinetic energy of the trapped ion cloud were made. This table is reproduced here as table 4-6 with additions that include the work of this thesis. It offers a good summary of how the results harvested from this work fit in with those already published. In many of these publications, the average kinetic energy, $\langle E \rangle$, has been measured and interpreted as an ion temperature. Moreover, $\langle E \rangle$ has mostly been measured as a function of the potential well depth of the trap and not as a function of ion number. While the dependence of ion temperature on ion number is a relatively simple and straightforward concept, only one such measurement has been reported. Furthermore, the results in table 4-6 are all measured very close to the space charge limit of the trap's capacity so the number of ions is quite large. This work presents time-of-flight measurements of the temperatures of an extracted ion cloud for relatively small clouds as a function of ion number rather than the trap well depth.

As stated previously, the original ideas concerning trapped ion dynamics were formulated by Dehmelt [DEHb]. These main ideas are: that cold ions fill up an RF-generated, pseudopotential well with constant density; that the ion macromotion is damped out leaving only a synchronous

Table 4-6: Summary of published ion temperature measurements in chronological order with those of this work included. The first part of the table originally appeared in [VED] with the exception of the ion cloud size and non-optical results as noted.

ion species	number of ions	temperature kT (eV)	well depth D (eV)	radial diameter (mm)	pressure (mPa)	reference
$^{1}H^{+}$	7×10^{3}	1.04†††	10.4	§§	10^{-6}	[CDE]‡
"	"	0.08	2.6	§§	10^{-6}	"
$^{135,137}Ba^{+}$	10^{5}	$0.11D$†*	25-64	§§	10^{-4}	[IWE]
$^{6}Li^{+}$	10^{5} §	0.43	18	11	10^{-4}	[KPR]
$^{137}Ba^{+}$	10^{6} **	$0.11D$	10-26	5.5, 3.8‡‡	10^{-4}	[SSW]
"	"	1.3*	40	§§	0.1 (He)	"
$^{205}Tl^{+}$	9.1×10^{6}	2.4*	40	16	§§	[GDM]‡
$^{173}Yb^{+}$	10^{5}	$0.126D$†*	10-40	§§	0.01 (He)	[MBG]
"	"	$0.112D$††*	10-40	§§	"	"
$^{199}Hg^{+}$	6×10^{5}	0.043	15	§§	2.0 (He)	[CFG,
"	2×10^{6}	0.049	15	5.0	"	CGM]
$^{199}Hg^{+}$	2.86×10^{5}	0.14†††	§§	3.8	§§	[MDJ]‡
"	3.66×10^{5}	0.03†††	§§	5.2	§§	"
"	2.00×10^{6}	0.29†††	§§	5.4	§§	"
"	2.26×10^{6}	0.20†††	§§	7.6	§§	"
"	3.20×10^{6}	0.30†††	§§	8.8	§§	"
$^{135,137}Ba^{+}$	10^{7}	$0.015D$*	18-62	12	0.001	[SBS]
$^{135,137}Ba^{+}$	10^{7} **	$0.004D$*	20-75	1.2	0.001	[SSB]
$^{39}K^{+}$	2.0×10^{3}	0.06	37	2.0‡‡	26.6 (He)	[this work]‡
"	1.0×10^{4}	0.125	37	3.0‡‡	"	"
"	0.5×10^{5}	0.25	64	2.8‡‡	"	"
"	2.3×10^{5}	0.75	60	5.6‡‡	"	"
$^{23}Na^{+}$	2.5×10^{3}	0.05	67	0.6‡‡	"	"
"	2.0×10^{4}	0.1	67	1.2‡‡	"	"
"	1.2×10^{5}	0.25	37	3.2‡‡	"	"
"	5.0×10^{5}	0.6	37	4.8‡‡	"	"

‡non-optical measurement
‡‡axial diameter
§reported in [VED] as 10^{3}
§§information not supplied in reference
*average kinetic energy (as opposed to temperature)
**ion number inferred from a related publication
†from the width of the resonance line
††from the centroid shift of the resonance line
†††ions cooled by damping circuit across trap endcaps

breathing of the ions at the micromotion, or RF, frequency; that a trapped ion cloud can be described by a temperature; and that ions can be cooled by collisions with light, neutral gas but can alternately be RF-heated by collisions with heavier ions and atoms which leads to evaporative cooling, or boiling of ions from the trap.

Church and Dehmelt [CDE] performed the first measurement of a trapped ion cloud temperature. These results constitute the first row of table 4-6. They measured temperatures for clouds of trapped protons under high vacuum but cooled by a dissipative circuit connected across the endcaps. The number of ions was relatively low but the trap was only 2.3 mm between endcaps compared to about 20-30 mm in all other cases. They found that the *cooled* ion temperature was in proportion to about *one-thirtieth* the well depth while *uncooled* ion temperatures varied as about *one-tenth* the well depth Their cooled ion temperature result of 0.08 eV is similar to the one of this work for roughly 10^3 ions but the well depths are quite different.

Iffländer and Werth [IWE] performed the first observation of a trapped ion cloud by laser illumination. Their result is actually a velocity spread which is derived from the doppler width of an observed hyperfine splitting peak. They determined that $\langle E \rangle$ varied in rough linear proportion to the trap well depth for a one trap loading. While the potential well was spherical, no indication was given as to which operating parameters were used to vary the well depth. Furthermore, they did not cool their ions so their values are about a factor of ten higher than those of this work.

A similar laser spectroscopy study was made by Knight and Prior [KPR] only they scanned the spatial extent of the trapped ion cloud with the laser beam. The measured Gaussian distributions showed that the concept of ion temperature was valid and the data were fit using thermodynamic arguments to derive a temperature. They found the ion cloud radius to be independent of the number of ions "...with the possible exception of very small numbers of ions." They went on to state that: "All subsequent data were...taken with a sufficient number of ions to eliminate error resulting from fluctuations." This means that the ion number and temperature were governed by evaporative cooling. They measured this ion cloud radius to be about 5.5 mm. In the original table in Vedel's paper [VED] the number of ions for this work was reported as 10^3. This is actually the number of fluorescing ions which have been first optically pumped into a metastable state and subsequently excited to a fluorescing state. The total number of ions in the trap, and therefore the number determining the ion cloud temperature, is actually 10^5. Their temperature compares favorably to that obtained in this work.

Schaaf *et al.* [SSW] also scanned a laser beam over a defined geometric area to observe Gaussian velocity and spatial distributions of trapped Ba^+ ions. These measurements also gave credence to the ion temperature idea. They determined that the uncooled $\langle E \rangle$ varies as about one-tenth the trap well depth and, using buffer gas cooling, that the cooled $\langle E \rangle$ was about one-thirtieth the well depth which is consistent with the results in [CDE] as well as those of this work. They

also found the spatial ion cloud widths to be independent of the trap well depth. They reported an average radial width of 3.8 mm and average axial width of 5.5 mm. These values are related by a factor of $\sqrt{2}$ which follows from the Boltzmann distribution for equal radial and axial well depths. If the well depths are equal, the macromotion frequencies must also differ by $\sqrt{2}$ (equation 2-12). If we assume equipartition of energy in each dimension then it follows that the amplitudes of oscillation, or cloud sizes, are related by $\sqrt{2}$ (equation 2-25). Though not reported in [SSW] the number of ions is taken to be 10^6 from a related publication by Blatt *et al.* [BSW].

Another average kinetic energy measurement of a $^{205}Tl^+$ ion cloud has been made by Gaboriaud *et al.* [GDM] using a resonant circuit connected across the endcaps with a local oscillator which is swept through the ion macromotion frequency. They measured the absolute ion number as well as a shift in macromotion due to space charge which indicates the ion density. From the density and number, a simple relationship for spherical trap volume gives an ion cloud radius of 8 mm from which $\langle E \rangle$ is calculated as 2.4 eV which is relatively large. The number of ions is also large, however, and the ions were not cooled. Though they report a well depth of only 5.4 eV, it is defined differently than the pseudopotential well depth generally used in the literature. Their well depth calculated in the general way (from equation 2-12) would give a value of 40 eV.

Münch *et al.* [MBG] have recently measured an average kinetic energy of Yb^+ using both the hyperfine resonance width and the frequency shift. These results yield two confirmations of the variation of $\langle E \rangle$ with approximately one-tenth of the trap well depth. Though helium buffer gas was used, the background pressure did not appear to be high enough for significant cooling.

The work of Cutler *et al.* [CFG, CGM] presents two determinations of trapped ion temperature in the framework of a second-order non-linear equation of ion density. This model also defines an ion cloud radius. The measurements are made using the second-order doppler shift of a laser-excited hyperfine transition in $^{199}Hg^+$, 10^6 ions of which are buffer gas cooled. Their calculated temperatures fall far lower than any published as well as those presented here, even for small numbers of ions. Furthermore, they state that: "For given values of m and ω...the relationship $T \propto N^{2/3}$ must hold," which is proved for the two temperature values published. Incorporated into their model is the frequency shift due to space charge mentioned above. They argue that as the cloud *cools*, the central density *increases*, causing a shift in the oscillation frequency due to space charge. Indeed, their reported ion densities of 3×10^7 cm^{-3} are about ten times higher than those determined from this work. One possible explanation for their extremely low temperatures is the larger mass difference between their Hg ion cloud (mass 199) and the He buffer gas (mass 4). In this case, the difference between He and K

(mass 39) or Na (mass 23) is much smaller. Because buffer gas cooling depends on the mass difference between the ion and the buffer gas, the larger difference may allow better cooling.†

The systematic measurements of ion temperature versus ion number presented in this thesis offer some insight into the temperature dependence of trapped ion clouds.

As discussed in chapter 2, RF heating of the ion cloud is the result of friction between the buffer gas and the cloud. If the volume of the cloud is proportional to the total ion number (as in the Dehmelt model that also assumes constant ion density), then its outer radius (assuming a spherical cloud) is proportional to $N^{1/3}$. The heat input to a system is defined as force times velocity. Existing data on ion mobility at low velocity (in the eV range) indicates that the frictional force presented to the ion by the buffer gas is proportional to the velocity.‡ This means that the rate of heat input is then proportional to the velocity squared. The RF quadrupole field strength experienced by the ions, and therefore the velocity of the RF micromtion, is proportional to the radius. Therefore, the heat input is proportional to $N^{2/3}$. Recall that in the plots of $k(T-T_b)$ versus N in figures 4-17 (K) and 4-22 (Na), the data were fit with slopes of 0.63 and 0.59, respectively. These values are within 6% and 12%, respectively, of the purported slope of two-thirds.

The above discussion assumes that the ion density n has no dependence on N. This is not necessarily the case if enough ions are cooled to a low enough temperature that the resulting space charge can cause a shift in the macromotion frequency of the cloud. The effect of space charge on the trapped ion phase space was first discussed by Vedel and André [VAN]. They also developed a temperature model for buffer gas cooled ions and determined that the ion cloud should cool to the temperature of the buffer gas but presented no experimental results [VAV].

The frequency shift induced by space charge is fundamental to the elegant, analytical model of Meis *et al.* [MDJ]. In this reference they present temperatures and densities for five trap loadings based on the number of ions and the measured macromotion frequency. Though not specifically tabulated in [MDJ], ion cloud radii can readily be obtained from the ion number and calculated ion density assuming a spherical cloud. These radii are included in table 4-6. Their reported temperatures are similar to those obtained in this work but generally a little lower. The ion densities are, in keeping with the lower temperature, slightly higher. This was possible since they did not use buffer gas to cool the ions but an external radiative cooling circuit.

---

† Private communication from Dr. Alan Madej of the National Research Council in Ottawa.

‡ Ellis *et al.* [EMA]. Mobility is a term used to describe the movement of ions through neutral gases. The velocity of ions in this situation is proportional to the applied electric field. The *ion mobility* is the proportionality factor.

In the statistical model formulated by Meis *et al.* the temperature also varies as the two-thirds power of the ion number but with the space charge manifested in the macromotion frequency shift according to the relation:

$$kT \propto \langle\omega_m\rangle^2 \left(\frac{N}{\omega^2 - \langle\omega_m\rangle^2}\right)^{2/3} \qquad (4\text{-}1)$$

where $\langle\omega_m\rangle$ is the measured (shifted) macromotion frequency and ω the computed value. The temperature results from [MDJ] are plotted versus ion number in figure 4-29. The reason for showing this is to demonstrate that, for ion densities high enough to exhibit space charge effects, the variation in temperature with ion number is more complicated than for buffer gas cooled clouds.

The results in figure 4-29 span a more limited range than those of this thesis and no information about the measurements accompanies them. Meis *et al.* refer to the frequency shift and ion number measurements of Gaboriaud *et al.* [GDM] of which only one shift is actually reported. One has the impression that the shifts were measured in this way but there seems to be no account of the experiments which furnished the numbers for these elegant calculations. The price of elegance, however, is preclusion. This model pivots about an implicit assumption of spherical symmetry as well as restricted operating parameters such that: $|a| << q << 1$.

Finally, a group at Hamburg have directly measured both the velocity and spatial distributions of trapped ion clouds using laser spectroscopy [SBS]. They have also developed a detailed Brownian motion model of trapped ion dynamics [BZH]. Their results in table 4-6 differ from those of other groups measuring $\langle E\rangle$ as a function of D indicating much lower average kinetic energies for similar well depths. Furthermore, the same group report even lower average kinetic energy in a paper by Schubert *et al.* [SSB] for the same ion and similar operating parameters. Siemers *et al.* [SBS] show that if the well depth is varied by changing Ω but keeping β constant, $\langle E\rangle$ changes linearly with D, but if D is varied by changing β and keeping Ω constant, this linear variation of $\langle E\rangle$ with D is no longer observed. These kinetic energy versus well depth curves from [SBS] are reproduced in figure 4-30. The linear dependence in the constant β case is obvious. The variation in the constant Ω case is not so obvious, though the deviation of $\langle E\rangle$ about an average value of about 0.4 eV is not exceptionally large. The reason for pointing this out is that the temperatures obtained in this work were not all measured at the same potential well depth. It was intended to keep the trap driving parameters the same for these measurements but a problem in RF calibration caused some deviation from this intent. The results of Siemers *et al.* indicate that $\langle E\rangle$ should not change too much if D is varied using the RF voltage only. It is only when D is varied using both RF voltage and frequency such that the ratio of V to Ω^2 is constant that $\langle E\rangle$ rises linearly with D. In the measurements of this thesis, only the

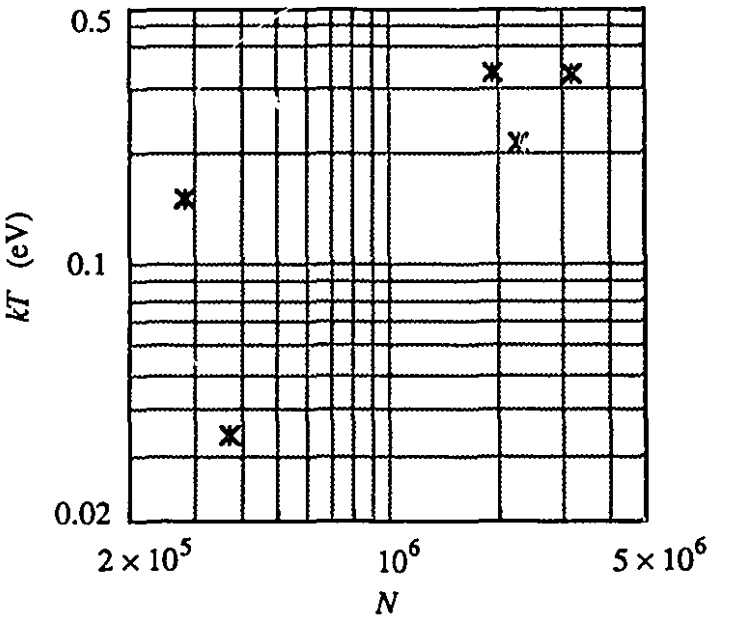

Figure 4-29: Ion temperature versus ion number results published by Meis *et al.* The graph is plotted on a log-log scale.

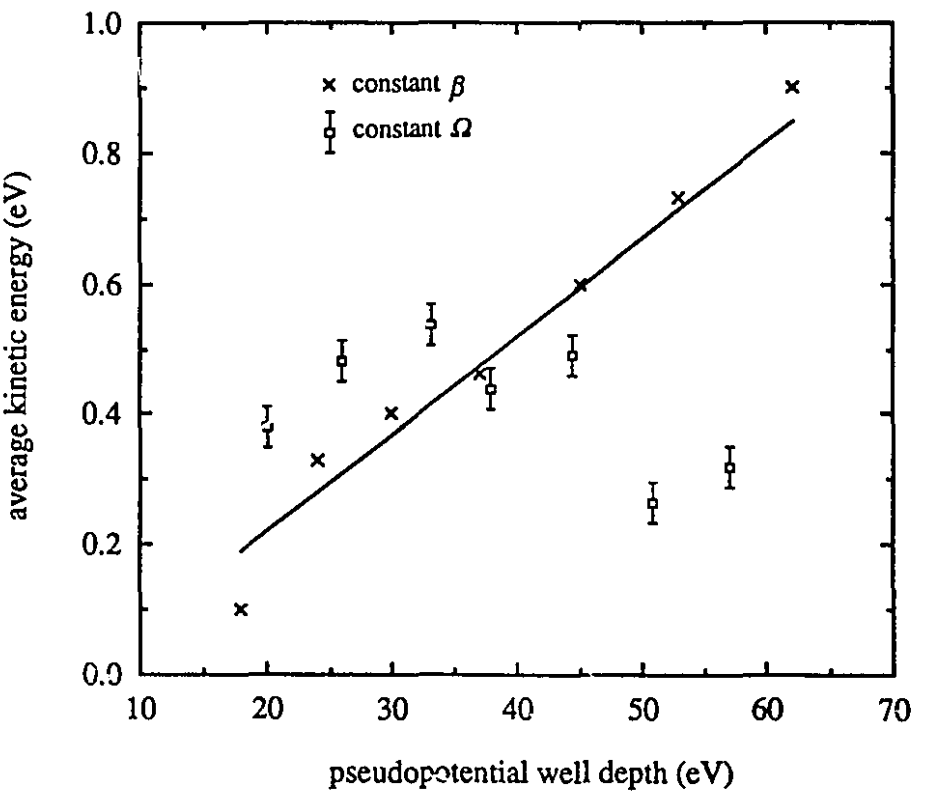

Figure 4-30: Comparison between measurements of average kinetic energy of the trapped ion cloud versus the trap potential well depth performed by Siemers *et al.* In the linear case, the trap Mathieu parameters were kept constant while the RF frequency was varied. In the other case, the frequency was kept constant while a and q were changed using the RF and DC voltages. Reproduced from [SBS].

RF voltage was changed so the effect of the changing well depth on the ion temperature, though not totally obvious, is much less than if the well depth were changed otherwise. Indeed, if the well depth affected the ion temperature in a linear fashion, the temperatures for the first two entries for $^{39}K^+$ in table 4-6 would be lower by about 60%, violating the $N^{2/3}$ dependence on temperature demonstrated earlier. In addition to the these results, they also measured the spatial distribution of the ion cloud by scanning the laser frequency in the ring plane an observing the fluorescence as a function of position. Again, since the drive parameters were not the same, rather incongruous measurements of the ion cloud radial diameter $\langle \Delta r \rangle$ were obtained for the same well depth, to wit: for a 30 eV well, a $\langle \Delta r \rangle$ of 1.2 mm was reported in [SSB] versus 12 mm in [SBS]. This difference may be related to the corresponding $\langle E \rangle$ values for this well depth of 0.1 and 0.4 eV, respectively.

In the more recent publication by Schubert *et al.* [SSB] four models of trapped ion dynamics were compared using a ratio of mean kinetic energy of the macromotion to the micromotion:

$$R = \frac{\langle E \rangle}{\frac{1}{2} m \Omega^2 \langle \Delta^2 \rangle} \tag{4-2}$$

where $\langle E \rangle$ is the average kinetic energy in one spatial direction and $\langle \Delta^2 \rangle$ is the spatial width in the same direction. R can be derived from experimental parameters and then compared to calculations by the different models: a pseudopotential model, a modified pseudopotential model, their own Brownian motion model [BZH], and the analytical model of Meis *et al.* [MDJ].

The first of these is the pseudopotential model which reinterprets the kinetic energy contained in the micromotion as a contribution to a pseudopotential $D(\Delta)$ for the macromotion:

$$D(\Delta) = \tfrac{1}{8} m \Omega^2 \beta^2 \Delta^2 \tag{4-3}$$

Assuming $|a| << q << 1$, the net result for R is:

$$R^{ps} = \tfrac{1}{4} (a + \frac{q^2}{2}) \tag{4-4}$$

Because of the limitations on a and q and the fact that the micromotion has been reinterpreted as potential energy and neglected as a contribution to total kinetic energy, this model is limited in usefulness. The modified pseudopotential model uses both contributions to the total kinetic energy; that of the macromotion: $D(\lambda)/2$, where $\lambda^2 = 2\Delta^2$, and that of the micromotion: $m\Omega^2\lambda^2\beta^2/16$. The net result for R in this case is:

$$R^{psm} = \tfrac{1}{4} (a + q^2) \tag{4-5}$$

The experimental value of R from [SBS] is 0.024. Using equations (4-4) and (4-5) yield values of 0.013 and 0.023, respectively, indicating the superiority of the modified

pseudopotential method. The results from this work have been cast in the framework of these models and presented in table 4-7. The values for kT and A (using A for Δ) are taken from tables 4-1 and 4-2.

Table 4-7: Comparison of the results obtained in this thesis to the various models of trapped ion dynamics presented by Schubert *et al.* [SSB] whose reported average value for R^{exp} is 0.024 for Mathieu parameters a_z = -0.003 and q_z = 0.55. The first seven rows are for potassium (taken from table 4-1) and the last four are for sodium (table 4-2). In all cases, the a-parameter is zero. The percentage differences are for R^{exp}.

kT (eV)	A (mm)	q	β	R^{exp}	R^{ps}	R^{psm}	R^{psm} %diff	$R^{\beta psm}$	$R^{\beta psm}$ %diff
0.75	1.6	0.72	0.59	0.043	0.016	0.032	34	0.044	0.04
0.25	1.3	0.55	0.42	0.022	0.010	0.019	17	0.022	0.55
0.20	0.8	0.74	0.61	0.047	0.017	0.034	37	0.047	0.47
0.13	0.8	0.60	0.46	0.027	0.011	0.023	19	0.026	1.41
0.13	0.8	0.60	0.46	0.026	0.011	0.023	16	0.026	1.35
0.06	0.6	0.60	0.46	0.027	0.011	0.023	21	0.026	2.99
0.05	0.5	0.60	0.46	0.027	0.011	0.023	19	0.026	1.58
0.60	1.4	0.73	0.60	0.045	0.017	0.033	36	0.045	0.48
0.25	0.9	0.73	0.60	0.045	0.017	0.033	36	0.045	0.29
0.10	0.3	0.86	0.81	0.082	0.023	0.046	78	0.081	1.19
0.05	0.2	0.86	0.81	0.082	0.023	0.046	77	0.081	0.64

The table shows that the pseudopotential model does a poor job of reproducing R^{exp}. For that matter the modified pseudopotential is not so great either. If we examine R^{exp} and compare it to R^{exp} of [SBS] we see that it is way off in cases where the q-parameter is very large (≈0.045 compared to 0.023). Indeed, the q-parameters are all larger than the usual approximation for β allows (i.e., $q < 0.4$). That same approximation has been used to formulate R^{psm} and R^{ps}. Since we have rigorously simulated the macromotion frequency (and hence, β), if the expression for R^{psm} is recast using β then the agreement with the R^{exp} should improve. Thus we have $R^{\beta psm}$ and the difference between this and R^{exp} is in the last column of table 4-7. Here the agreement is much better. One thing to note is that the value of A is directly governed by the choice of temperature in the fit of the data. In the case of [SBS], the two values are independently measured. However, it is somewhat edifying to find consistency in the model used for this work as compared to other models.

One significant question about much of the work cited in table 4-6 concerns the relationship of average kinetic energy and temperature. This issue is not completely resolved in the literature due to the coherent nature of the trapped ion micromotion. Much of the published work has been reported as measurements of the average kinetic energy which has been found to increase as a function of the trap well depth. This result is expected considering that the RF voltage must be raised to increase the well depth and the oscillation frequencies increase as a result. For an ion cloud at some temperature, increasing the RF energy will simply increase the kinetic energy of the micromotion and will not increase the temperature. The ion cloud phase space diagram will be distorted to a more extreme ellipse (figure 2-6) but the area will still be the same. In practice, the higher RF field will increase the temperature somewhat due to RF heating (collisions with the background gas causing loss of macromotion coherence). However, the temperature is not increased by the higher kinetic energy of the micromotion because it is coherent (*i.e.*, it is the driving motion). By assigning a temperature to an ion cloud, a phase space distribution is also defined, the time component of which can be measured quite accurately. Any change in the RF field is accounted for by the RF distortion of the phase space volume as discussed in chapter 2. This provides a consistent determination of the ion temperature which is not provided on the basis of average kinetic energy.

Most of the trapped ion temperature measurements discussed above were made *in situ* using laser spectroscopy. The technique presented here is different but still requires knowledge of the ion phase space distribution inside the trap since it determines the extracted phase space volume. Thusfar, we have presented a totally self-consistent model for trapped ion dynamics, not restricted by operating parameters, yielding results that fall within the range of those published.

It remains to use this model to predict the dynamics of extracted ions under conditions of higher trap loading as would be present in a Paul trap beam buncher. This has been done by simulating K ion clouds of five different temperatures and observing the resulting phase space boundaries. These boundaries: dE, dt, dp and dz, are determined simply by the difference in maximum and minimum values. Simulations were run for temperatures of 0.01, 0.1, 0.5, 1.0, 2.0 and 5.0 eV. The resultant boundaries are listed in table 4-8 as well as the ion cloud displacement (determined by equation 2-25). These values are plotted on a log-log scale in figure 4-31 (the different quantites are scaled to fit on the same graph). A deviation is evident from the graph at about 1 eV. This is the point at which the phase space starts to become so big as to be distorted by the large RF field experienced during extraction.

Table 4-8: Axial phase space boundaries of a K ion cloud computed for five initial temperatures. The ions were extracted with a 200 V pulse applied at 197° of the RF phase. The applied trap voltage is 420 V at 0.65 MHz with no DC yielding a 151 kHz collective oscillation frequency.

kT (eV)	z_i (mm)	dE (eV)	dt (μs)	dp (eV-μs/mm)	dz (mm)
0.01	0.4	13	0.06	0.32	2
0.1	1.3	41	0.19	1.05	7
0.5	2.9	108	0.44	2.86	15
1.0	4.0	193	0.66	5.51	19
2.0	5.8	283	0.82	8.98	24
5.0	9.0	380	1.45	13.76	40

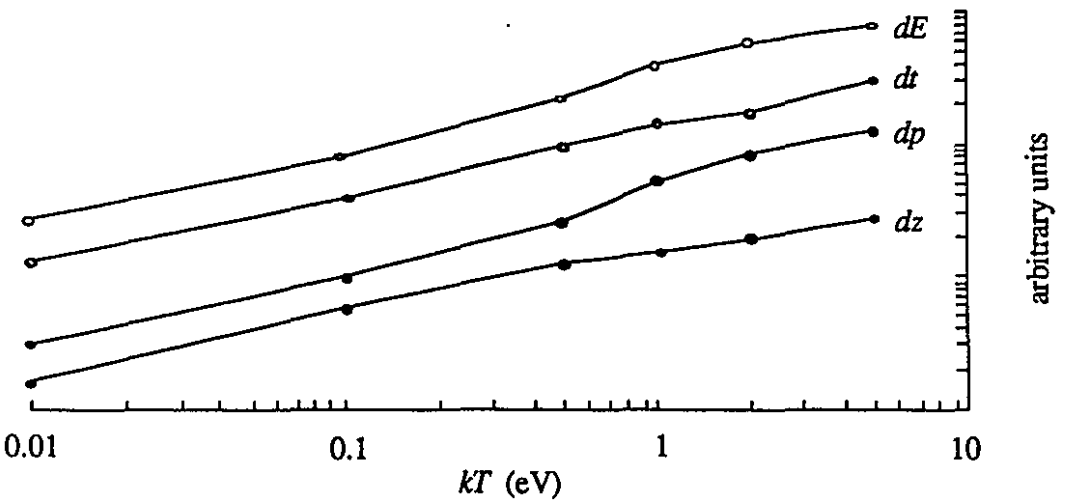

Figure 4-31: Axial phase space boundaries of table 4-8 plotted versis ion temperature on a log-log scale.

Figure 4-32 shows the phase space diagrams for 1.0 and 5.0 eV temperatures at $z = z_o$. The phase space is plotted in both momentum-displacement space and energy-time space. The difference in shape between these two diagrams only becomes apparent with high temperature where the phase space distortions are manifest.

At 5 eV the curves of figure 4-31 show another inflection. This is because distortion of the phase space for a 5 eV ion cloud is quite severe and the boundaries were actually determined by "clipping" the phase space diagram. If this is not done, the curves of figure 4-31 diverge wildly after a temperature of 2 eV. Using the two-thirds dependence of ion number on temperature, a

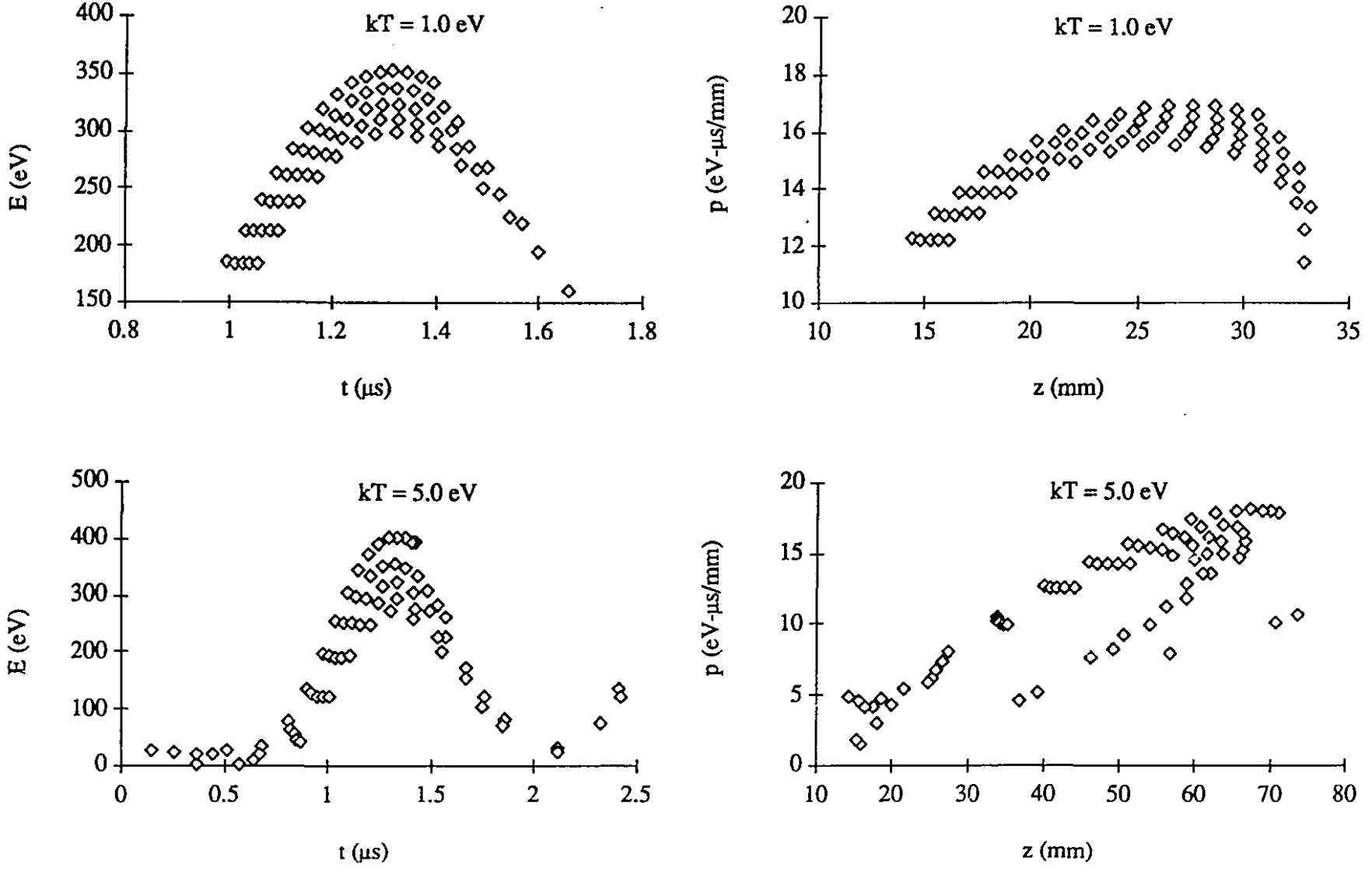

Figure 4-32: Axial phase space diagrams in energy-time and momentum-displacement representations for 2 and 5 eV initial ion temperatures.

5 eV temperature would correspond to about 5 million ions if we extrapolate from the experimental data in table 4-2.

Shown in table 4-9 are computed values for the axial phase space and phase space volumes for the same simulations in table 4-8. These quantities are determined from equations 2-22 and 2-24. In addition, the corresponding number of ions based on the extrapolation mentioned above is given. The Δt column in table 4-9 is a time duration which corresponds to the equivalent phase space volume of a continuous beam of the same mass. This parameter depends on the transverse emittance and central energy of such a beam. Here, we assume values given by the ISOLDE facility at CERN [ISO]: a 6 eV energy spread on a 60 kV beam with transverse emittance of 20 π-mm-mrad in each coordinate. Using equation 2-27, these figures yield a phase space volume of 1125 (eV-μs)^3 per μs of beam. Therefore the second last entry in table 4-9 is the time in μs when the corresponding trap phase space volume is divided by this number. The extreme case of a 5 eV trapped ion temperature corresponds to an impressive collection of almost 0.8 ms of DC ISOLDE beam. However, the validity of the model is compromised at this high temperature due to space charge and evaporative cooling so the results corresponding to temperatures between 1 and 2 eV are more plausible. The amount of beam collected in this case is not so high. It becomes necessary, therefore, to increase the capacity of the trap by increasing its size.

Table 4-9: Axial phase space area, phase space volume, corresponding DC beam time duration and ion number computed for the five initial ion temperatures of table 4-8.

kT (eV)	z_i (mm)	S_z (eV-μs)	S (eV-μs)^3	Δt (μs)	N
0.01	0.4	0.2	0.008	6×10^{-6}	5.0×10^2
0.1	1.3	2.0	8.0	7×10^{-3}	1.5×10^4
0.5	2.9	10	960	0.9	1.5×10^5
1.0	4.0	20	7×10^3	6.0	4.5×10^5
2.0	5.8	40	6×10^4	56	1.2×10^6
5.0	9.0	95	9×10^5	800	5.0×10^6

Some rough calculations have been performed to establish the potential of continuous beam capture using traps. If the size of the trap is increased by a factor of 4, in order to maintain the same macro-oscillation frequency, the RF voltage must be increased by a factor of 4^2 (from equations 2-9 and 2-11). Extrapolating from the 1.0 eV temperature case of table 4-9, we had used a maximum oscillation amplitude of about 30% of z_0 and therefore our maximum for the bigger trap would be 18 mm. Calculating the phase space volume for the 18 mm oscillation of a mass 39 ion at 0.15 MHz yields 5.6×10^7 (eV-μs)^3 or 50 ms of DC beam. To appreciate the

potential improvement of an experiment, we must consider the current of such a DC beam. For the ISOLDE beam parameters mentioned above, the corresponding beam current is about 10^9 ions per second (160 pA). A 100 ms section of this beam is therefore 10^8 ions. Though less than the DC beam yield, this number of ions can, in principle, be extracted from the trap and delivered to an experiment in a 1 μs bunch. This corresponds to a reduction in background by a factor of 10^5 which would is quite significant.

Realistically, several mitigating factors must be examined, however. The capture efficiency of the trap will reduce this gain by a factor of almost 1000 according to the most recent results of Rouleau [ROU]. The small time spread of the extracted ion bunch comes at the expense of a large energy spread which could affect the experiment in question unless energy-correction measures are taken. Space charge may also cause problems with the phase space density of the ions in the trap. These considerations regarding the capabilities of larger traps have been addressed in more detail by Moore *et al.* [MLR]. Furthermore, the ion mobility behavior for the higher velocities resulting from these larger clouds will tend to cause greater friction [EMA].

The possibility of beam collection using Paul traps poses, at once, intriguing yet challenging questions. The engineering of such a system would require quite stringent specifications regarding timing, machining and high-voltage. However the purpose of this work was not to study the feasibility of beam collection but to determine the temperature of trapped ion clouds over a range of trap loading. In performing this task, it was found that the temperatures of small ion clouds are actually quite low.

Using the trap as a source of cold ions offers other interesting possibilities in the field of nano-circuit fabrication. In a recent review article by Smith and Craighead [SCR] several comparisons are made between focused ion beam lithography and electron beam lithography. Ion beams offer many advantages over electron beams but suffer from low source brightness and beam diffuseness. Furthermore, such ion beams are a result of severe collimation which simply throws away almost all the beam. Ion traps offer interesting possiblities as the ions can be collected and cooled. A cooled ion cloud would have a radius of some hundreds of μm in size for a room temperature buffer gas. In principle the buffer gas can be cooled to liquid helium temperature (4 °K or 0.3 meV) and the trap can be made smaller to further reduce the phase space volume. A trap of the order of a few millimeters endcap separation could produce an extracted beam of a few microns radius. This beam could then be focused to submicron spot sizes in focal lengths of a few microns. Such a small beam focus would be very useful for ion beam lithography applications.

CHAPTER 5: CONCLUSION

Offer up your best defense because this is the end.
This is the end of the innocence.

Don Henley

The phase space volume of ion traps is a topic that continues to receive considerable attention from researchers with wide ranging backgrounds. Most of this work, however, has not been pursued from the perspective of phase space volume but by a related quantity: temperature. The temperature of a trapped ion cloud determines all of its dynamic characteristics. Due to the nature of ion motion in the Paul trap, the concept of trapped ion temperature has had conflicting interpretations in the literature. The radiofrequency trapping field causes the ions to have a large average kinetic energy but with a motion that is coherent and therefore one that does not necessarily affect the temperature of the ion cloud. Most reported results are actually measurements of average kinetic energy and not temperature.

This thesis has presented a self-consistent model of trapped ion dynamics based on the Gibbs distribution that has accounted for the measurements of ion temperature versus ion number. Accuracies of a few percent in time-of-flight of extracted ion clouds were achieved over the entire range of RF phase at extraction for three extraction fields and two different masses. The temperatures measured in this work reveal that buffer-gas cooled ion clouds are significantly cooler than DC beams produced at isotope separators. Such low temperature ion clouds not only offer the possibility to collect weakly produced radioisotopes but also considerably ease the engineering requirements for the transfer of these beams to other apparatus.

The Gibbs phase space model has also provided the means of dynamically manipulating the ion cloud phase space volume that was demonstrated in this work. This result in itself is very important for the future use of beams extracted from traps. However, while this manipulation has been demonstrated, considerable development will be needed before a beam collected in a trap could be used for laser spectroscopy. Another remaining problem is the detailed analysis of the transverse qualities of these pulsed beams.

Continuation of this work will require further development of the transport system to measure transverse beam qualities and improved knowledge of the overall transmission of the ion beam. Some energy retardation measurements could be made in order to verify some of the predictions of the phase space model regarding energy distributions. The engineering of a larger ion trap would also have to be undertaken to improve the bunching capacity as well as a pre-bunching system to manipulate the incoming ion beam for more efficient collection.

This work has provided a good example of the versatility of the ion trap which offers myriad possiblities and all in a benchtop experiment. These are desirable commodities in an era of big science projects.

APPENDIX 1:

Feasibility Study for Laser Spectroscopy on Bunched Ion Beams

INTRODUCTION

Laser spectroscopy is an experimental technique used to study nuclear properties by probing the effects of the nucleus on the atomic electron energy levels of a particular isotope. It is an elegant and extremely powerful technique which has been very fruitful for research in nuclear ground state properties. It was to enhance the technique of collinear laser spectroscopy that the study of collected and extracted ion beams in Paul traps was initiated.

Since the energy levels of the electrons orbiting the nucleus are quantized, it is possible to excite an electron from its ground state to an excited state. The development of the laser enabled this to be done in systematic fashion. Monochromatic laser light can be tuned with sufficient accuracy to excite the electron which resonantly absorbs the light. When the electron decays back down to the ground state, the re-emitted light can be detected with a photo-multiplier tube. The advent of the tuneable dye laser has enabled the energy levels, and hence the nuclear properties, of many radioisotopes to be probed in this way.

Laser spectroscopy is important for nuclear physics because this method of resonant excitation is so accurate that it can be used to detect the minute shifts in atomic energy levels caused by their interaction with the atomic nucleus. There are two atomic observables from which information about the nucleus can be derived: hyperfine splitting and isotope shift. The basis of hyperfine structure is briefly discussed below. The technique of collinear laser spectroscopy is one in which the excitation is done collinearly with radionuclides produced at an isotope separator facility and delivered as a beam. This technique is also briefly summarized. Finally, some laser spectroscopy measurements that were made for the initial work of this thesis are presented and discussed within the context of Paul trap beam collectors.

HYPERFINE STRUCTURE

The *fine* structure of the atom is a result of coupling between the orbital angular momentum L and the spin of an electron S. This coupling splits the level into two components. *Hyperfine* structure arises from coupling of the electronic and nuclear angular momenta as well as the interaction of the electrons with the electric and magnetic moments of the nucleus. The total electronic momentum J, is simply L + S. The nuclear angular momentum is designated by I so that the total quantized angular momentum of the atom is F = J + I.

The energy W associated with a particular hyperfine level F is expressed by:

$$W_F = A\ f(I,J,F) + B\ g(I,J,F) \qquad \text{(A1-1)}$$

where A is a function of the magnetic moment of the nucleus and B is a function of the electric field gradient of the nucleus.† By measuring the energy of the various hyperfine splitting levels and making the correct angular momenta assignments, these fundamental nuclear quantities may be determined. The various hyperfine levels can be measured for a long chain of isotopes over which a variation can be determined that is called the *isotope shift*. The isotope shift will not be discussed here as it is not relevant for this work.

Sodium was chosen for the experiment because it is easily produced and the excitation wavelength is easily reached with a tunable dye laser. To illustrate what is observed in the experiment, the hyperfine structure of ^{23}Na is derived here.

Atomic states are labeled using the spectroscopic notation $n^{2S+1}L_J$, where L indicated by the designations S, P, D... for L = 0, 1, 2... and the principal quantum number n is sometimes omitted. The 11 electrons of Na fill these levels up to $3^2S_{1/2}$ which means the first excited states are the 3p states which have fine structure levels: $3^2P_{1/2}$ and $3^2P_{3/2}$. In this work the $3^2P_{3/2}$ level was used, the observed transition of which is called the D_2 line (the $^2P_{1/2}$ state is the D_1 line). The excitation wavelength of this transition is 589.6 nm. The well-known nuclear spin of sodium is I = 3/2. Therefore the hyperfine states are defined by $|I - J| \leq F \leq |I + J|$ which gives F' = 1 and 2 for the $^2S_{1/2}$ (J = 1/2) state and F = 0, 1, 2, 3 for the $^2P_{3/2}$ (J = 3/2) state. Hyperfine transitions are subject to quantum mechanical selection rules and for the electric dipole transitions in this case the rule $\Delta F = 0, \pm 1$ is followed. For example, the excitation of the $^2S_{1/2}$ (F') to $^2P_{3/2}$ (F) transition (F' = 1→ F = 0, 1, 2) is allowed while (F' = 1→ F = 3) is not. The hyperfine level structure for Na is illustrated in figure A1-1. The energy spacings between the levels are determined by the corresponding A and B factors and are indicated in the figure. (The energy units used in laser spectroscopy are MHz as determined from $E = h\nu$ where h is Plank's constant and ν is the radiation frequency.) The six transitions form two groups (numbered 1, 2, 3 and 4, 5, 6 in figure A1-1) according to which ground state level the electrons de-excite. Each peak has a natural linewidth of about 10 MHz that is characteristic of the particular atom and state in question and is determined by the lifetime of the state which, in this case, is about 16 ns [CAR].

EXPERIMENTAL TECHNIQUE

The method used to measure these hyperfine transition energies was collinear fast-beam laser spectroscopy, the principle of which is illustrated by figure A1-2a.‡ The resolving power of the collinear method is dependent upon the doppler width, $\delta\nu_d$. This quantity, defined by the initial

† A good reference which discusses hyperfine structure and nuclear moments is [KRA].

‡ For reviews of laser spectroscopy and the fast beam technique see [OTT] and [NEU], respectively.

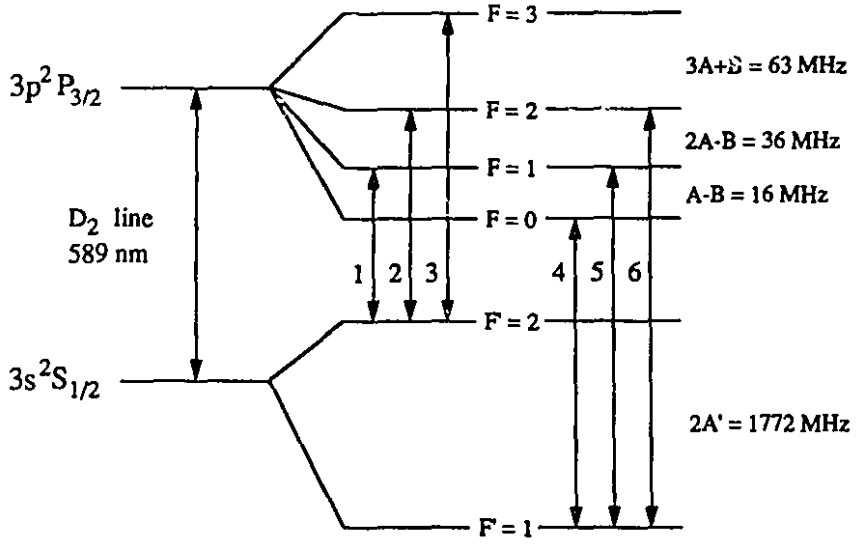

Figure A1-1: Hyperfine structure of the D_2 line of sodium (not to scale). The transitions are numbered with increasing frequency. The level splittings are determined by the nuclear A and B factors as indicated[SAG].

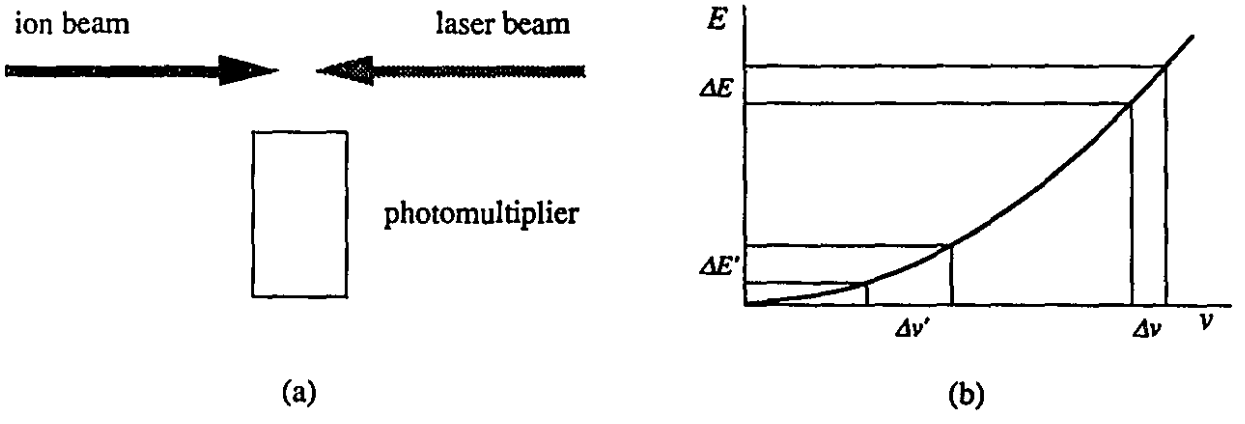

Figure A1-2: Principles of the collinear fast-beam technique of laser spectroscopy.
(a) Geometry of ion beam, laser beam and photomultiplier.
(b) Reduction of velocity spread for a given energy spread at increasing velocity.
For $\Delta E = \Delta E'$, $\Delta\nu < \Delta\nu'$ at higher ν.

energy spread of the ion source, determines how well the hyperfine peak positions can be resolved. For a given energy spread, the corresponding velocity spread can be reduced at higher velocities as shown in figure A1-2b as a greater fraction of the ion beam is simultaneously brought into resonance. This is the *fast*-beam aspect of the technique. With sufficient acceleration, the velocity spread of an ion beam can be reduced to within the natural linewidth. From the expression for the doppler shifted frequency ν_d:

$$\nu_d = \nu_o\left(1 - \frac{v}{c}\right) \qquad \text{(A1-2)}$$

the doppler width $\Delta\nu_d$ is defined as:

$$\Delta\nu_d = \nu_o\frac{\Delta v}{c} \qquad \text{(A1-3)}$$

where the velocity spread Δv is obtained from the energy spread:

$$\Delta E = mv\Delta v \qquad \text{(A1-4)}$$

If the beam is accelerated to a voltage V then the doppler width becomes:

$$\Delta\nu_d = \nu_o\frac{\Delta E}{\sqrt{2eVmc^2}} \qquad \text{(A1-5)}$$

that, for a given energy spread, is reduced for higher acceleration voltages.

APPARATUS

The apparatus used for the laser spectroscopy measurements is the same as that described in chapter 3 which was subsequently modified for the time of flight work. The experiments were done with a 5 kV sodium beam. A *Coherent* CR-699-21 ring dye laser was used with *Rhodamine 6G* liquid dye to produce the excitation wavelength of 589.6 nm. The dye laser is pumped by a *Coherent* CR-12 Argon ion laser which generates about 5 W of power at 514 nm. The dye laser produced about 100 mW when operating single-mode with a bandwidth of less than 0.5 MHz. The wavelength was monitored by a *Burleigh* WA-20 wavemeter and the laser stability by a *Burleigh* RC-45 Fabry-Perot Interferometer. The laser beam is directed, by mirrors, through a polarizer which was used to adjust the power. More details of the apparatus are given by Nantel [NAN].

The beamline is shown in figure A1-3. It is the same as shown in figure 3-1 but with a laser entrance window at the opposite end to the ion trap and a photomultiplier tube and light

collection system at the downstream (relative to the trap) multichannel plate detector position. (This is referred to as the interaction region.) The ion trap was actually in place but there was no RF voltage applied. In the place of the cavity system was an ion optic lens and beam deflection plates to control the geometric overlap of the ion beam and laser beam. Immediately preceding the interaction region was a charge exchange cell used to neutralize the ion beam for laser excitation. The charge exchange cell consists of a heated reservoir of neutral sodium (for resonant charge-transfer with the sodium ion) which produces a sodium vapor through which the ion beam passes, exchanging an electron with the neutral vapor as it does. The cell is cooled at the ends to avoid sodium being deposited throughout the system and a mesh is inserted that recirculates the sodium by capillary action. Details concerning the charge exchange cell are given by Nantel [NAN]. The interaction region consists of an *RCA* 8850 photomultiplier tube with a 2-inch diameter cathode, mounted perpendicularly to the ion beam, and a spherical mirror to reflect light emitted in the opposite direction. The solid angle subtended by the photomultiplier window results in about 10% of the emitted light being collected. The photomultiplier has a quantum efficiency of 2.5% at 589 nm. Apertures are placed along the entrance to interaction region to reduce stray light reflection which contributes to the background. Light collected by the photomultiplier is converted to an electronic pulse and then amplified by an *Ortec* 9301 fast pre-amp. The amplified pulses are passed through an *Ortec* 584 Constant Fraction Discriminator to avoid spurious signals and input to a *Kinetic Systems* 3553 Analog-Digital Converter which is part of a *CAMAC*-based data acquisition system. The *CAMAC* system is interfaced to an *IBM-PC* microcomputer via a *Transiac* 6002 controller and a *Real*Corriveau* software package. The output of the discriminator is also monitored by an *Ortec* 449 ratemeter and a *Nicolet* 3091 storage oscilloscope.

The experiment begins with the heating of the charge exchange cell which must be done slowly so as not to evaporate all the sodium. The ion source is then slowly heated and the beam current is monitored before and after the cell to determine the charge transfer efficiency. When the beam current reaches about 10 nA and the cell (at a temperature of about 340 °C) is operating at about 80%, the laser is sent through the beam line and frequency-scanned to look for the fluorescence signals.

RESULTS

Shown in figure A1-4 are two hyperfine spectra for the sodium D_2 line. Also indicated are the theoretical spacings [SAG] and intensities [KOP] of the lines indicated in figure A1-2 (the lines numbered 1 through 6 in figure A1-2 appear from right to left in figure A1-4). The lower spectrum, recorded with a 0.3 mW laser beam, is a result of 24 averaged scans. The upper spectrum represents only 10 scans using a 1 mW beam and is considerably noisier. The sodium

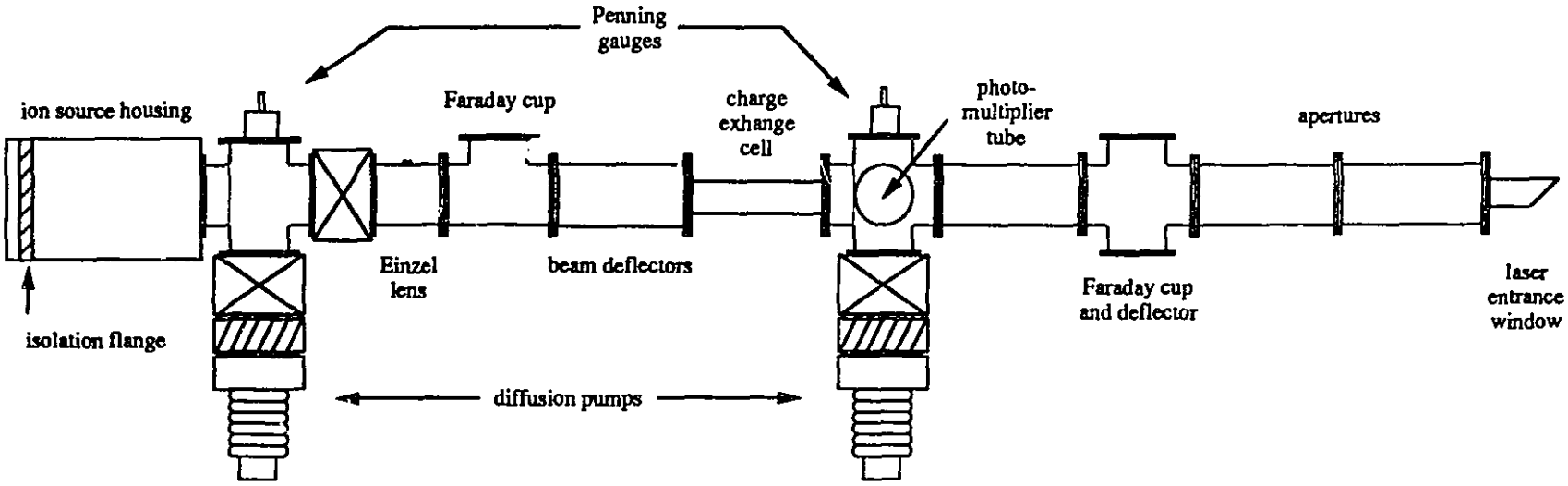

Figure A1-3: Schematic diagram of the beamline used for the collinear laser spectroscopy on fast sodium beams. The overall length of the beamline is 2.6 meters.

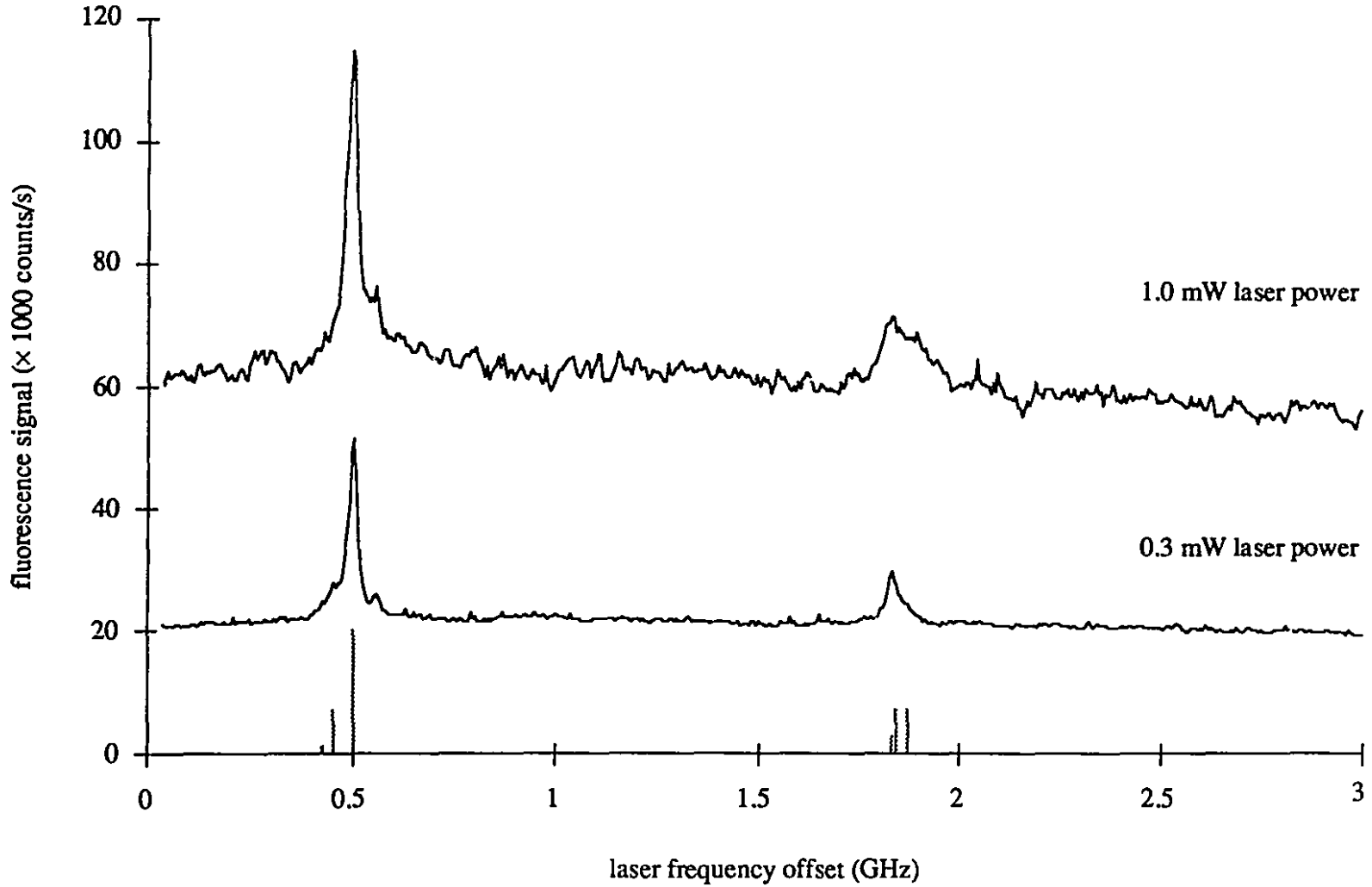

Figure A1-4: Fluorescence signals detected from collinear excitation of the D2 line in sodium. The theoretical hyperfine components are plotted with correct frequency and relative intensity.

beam current in each case was about 22 nA. The peaks of the upper spectrum are considerably wider which is due to a phenomenon called power broadening.† The lower spectrum is also power broadened to some extent as the laser power could not be further reduced during the run. The laser was scanned over 3 GHz at 40 ms per channel (512 channels). The first peak occurred at the doppler shifted frequency of 508508.863 GHz (589.552 nm, or 16962.03 cm^{-1} on the wavemeter) with the ion beam accelerated to 4790 V. Once the laser is scanning in stable fashion, the ion acceleration voltage is used to position the fluorescence peaks over the laser scan range. The peak is shifted by 36 MHz/V as calculated from equation A1-2. The background results mostly from stray laser light. The laser was blocked at one point and a background of about 5000 counts/s was recorded this due to florescence produced by residual gas that has been excited by the fast ion beam. The photomultiplier also has a dark current of about 400 s^{-1}.

It is obvious from the spectra that not only are the individual components not resolved but the relative intensities do not correspond to the theoretical ones. To ensure that all the peaks were observed in the right place, the spectra were fit with Lorentzian peaks as shown in figure A1-5. The lines from the first group (transitions 1, 2, and 3) are fit quite well while the second group is fit less so due to the closer spacing. Moreover, there an extra peak visible higher in frequency from the first group. These observations can all be easily accounted for. The resolution of the system, or linewidth, can be evaluated using equation A1-5. The ion source is the surface ionization type described in chapter 3 that has an energy spread of roughly 1 eV which can be estimated from surface ionization considerations. With an acceleration voltage of 4790, equation A1-5 gives a doppler width of 27 MHz which is almost triple the natural linewidth of 10 MHz. Reducing this doppler width to the natural linewidth would require an acceleration voltage of 35.59 kV which was not feasible with this system. The linewidth can also be determined by calibrating the scanning channels with the ground state separation of 1772 MHz between the lines 1 and 5 or 2 and 6 in figure A1-2. This calibration gives a linewidth of about 30 MHz for the largest peak and closer to 40 MHz for the smaller peaks. Power broadening also accounts for some of the additional linewidth.

The intensity disparity is easily explained using the concept of hyperfine pumping [BDS]. When an atom is excited, it can decay to the ground state by spontaneous emission rather than stimulated emission. If this happens, it may decay to a different ground state than that from which is was excited. Referring to figure A1-1, of the four hyperfine components of the $^2P_{3/2}$ state, the middle two (F = 1, 2) have allowed transitions to both hyperfine levels in the $^2S_{1/2}$ ground state. These are the transitions numbered 1, 2, 5, and 6. The F = 3 state can only decay

† Power broadening is the result of the populations of the excited and ground states being affected by the radiation field of the laser which leads to a shortening of the lifetime of the state. This causes the linewidth to broaden. A more detailed discussion is given by [DEM].

Figure A1-5: Data from the first hyperfine group of figure A1-4 fit with Lorentzian peaks.

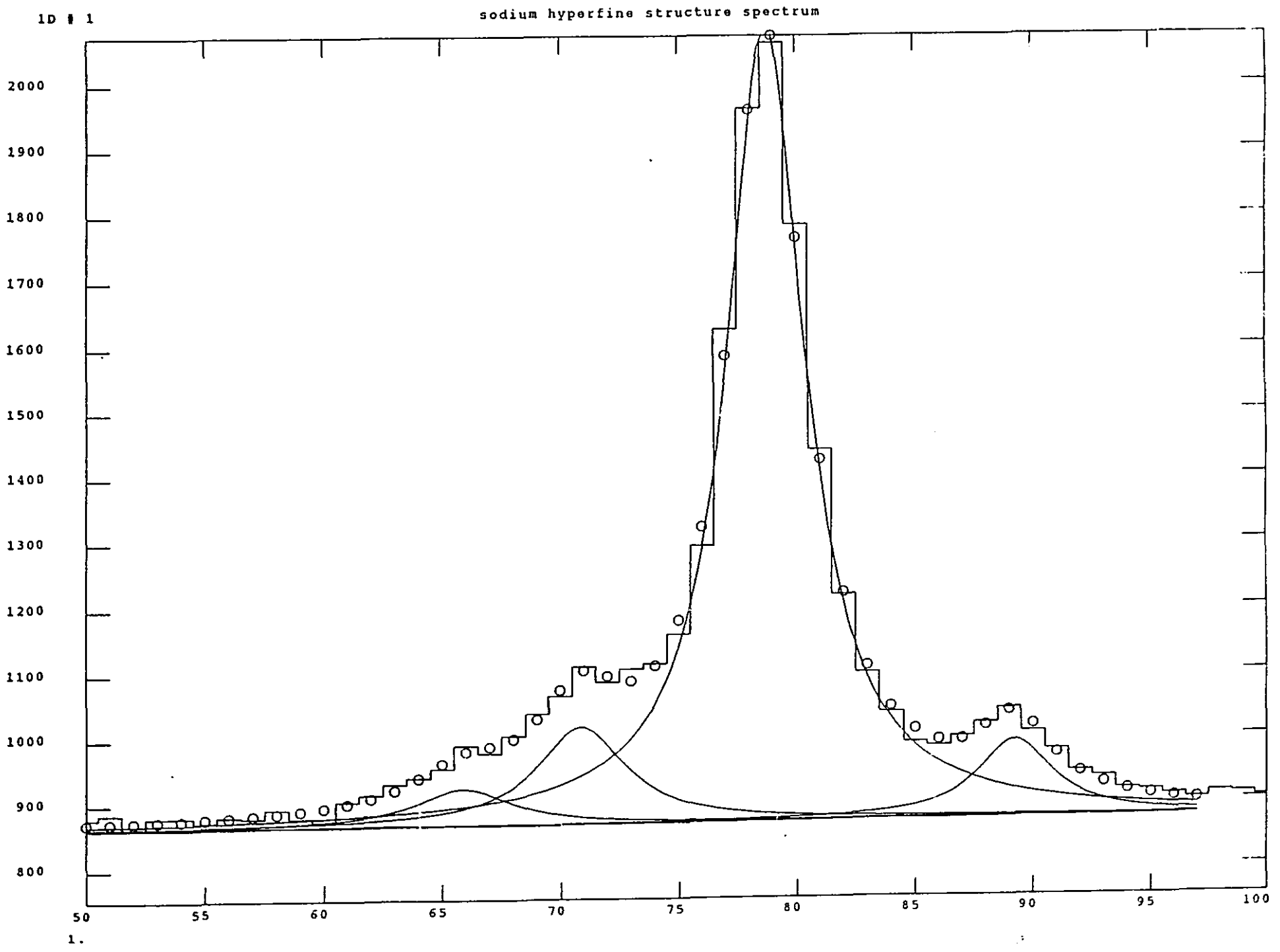
1D # 1
sodium hyperfine structure spectrum
2000
1900
1800
1700
1600
1500
1400
1300
1200
1100
1000
900
800
50
55
60
65
70
75
80
85
90
95
100
1.

to the F' = 2 state and F = 0 only to F' = 1. As the laser sweeps through the excitation frequency of either transition 1 or 2 the atom absorbs and emits several times. If at any point the atom spontaneously emits via transitions 5 or 6, respectively, further absorptions are impossible since the electron has been pumped into a ground state from which it cannot be re-excited at that frequency. It is only transitions 3 and 4 which are immune to this phenomenon as even the spontaneous emissions must return to the same ground state. For this reason, those transition intensities are greatly enhanced in the measured spectra. One way of avoiding this is to shorten the channel time widths. Another is to detune the atomic levels with a magnet while the atoms are outside the field of view of the photomultiplier.

The last feature of the spectra in figures A1-4 and A1-5 to account for is the small peak located to the right of the large F = 3 → F' = 2 peak by 76 MHz. During collisional charge exchange there is a chance for the neutralized sodium atom to be in the excited $^2P_{3/2}$ state after the collision according to the reaction:

$$Na^+ (3s) + Na \rightarrow Na (3p) + Na^+ - E \qquad \text{(A1-5)}$$

where E is the separation energy between the 3s and 3p state. In principle there should be a satellite peak for each hyperfine component but the others are not seen due to the lower intensities. The energy of the F = 3 → F' = 2 peak (at 16962.03 cm^{-1}) is 2.103 eV which means the effective beam energy of an atom thus excited is doppler shifted by a frequency corresponding to this energy. From equation A1-3, this shift is 71.5 MHz which is in fair agreement with what is measured from the fit of figure A1-5. The collisionally excited satellite peaks for the second group were not discernable.†

DISCUSSION

The main goal of the laser spectroscopy measurements was not to resolve the hyperfine components of sodium but to build and analyze the feasibility of a system to perform laser spectroscopy on a beam collected and extracted from a Paul trap. In order to gauge this, the overall detection sensitivity of the laser spectroscopy system must be established. From the results shown above and other trials an overall detection efficiency of 4×10^{-7} photons/ion was attained knowing the beam current (ions/s) used and the photon counting rate from the photomultiplier. This can be broken down as follows:

---

† A beautiful measurement of the Na D_2 line hyperfine structure using collimated atomic beam spectroscopy was published by [LLN].

photomultiplier quantum efficiency	2.5%
solid angle of detection	10%
ion beam transmission	50%
beam purity (Na/Na+K)	50%
charge exchange efficiency	80%
spectral overlap (linewidth ratios)	25%
geometric overlap	1%
hyperfine pumping	10%
excitations per atom	300%‡

The last three parameters are estimated based on the overall detection efficiency as they are difficult to measure. Signal to background ratios were fairly uniform at about 2.0 ± 0.5 with the best background counting rates not falling much below 25,000 photons/s.

If we refer back to table 4-2, the largest extracted cloud of Na ions was 5000. This was done at a rate of 130 Hz which corresponds to 6.5×10^5 ions/s. When multiplied by the detection efficiency of this corresponds to a signal of 0.325 photons/s. Though small, this signal comes in a tremendously short time window of about 0.75 μs. If the photomultiplier were gated with a 1 μs time window at 130 Hz, it would see 3.25 of the 25,000 photons/s background which would give a signal to background ratio of 0.1 which is not too impressive. Furthermore, the energy spread of this ion bunch is on the order of 100 eV so that the overall detection efficiency is reduced by another two orders of magnitude. Even if the energy spread were totally corrected, and the signals summed to reduced background statistically, 30 scans of about 25 s/scan would be required to achieve a signal to background approaching 1:1.

CONCLUSION

Three specific problems have hindered the spectroscopy attempts on bunched beams: the scant amounts of beam, the low detection efficiency and the large energy spread of the sample. Getting larger beams from traps is possible but will represent a major developmental effort. The low detection efficiency of the spectroscopy system could be improved but an order of magnitude improvement would only come with considerable work. The stray light background could also be reduced. Though energy spread reduction of extracted beams has been demonstrated in this thesis, the present reduction of about 30% would need considerable improvement.

‡ This figure is estimated from the number of times a single atom may fluoresce while in the field of view of the photomultiplier tube. The flight time of an atom through the field of view is about 0.2 μs so one could expect about 10 counts from the florescence rate of about 5×10^7 s^{-1} based on the 16 ns lifetime of the state [CAR]. Laser spectral density considerations [EIN] further reduce this to about a factor of 3 photons per atom.

APPENDIX 2:

The Computation of Electric Fields for Numerical Integration of Charged Particle Motion

This paper was presented at the 1991 Conference on Electric Field Computation which was held September 30-October 1, 1991 in Toronto, Canada. It was refereed and published in: I.E.E.E. Transactions on Magnetics, Vol. 27, No. 5, September 1991, pp. 4174-4176.

Note that equation (5) in the publication is incorrect and should read:

$$\cos\theta = \frac{z}{r} = \frac{z}{\sqrt{z^2 + r^2}}$$

vice:

$$\cos\theta = \frac{z}{r} = \frac{z}{z^2 + r^2}$$

APPENDIX 3:

Reconstruction of Phase Space Diagrams using the Projection-Slice Theorem

INTRODUCTION

The detailed phase space diagram of a trapped ion cloud is extremely difficult to measure because the two components, time and energy, are convolved. Sampling these quantities is difficult whether studying the cloud *in situ* or extracting the cloud from the trap for observation.

From the measurements presented in this thesis, it was shown that the variation of the extraction time with RF phase of the trapping field changes the relative orientation of the phase space distribution of the extracted ion cloud as reflected by the resulting intensity versus time signals. This change in orientation offers a way of viewing the ion cloud phase space from various perspectives, exactly the way an observer walks around an object so as to divine its overall form. The information processing that accompanies such observation is known as *tomography* which is the reconstruction of an image from its projections. Probably the best known example of tomography is the CAT (computer-aided tomography) scan in which images of the brain are reconstructed from transmitted X-ray beams detected at various positions around the circumference of the head.

The application of the image reconstruction principle to phase space space diagrams differs in that the source is actually changing its perspective relative to a fixed detector. Also, the conditions under which each projection is measured are not identical. Nevertheless, the problem is fundamentally the same. If a time projection for several orientations of the phase space diagram can be made, the detailed structure can be reconstructed from the projections. This would offer a way of studying the dynamics of the trapped ion cloud independently of a thermodynamic or space charge model.

THE PROJECTION-SLICE THEOREM

The projection-slice theorem (or Fourier-slice theorem, as it sometimes called) states that: the Fourier transform of a parallel projection of an image at a given angle, represents a slice of the two-dimensional transform at the same angle. The object can then be estimated by taking the inverse Fourier transform of the sum of the projections at all angles.†

A geometrical description of the reconstruction problem is illustrated in figure A3-1. The image is $f(x,y)$ and a projection $P_\theta(t)$ is shown as a function of t for a particular angle θ. Also shown is the Fourier transform of $P_\theta(t)$, denoted by $F(u,v)$, where $u = \omega\cos\theta$ and $v = \omega\sin\theta$ t.

---

† For a detailed derivation of the projection-slice theorem and reconstruction algorithms in general, see [KSL]. For a review of the many applications using the projection-slice theorem, see [HER].

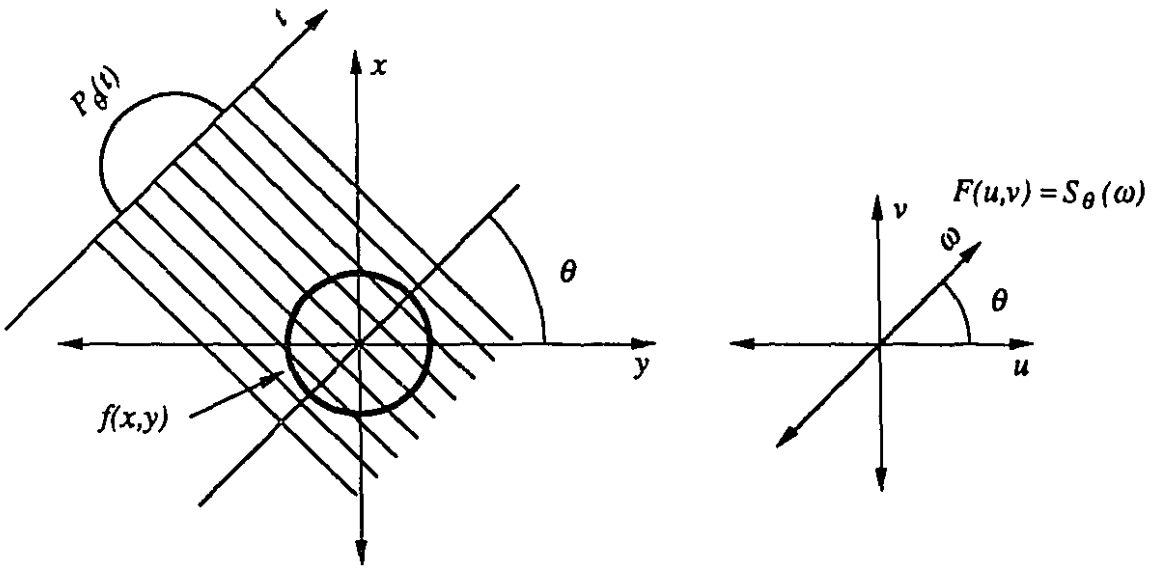

Figure A3-1: Projection $P_\theta(t)$ of an image $f(x,y)$ at angle θ with corresponding Fourier transform $F(u,v)$.

The slice of $F(u,v)$ at angle θ, defined as $S_\theta(\omega)$, forms a slice of $f(x,y)$ in Fourier space according to the projection-slice theorem:

$$S_\theta(\omega) = F(u,v) \tag{A3-1}$$

The image is then obtained from the inverse Fourier transform, $F^{-1}(u,v)$:

$$f(x,y) = F^{-1}(u,v) = \int_{-\infty}^{\infty} \int_{-\infty}^{\infty} F(u,v)\, e^{i\omega t}\, du\, dv \tag{A3-2}$$

Using equation A3-1 and substituting the Jacobian of $du\, dv = |\omega|\, d\omega\, d\theta$:

$$f(x,y) = \int_{0}^{\pi} d\theta \int_{-\infty}^{\infty} S_\theta(\omega)\, |\omega|\, e^{i\omega t}\, d\omega)\, d\theta \tag{A3-3}$$

We define a filtering function $\Phi(t)$ as the inverse Fourier transform of ω:

$$\Phi(t) = F^{-1}(\omega) = \int_{-\infty}^{\infty} |\omega|\, e^{i\omega t}\, d\omega \tag{A3-4}$$

so that in the time domain:

$$f(x,y) = \int_0^{\pi} d\theta \, [P_\theta(t) * \Phi(t)] = \int_0^{\pi} d\theta \int_{-\infty}^{\infty} P_\theta(\alpha)\Phi(t-\alpha)\, d\alpha \qquad \text{(A3-5)}$$

which is the convolution function of $P_\theta(t)$ and $\Phi(t)$ which follows from the convolution theorem.† Reconstruction of an image using this technique is the filtered convolution-backprojection algorithm an example of which is described by [SLO]. A backprojection of the image of figure A3-1 is shown in figure A3-2. For the simple example of a circle, all the angular projections are the same. Figure A3-2 illustrates how the projections form the reconstruction. It is obvious from the figure that more projections reconstruct the image with greater accuracy.

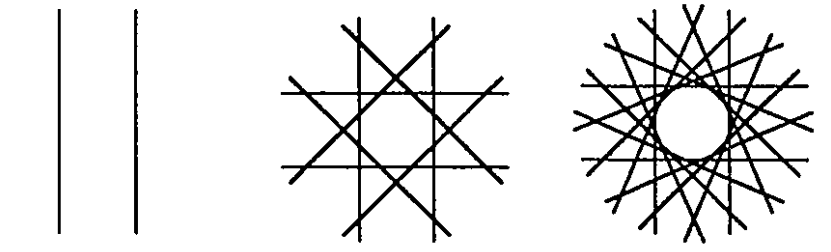

Figure A3-2: Reconstruction of a circular image from several one-dimensional projections.

RECONSTRUCTION OF PHASE SPACE DIAGRAMS

To illustrate the idea of the time projection of a phase space diagram, a simple example is shown in figure A3-3. A simple distribution in energy versus time drifts as shown. At some postion the ion bunch is detected in time. A parallel projection at this point can be mapped back to the original distribution as illustrated forming a projection angle of, in this example, 45°. What is required to reconstruct the phase space diagram is a method of systematically varying the projection angle to sample as many viewing angles as possible.

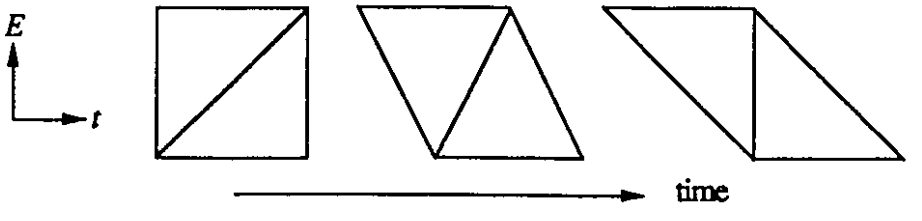

Figure A3-3: Parallel projection of a drifted phase space diagram (energy verus time) mapped back through the original orientation. Different drift times produce different angluar projections.

† The convolution theorem states that the convolution of two functions is equivalent to the multiplication of their Fourier transforms.

In the case of a trapped ion cloud, the RF phase at extraction offers a fortuitous method of varying the projection angle. Shown on the right side of figure A3-4 are the simulated phase space diagrams of figure 3-6. The phase space plot at any given RF phase corresponds to a single projection through the original phase space diagram. The vertical lines through the diagrams correspond to time bins into which the projection is sampled. Because each ion in the ensemble is coded, it is easy to map back to the original, symmetrical distribution and determine the projection angle for the ensemble at a particular RF phase. This is done on the left side of figure A3-4 for each phase of extraction. By systematically varying the phase at extraction, a series of angular projections of the axial ion phase space diagram can be measured and reconstructed.

As demonstrated in chapter 4, the centroids of the ion cloud time-of-flight peaks at each phase are accounted for to within a few percent. This means that if the measured projections are mapped back to the center point of the trapped ion ensemble, information about the distribution could be gleaned from the profile of the reconstruction. This information comes without any assumptions about the initial ion cloud phase space (except that it symmetric). The results presented in this thesis, though consistent, were obtained under the assumption of a particular temperature and model (the Gibb's distribution) with no space charge considerations.

The development of the projection-slice theorem and back-projection algorithm for this problem poses interesting possibilities for future work. The main problem associated with the technique is that the projections are generally not parallel as seen in figure A3-4. Furthermore, though straight lines have been used in the figure, the projections are not linear. This complicates the use of existing algorithms but with some work, a technique could be developed probably involving conformal mapping of the projections. The non-parallel aspect can be dealt with using existing formulations for fan-beam projections.

The projection-slice theorem also has potential application to the problem of measuring transverse emittance of DC beams. This measurement is quite tedious as it requires selective scanning over the entire beam cross-section. An emittance meter consists of a large plate with a regularly spaced array of holes behind which a detector is moved. This allows the sampling of the beam divergence as a function of position so as to map out the transverse emittance.

The idea of projecting the transverse emittance over several angles and then reconstructing it offers potential improvement of this measurement. A calibrated quadrupole magnet could be used to sweep the beam through a focus in each transverse direction with a position sensitive detector used to sample the projection. The resulting projections are measured at each quadrupole setting and reconstructed to obtain the transverse emittance. Such an emittance meter would be superior to what is now available as the speed limitations due to mechanical motions as well as the inherent instability would be circumvented.

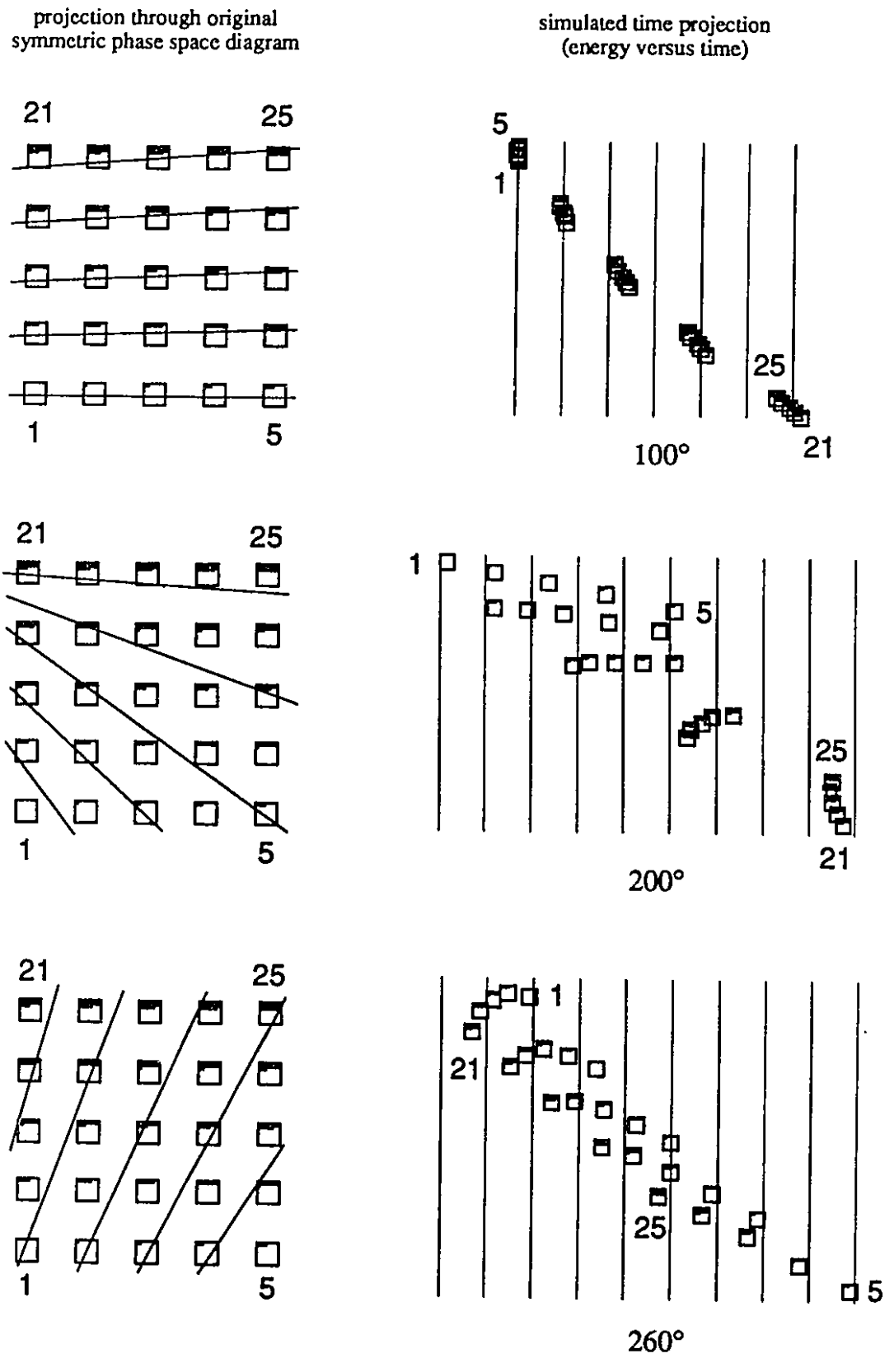

Figure A3-4: Projection angles of a trapped-ion phase space diagram for three different RF extraction phases. (The energy-time simulations are those in figure 3-6.) The projections of the phase space diagrams in time are shown along with the corresponding projection angles in the original ion distribution. As the RF phase at extraction is increased, the projection angle sweeps from 180° to about 60°.

REFERENCES

[BBK] St. Becker, G. Bollen, F. Kern, H.-J. Kluge, R.B. Moore, G. Savard, L. Schweikhard, H. Stolzenberg and the ISOLDE Collaboration, "Mass Measurements of Very High Accuracy by Time-Of-Flight Ion Cyclotron Resonance of Ions Injected into a Penning Trap," Int. J. Mass Spec. Ion Proc. 99 (1990) 53-77.

[BCZ] G. Brincourt, R. Catella, Y. Zerega and J. André, "Time-of-Flight Detection of Ions Ejected from a Radiofrequency Quadrupole Trap: Experimental Determination of their Secular Frequency", Chem. Phys. Lett 174 (1990) 626-630.

[BDS] N. Bendali, H.T. Duong, J.M. Saint Jalm and J.L. Vialle, "Observation of optical pumping effects in collinear atomic beam-laser beam(s) interaction," J. Physique 44 (1983) 1019-1023.

[BER] K. Berkling, "Der Entwurf eines Partialdruckmessers," Bonn University, 1956.

[BGA] L.S. Brown and G. Gabrielse, "Geonium Theory: Physics of an Electron or Ion in a Penning Trap," Rev. Mod. Phys. 58 (1986) 233-311.

[BHI] J.J. Bollinger, D.J. Heinzen, W.M. Itano, S.L. Gilbert and D.J. Wineland, "A 303-MHz Frequency Standard Based on Trapped Be+ Ions," IEEE Trans. Ins. Meas. 40 (1991) 126-128.

[BHU] J.C. Bergquist, R.G. Hulet, W.M. Itano and D.J. Wineland, "Observation of Quantum Jumps in a Single Atom," Phys. Rev. Lett. 57 (1986) 1699-1702.

[BSE] M. Baril and A. Septier, Piégeage des Ions dans un Champ Quadrupolaire Tridimensional a Haute Fréquence", Rev. Phys. Appl. 9 (1974) 525-531.

[BSW] R. Blatt, U. Schmeling and G. Werth, "On the Sensitivity of Ion Traps for Spectroscopic Applications," Appl. Phys. 20 (1979) 295-298.

[BWI] J.J. Bollinger and D.J. Wineland, "Microplasmas," Scientific American, January (1990) 124-130

[BZH] R. Blatt, P. Zoller, G. Holzmüller and I. Siemers, "Brownian Motion of a Parametric Oscillator: A Model for Ion confinement in Radio Frequency Traps", Z. Phys. D4 (1986) 121-126.

[BZO] R. Blatt and P. Zoller, "Quantum Jumps in Atomic Systems," Eur. J. Phys. 9 (1988) 250-256.

[CAR] J. Carlsson, Z. Phys. D9 (1988) 2.

[CCL] R.J. Campeau, A. Crubelier, R. Leroux, D. Marinescu and D. Pavolini, "Ions in R.F. Traps. Theoretical Study of Laser Evaporative Cooling of Trapped Negative Ions. Experimental Investigations of R.F. Phase Stopped Ejection", Proceedings of 22nd EGAS, Uppsala 1990, 464-66.

[CDE] D.A. Church and H.G. Dehmelt, "Radiative Cooling of an Electrodynamically Contained Proton Gas", J. Appl. Phys, 40 (1969) 3421-4.

[CFG] L.S. Cutler, C.A. Flory, R.P. Giffard and M.D. McGuire, "Doppler Effects due to Thermal Macromotion of Ions in an RF Quadrupole Trap", Appl. Phys. B 39 (1986) 251-259.

[CGM] L.S. Cutler, R.P. Giffard and M.D. McGuire, "Thermalization of 199Hg Ion Macromotion by a Light Background Gas in an RF Quadrupole Trap", Appl. Phys. B 36 (1985) 137-142.

[DAW] P.H. Dawson (editor), "Quadrupole Mass Spectrometry and its Applications," Elsevier, Amsterdam, 1976.

[DEHa] H. Dehmelt, "Experiments with an Isolated Subatomic Particle at Rest", Rev. Mod. Phys. 62 (1989) 525-530.

[DEHb] H.G. Dehmelt, "Radiofrequency Spectroscopy of Stored Ions I; Storage", Adv. At. Mol. Phys. 3 (1967) 53-72 and H.G. Dehmelt, "Radiofrequency Spectroscopy of Stored Ions II; Spectroscopy", Adv. At. Mol. Phys. 5 (1969) 109-54.

[DEM] W. Demtröder, "Laser Spectroscopy," Springer-Verlag, Berlin, 1982, chapter 3.

[DFI] F. Diedrich, J.C. Bergquist, W.M. Itano and D.J. Wineland, "Laser Cooling to the Zero Point of Motion," Phys. Rev. Lett. 62 (1989) 403-406.

[DPC] F. Diedrich, E. Peik, J.M. Chen, W. Quint and H. Walther, "Observation of a Phase Transition of Stored Laser-Cooled Ions," Phys. Rev. Lett. 58 (1987) 2931-2934.

[DLA] P.H. Dawson and C. Lambert, "Pulse-Out Synchronization in the Quadrupole Ion Trap," Int. J. Mass Spectrom. Ion Phys. 14 (1974) 339-347.

[DWA] F. Diedrich and H. Walther, "Nonclassical Radiation of a Single Stored Ion," Phys. Rev. Lett. 58 (1987) 203-306.

[EIN] A. Einstein, Phys. Zeitschrift 18 (1917) 121.

[EMA] H.W. Ellis, E.W. McDaniel, D.L. Albritton, L.A. Viehland. S.L. Lin and E.A. Mason, "Transport Properties of Gaseous Ions over a Wide Energy Range. Part II," Atomic Data and Nuclear Data Tables 22 (1978) 495-514.

[EWI] P. Ekstrom and D. Wineland, "The Isolated Electron," Scientific American, August (1980) 111-121.

[FIS] E. Fischer, "Die Dreidimensionale Stabilisierung von Ladungstraegern in einem Vierpolfeld," Z. Phys. 156 (1959) 1-26.

[GBW] S.L. Gilbert, J.J. Bollinger and D,J. Wineland, "Whell Structure of Magnetically Confined Strongly Coupled Plasmas," Phys. Rev. Lett. 60 (1988) 2022-2025.

[GDK] G. Gabrielse, H. Dehmelt and W. Kells, "Observation of a Relativistic, Bistable Hysteresis in the Cyclotron Motion of a Single Electron," Phys. Rev. Lett. 54 (1985) 537-539.

[GDM] M.N. Gaboriaud, M. Desaintfuscien and F.G. Major, "Absolute Measurement of the Total Number of Ions Stored in an RF Quadrupole Trap," Int. J. Mass Spectrom. Ion Phys. 41 (1981) 109-123.

[GFO] G. Gabrielse, X Fei, L.A. Orozco, R.L. Tjoelker, J. Haas, H. Kalinowsky, T.A. Trainor and W. Kells, "Thousandfold Improvement in the Measured Antiproton Mass," Phys. Rev. Lett. 65 (1990) 1317-1320.

[GIB] J.S. Gibbs, "Elementary Principles in Statistical Mechanics," Dover Publications, New York, 1960 (first published in 1902 by the Yale University Press). A good biography of Gibbs and summary of his work is given by M. Klein, "The Physics of J. Willard Gibbs in his Time," Physics Today, Vol. 43, No. 9, September, 1990, pp. 40-48.

[GOL] H. Goldstein, "Classical Mechanics," Addison-Wesley, Reading, 1980.

[GUL] S.L. Gulick, "Ion Injection into Radiofrequency Quadrupole Field Devices," M.Sc. Thesis, McGill University, Montreal, 1986.

[HDR] J. Hoffnagle, R.G. DeVroe, L. Reyna and R.G. Brewer, "Order-Chaos Transition of Two Trapped Ions," Phys. Rev. Lett. 61 (1988) 255-258.

[HER] G.T. Herman (editor), "Image Reconstruction from Projections," Springer-Verlag, Berlin, 1979.

[HUA] K. Huang, "Statistical Mechanics," John Wiley and Sons, New York, 1987.

[ILS] Bull. Am. Phys. Soc. 36 (1991) 1973-1974.

[ISO] ISOLDE Users' Guide, edited by H.-J. Kluge, European Organization for Nuclear Research (CERN), report number CERN 86-05, Geneva, 1986.

[IWE] R. Iffländer and G. Werth, "Optical Detection of Ions Confined in a RF Quadrupole Trap", Metrologia 13 (1977) 167-170.

[KNI] R.D. Knight, "The genral form of the quadrupole ion trap potential", Int. J. Mass Spectrom. Ion Phys. 51 (1983) 127-131.

[KOP] H. Kopfermann, "Nuclear Moments," Academic Press, New York, 1958, p.441.

[KPR] R.D. Knight and M.H. Prior, "Laser Scanning Measurement of the Density Distribution of Confined $^6Li^+$ Ions", J. Appl. Phys. 50 (1979) 3044-3049.

[KRA] K.S. Krane, "Introductory Nuclear Physics," Wiley, New York, 1988, chapter 16.

[KSL] A.C. Kak and M. Slaney, "Principles of Computerized Tomographic Imaging," I.E.E.E. Press, New York, 1988, chapter 3.

[LLB] W. Lange, J. Luther, B. Nottbeck and H.W Schröder, "High Resolution Fluorescence Spectroscopy by use of a CW Dye Laser," Optics Communications 8 (1973) 157-159.

[LLI] L.D. Landau and E.M. Lifshitz, "Statistical Physics," Pergamon Press, Oxford, 1980.

[LMO] M.D. Lunney and R.B. Moore, "The Computation of Electric Fields for Numerical Integration of Charged Particle Motion," IEEE Trans. Mag. 27 (1991) 4174-4176.

[LTB] G. Lawson , J.F.J. Todd and R.F. Bonner, "Theoretical and Experimental Studies with the Quadrupole Ion Storage Trap ("Quistor")," in "Dynamic Mass Spectrometry," Edited by D. Price and J.F.J. Todd, Vol. 4, pp. 39-81, Heydon, London, 1974.

[LUN] M.D.N. Lunney, "Dynamics of Ions in Radiofrequency Quadrupole Traps," M.Eng. Thesis, McGill University, Montreal, 1986.

[LWM] M.D.N. Lunney, J.P. Webb and R.B. Moore, "Finite Element Analysis of a Radiofrequency Quadrupole Ion Trap," J. Appl. Phys. 65 (1989) 2883-2888.

[MAR] J.B. Marion, "Classical Dynamics of Particles and Systems," Academic Press, New York, 1965

[MBG] A. Münch, M. Berkler, Ch. Gertz, D. Wilsdorf and G. Werth, "Precise ground-state hyperfine splitting in ^{173}Yb II," Phys. Rev. A, 35 (1987) 4147-4150.

[MDE] F.G. Major and H.G. Dehmelt, "Exchange-Collision Technique for the RF Spectroscopy of Stored Ions," Phys. Rev. 170 (1968) 91-107.

[MDJ] C. Meis, M. Desaintfucien and M. Jardino, "Analytical Calculation of the Space Charge Potential and the Temperature of Stored Ions in an rf Quadrupole Trap," Appl. Phys. B, 45 (1988) 59-64.

[MGU] R.B. Moore and S. Gulick, "The Transfer of Continuous Beams and Storage Ring Beams Into Electromagnetic Traps", Phys. Scr. T22 (1988) 28-35.

[MHU] R.E. March and R.J. Hughes, "Quadrupole Storage Mass Spectrometry," Wiley, New York, 1990.

[MLR] R.B. Moore, M.D. Lunney, G. Rouleau and G. Savard, "Collection, cooling and delivery of ISOL beams," Nucl. Inst. Meth. B70 (1992) 482-489.

[MRO] R.B. Moore, G. Rouleau and the ISOLDE Collaboration, "In Flight Capture of an Ion Beam in a Paul Trap" , J. Mod. Optics 39 (1992) 361-371.

[MTO] R.E. Mather and J.F.J. Todd, "The Quadrupole Ion Store (QUISTOR). Part V. A Simple Model for the Ion Ejection Process," Int. J. Mass Spectrom. Ion Phys. 31 (1979) 1-13.

[MVZ] E.R. Mosburg, Jr., M. Vedel, Y. Zerega, F. Vedel, and J.A. André, "A Time-of-Flight Method for Studying the Properties of an Ion Cloud Stored in an RF Trap", Int. J. Mass Spectrom. Ion Proc. 77 (1987) 1-12.

[NAN] M. Nantel, "Bunched Beams from RFQ traps for Laser Spectroscopy Studies," M.Sc. Thesis, McGill University, 1989.

[NEU] R. Neugart, "Collinear Laser Spectrsocopy on Unstable Isotopes - A Tool of Nuclear Physics," Hyperfine Interactions 24-24 (1985) 159-180.

[NHTa] W. Neuhauser, M. Hohenstatt, P. Toschek and H. Dehmelt, "Optical-Sideband Cooling of Visible Atom Cloud Confined in Parabolic Well", Phys. Rev. Lett. 41 (1978) 233-6.

[NHTb] W. Neuhauser, M. Hohenstatt, P. Toschek and H. Dehmelt, "Visual Observation and Optical Cooling of Electrodynamically Contained Ions", Appl. Phys. 17 (1978) 123-129.

[NHTc] W. Neuhauser, M. Hohenstatt, P. Toschek and H. Dehmelt, "Localized Visible Ba+ Mono-Ion Oscillator", Phys. Rev. A 22 (1980) 1137-1140.

[NSD] W. Nagourney, J. Sandberg and H.G. Dehmelt, "Shelved Electron Amplifier: Observation of Quantum Jumps," Phys. Rev. Lett. 56 (1986) 2797-2799.

[OTT] E.W. Otten, "Nuclear Radii and Moments of Unstable Isotopes," in "Treatise on Heavy-Ion Science," Vol. 8, edited by D.A. Bromley, Plenum, New York, 1989.

[PAU] W. Paul, "Electromagnetic Traps for Charged and Neutral Particles," Rev. Mod. Phys. 62 (1989) 531-540.

[PDM] J.D. Prestage, G.J. Dick and L. Maleki, "Linear Ion Trap Based Atomic Frequency Standard," IEEE Trans. Ins. Meas. 40 (1991) 132-136.

[PEN] F.M. Penning, "Glow Discharge at Low Pressure Between Coaxial Cylinders in an Axial Magnetic field," Physica 3 (1936) 873-894.

[PFT] W.H. Press, B.P. Flannery, S.A. Teukolsky and W.T. Vetterling, "Numerical Recipes," Cambridge University Press, Cambridge, 1986.

[PST] W. Paul and H.A. Steinwedel, "A New Mass Spectrometer Without a Magnetic Field," Z. Naturforsch. 8A (1953) 448-450.

[RHH] J.A. Richards, R.M. Huey and J. Hiller, Int. J. Mass Spectrom. Ion Phys. 12 (1973) 317.

[RKS] H.-P. Reiser, R.E. Kaiser, P.J. Savickas and R.G. Cooks, "Measurement of Kinetic Energies of Ions Ejected from a Quadrupole Ion Trap," Int. J. Mass Spectrom. Ion Processes 106 (1991) 237-247.

[ROU] G. Rouleau, "A tandem Paul-Penning trap mass measurement system for radionuclides," Doctoral Thesis, McGill University, 1992.

[SAD] B.M. Schwarzchild, "Low-Energy Lone Electron Exhibits Relativistic Hysteresis," Physics Today, May (1985) 17-19; B. Gross Levi, "Clouds of Trapped Cooled Ions Condense into Crystals," Physics Today, September (1988) 17-20; B.M. Schwarzchild, "Antiprotons Cooled to 4K and Weighed in a Penning Trap," Physics Today, July (1990) 17-20.

[SAG] P. L. Sagalyn, "The Hyperfine Structure of the $3P_{3/2}$ State of Na^{23}," Phys. Rev. 94 (1954) 885-892.

[SBB] H. Stolzenberg, St. Becker, G. Bollen, F. Kern, H.-J. Kluge, Th. Otto, G. Savard, L. Schweikhard, G. Audi and R.B. Moore, "Accurate Mass Determination of Short-Lived Isotopes by a Tandem Penning-Trap Mass Spectrometer," Phys. Rev. Lett. 65 (1990) 3104-3107.

[SBN] Th. Sauter, R. Blatt, W. Neuhauser and P.E. Toschek, "Quantum Jumps Observed in the Fluorescence of a Single Ion," Opt. Commun. 60 (1986) 287-292.

[SBS] I. Siemers, R. Blatt, Th. Sauter and W. Neuhauser, "Dynamics of ion clouds in Paul traps," Phys. Rev. A, 38 (1988) 5121-5128.

[SCR] H.I. Smith and G.G. Craighead, "Nanofabrication," Physics Today, Vol. 43, No. 2, February 1990, pp. 24-30.

[SFD] H.A. Schuessler, E.N. Fortson and H.G. Dehmelt, "Hyperfine Structure of the Ground State of 3He+ by the Ion-Storage Exchange-Collision Technique," Phys. Rev. 187 (1969) 5-38.

[SLO] L.A. Shepp and B.F. Logan, "The Fourier Reconstruction of a Head Section," IEEE Trans. Nucl. Sci. NS-21 (1974) 228-236.

[SSB] M. Schubert, I. Siemers and R. Blatt, "Kinetic Energy and Spatial Width of Ion Clouds in Paul Traps," Appl. Phys. B, 51 (1990) 414-417.

[SSW] H. Schaaf, U. Schmeling and G. Werth, "Trapped Ion Density Distribution in the Presence of He-Buffer Gas", Appl. Phys. 25 (1981) 249-251.

[THOa] R. Thompson, "First Trap Your Atom," New Scientist, September 1987, pp. 56-59.

[THOb] R.C. Thompson, "Precision Measurement Aspects of Ion Traps," Meas. Sci. Technol. 1 (1990) 93-105.

[TLA] J.F.J. Todd and G. Lawson, M.T.P. International Review of Science, Physical Chemistry, Series 2, Volume 5, edited by A. Maccoli, Butterworths, London, 1975.

[VAN] F. Vedel and J. André, "Influence of space charge on the computed statistical properties of stored ions cooled by buffer gas in a quadrupole rf trap", Phys. Rev. A 29 (1984) 2098-2101.

[VAV] F. Vedel, J. André, M. Vedel and G. Brincourt, "Computed energy and spatial statistical properties of stored ions cooled by a buffer gas", Phys. Rev. A 27 (1983) 2321-2330.

[VED] F. Vedel, "On the Dynamics and Energy of Ion Couds Stored in an R.F. Quadrupole Trap," Int. J. Mass Spectrom. Ion Processes, 106 (1991) 33-61.

[VSDa] R.S. Van Dyck Jr., P.B. Schwinberg and H.G. Dehmelt, "Electron Magnetic Moment from Geonium Spectra: Early Experiments and Background Concepts," Phys. Rev. D 34 (1986) 26.

[VSDb] R.S. Van Dyck Jr., P.B. Schwinberg and H.G. Dehmelt, "New High Precision Comparison of Electron/Positron g-Factors," Phys. Rev. Lett. 59 (1987) 26.

[VSK] R.S. Van Dyck Jr., H.A. Schuessler, R.D. Knight, D. Dubin, W.D. Phillips and G. Lafaytis, "Summary of the Physics in Traps Panel," Phys. Scr. T22 (1988) 228-237.

[WDU] F.L. Walls and G.H. Dunn, "Storing Ions for Collision Studies," Physics Today, August (1974) 30-35

[WDW] D.J. Wineland, E.E. Drullinger and F.L. Walls, "Radiation-Pressure Cooling of Bound Resonant Absorbers", Phys. Rev. Lett. 40 (1978) 1639-42.

[WERa] G. Werth, "Trapped Ion Spectroscopy," in "Progress in Atomic Spectroscopy: Part C," edited by H.J. Beyer and H. Kleinpoppen, Plenum Press, New York (1982) 151-175.

[WERb] G. Werth, "Precision Microwave Spectroscopy on Trapped Ions," Phys. Scr. T22 (1988) 191-194.

[WIN] D.J. Wineland, "Frequency Standards Based on Stored Ions," Proc. IEEE 74 (1986) 147-150.

[WITa] D.J. Wineland and W.M. Itano, "Spectroscopy of a Single Mg^+ Ion," Phys. Lett. 82A (1981) 75-78.

[WITb] D.J. Wineland and W.M. Itano, "Laser Cooling," Physics Today, June (1987) 34-40.

[WSL] R.F. Wuerker, H. Shelton and R.V. Langmuir, "Electrodynamic Containment of Charged Particles," J. Appl. Phys. 30 (1959) 342-349.

[WTO] R.M. Waldren and J.F.J. Todd, "The Quadrupole Ion Store (QUISTOR). Part III. Studies on Phase-Synchronised Ion Ejection: The Effects of Ejection Pulse Width and Detection Pulse Delay," Int. J. Mass Spectrom. Ion Phys. 29 (1979) 315-335; "Part VI. Studies on Phase-Synchronised Ion Ejection: The Effects of Ejection Pulse Amplitude," Int. J. Mass Spectrom. Ion Phys. 31 (1979) 15-29.